



5-1998

## Determination of the Dose Rate From Naturally Occurring Radionuclides in Soil

Daniel James Chase  
*University of Tennessee, Knoxville*

Follow this and additional works at: [https://trace.tennessee.edu/utk\\_gradthes](https://trace.tennessee.edu/utk_gradthes)

 Part of the [Nuclear Engineering Commons](#)

---

### Recommended Citation

Chase, Daniel James, "Determination of the Dose Rate From Naturally Occurring Radionuclides in Soil. " Master's Thesis, University of Tennessee, 1998.  
[https://trace.tennessee.edu/utk\\_gradthes/4159](https://trace.tennessee.edu/utk_gradthes/4159)

This Thesis is brought to you for free and open access by the Graduate School at TRACE: Tennessee Research and Creative Exchange. It has been accepted for inclusion in Masters Theses by an authorized administrator of TRACE: Tennessee Research and Creative Exchange. For more information, please contact [trace@utk.edu](mailto:trace@utk.edu).

To the Graduate Council:

I am submitting herewith a thesis written by Daniel James Chase entitled "Determination of the Dose Rate From Naturally Occurring Radionuclides in Soil." I have examined the final electronic copy of this thesis for form and content and recommend that it be accepted in partial fulfillment of the requirements for the degree of Master of Science, with a major in Nuclear Engineering.

Laurence F. Miller, Major Professor

We have read this thesis and recommend its acceptance:

Lawrence W. Townsend, Mike Elam

Accepted for the Council:

Carolyn R. Hodges

Vice Provost and Dean of the Graduate School

(Original signatures are on file with official student records.)

To the Graduate Council:

I am submitting herewith a thesis written by Daniel Chase entitled "Determination of the Dose Rate from Naturally Occurring Radionuclides in Soil." I have examined the final copy of this thesis for form and content and recommend that it be accepted in partial fulfillment of the requirements for the degree of Master of Science, with a major in Nuclear Engineering.

—Laurence F. Miller—  
Laurence F. Miller, Major Professor

We have read this thesis  
and recommend its acceptance:

Laurence W. Townsend  
J. H. E.

Accepted for the Council:

—Leuwink—  
Associate Vice Chancellor and  
Dean of The Graduate School

Daniel James Chase  
May 1999

# **DETERMINATION OF THE DOSE RATE FROM NATURALLY OCCURRING RADIONUCLIDES IN SOIL**

**A Thesis  
Presented for the  
Master of Science  
Degree  
The University of Tennessee, Knoxville**

**Daniel James Chase  
May 1998**



## **DEDICATION**

**This thesis is dedicated to my wife, Valerie. Without her patience and support, completion of this project would not have been possible.**

## **ACKNOWLEDGEMENTS**

I would like to thank Larry Miller and Mike Elam for their assistance and guidance on this project.

## ABSTRACT

This thesis addresses the problem of determining the dose rate that an artifact is exposed to while buried in soil. The determination of this dose rate is critical to obtaining an accurate age estimate for an artifact using the Thermoluminescent (TL) Dating technique. Determining the dose rate requires a two step process involving the measurement of the soil activity, and then calculation of the dose rate from this measured activity. For this paper soil samples taken from the Wickliffe Mound site located in Western Kentucky.

The activity of the soil is measured using a High Purity Germanium (HPGe) gamma spectrometry system. Specifically, the activity of each of the naturally occurring radionuclides (Th-232, U-238, and K-40) are determined. These measured activities are then converted into dose rate factors (DRF's) are then calculated for each of the nuclides in these decay chains. These calculated factors are compared to existing data used for typical dating applications.

The gamma spectrometry measurements resulted in a calculation of soil activity that produced results that are consistent with known data. In addition, the spectra produced by the different soil samples are consistent and in reasonable agreement. The calculation of dose rate factors produced results that are within 10% of previously published data for five out of six calculated DRF's. The exception to this is with the K-40 gamma DRF, which varies 14%.

The results of this paper warrant the conclusion that the use of the equipment and techniques used here would be suitable for dose rate determination of soil. Although the error estimation would seem to be high in some instances, it is within the range of previously published data in the field of Radiation Damage Dating.

# TABLE OF CONTENTS

<b>CHAPTER</b>		<b>PAGE</b>
<b>I.</b>	<b>Introduction.....</b>	<b>1</b>
	1.1 Background.....	1
	1.2 Radiation Damage Dating.....	2
	1.3 Techniques Used for Dose Rate Analysis.....	5
	1.4 Objectives of this Thesis.....	7
	1.5 Organization of this Thesis.....	8
<b>II.</b>	<b>Principles of Radiation Damage Dating.....</b>	<b>10</b>
	2.1 Introduction.....	10
	2.2 Thermoluminescence.....	11
	2.2.1 Basic Principles.....	11
	2.2.2 Glow Peak Formation.....	16
	2.2.3 Lifetime.....	19
	2.3 Measurement of Thermolumuniscence.....	22
	2.3.1 Background.....	22
	2.3.2 Sample Preparation.....	22
	2.3.3 Dose Evaluation.....	25
	2.4 Determining Dose Rate.....	31
	2.4.1 Introduction.....	31
	2.4.2 Contribution to Annual Dose.....	31
	2.4.3 Measurement Techniques.....	33
	2.4.4 Disequilibrium.....	34
	2.4.5 Effects of Moisture Attenuation.....	34

2.5 Other Applications.....	35
<b>III. Activity Measurements.....</b>	<b>37</b>
3.1 Introduction.....	37
3.2 Principles of Gamma Ray Spectrometry.....	39
3.2.1 Detector Types.....	39
3.2.2 Gamma Ray Spectra Characteristics.....	40
3.2.3 Gamma Spectrometry System Setup.....	43
3.3 Calibration.....	48
3.3.1 Energy Calibration.....	48
3.3.2 Efficiency Calibration.....	48
3.4 Sample Preparation and Counting.....	56
3.5 Activity Calculations.....	58
3.6 Statistical Analysis.....	59
3.6.1 Energy Resolution.....	62
3.6.2 MCA Emulation Peak Calculations.....	64
3.6.3 Calibration Curve.....	68
<b>IV. Dose Rate Determination.....</b>	<b>69</b>
4.1 Background.....	69
4.2 Dose Rate Calculations Using Dose Rate Factors.....	73
4.2.1 Background.....	73
4.2.2 Dose Rate Factors.....	74
4.3 Calculations in Soil.....	78
<b>V. Results.....</b>	<b>80</b>

5.1 Results of Gamma Spectrometry.....	80
5.1.1 Gamma Spectrum Analysis.....	80
5.1.2 Activity Calculations.....	86
5.1.3 Disequilibrium Determination.....	87
5.2 Dose Rate Calculations.....	91
5.3 Total Calculated Dose Rate.....	95
<b>VI Conclusions and Suggestions.....</b>	<b>98</b>
6.1 Conclusions.....	98
6.2 Suggestions for Future Work.....	99
<b>References.....</b>	<b>100</b>
<b>Appendix .....</b>	<b>104</b>
<b>Vita.....</b>	<b>125</b>

## List of Tables

Table	Page
2-1 Estimate of electron trap lifetimes.....	15
3-1 Gamma rays emitted from Eu-152.....	49
3-2 Peak identification for known sample.....	53
3-3 Results of activity calculations with known samples.....	57
5-1 Soil sample weights.....	81
5-2 Peak identification for soil sample spectra.....	85
5-3 Activity for each soil sample.....	88
5-4 Total activity of soil samples.....	89
5-5 Disequilibrium in uranium decay chain.....	90
5-6 Calculated dose rate factors.....	93
5-7 Dose rate factors listed for each decay chain.....	94
5-8 Comparison of calculated DRF's to published dose conversion factors.....	96
5-9 Total calculated dose rate.....	97



## List of Figures

Figure	Page
2-1 Electron movement in TL material.....	13
2-2 Typical natural glow curve for calcite.....	17
2-3 Typical glow curve for crystals extracted from pottery samples.....	18
2-4 A typical TLD glow curve.....	20
2-5 An example of glow curves from pottery grains.....	27
2-6 An example of the results of the plateau test.....	28
2-7 Illustration of the additive dose method.....	30
3-1 Comparison of HPGe and NaI pulse height spectra.....	38
3-2 Example of the compton continuum.....	42
3-3 HPGe system setup.....	44
3-4 Vertical HPGe detector configuration.....	47
3-5 Spectrum for sample of known activity.....	51
3-6 Efficiency curve generated from known sample.....	55
3-7 Uranium-238 decay chain.....	60
3-8 Thorium-232 decay chain.....	61
3-9 Depiction of detector energy resolution.....	65
5-1 Spectrum for soil sample.....	82

## **List of Abbreviations**

<b>C</b>	<b>Celsius</b>
<b>DCF</b>	<b>Dose Conversion Factors</b>
<b>DRF</b>	<b>Dose Rate Factor</b>
<b>eV</b>	<b>Electron Volt</b>
<b>FWHM</b>	<b>Full Width at Half Maximum</b>
<b>HPGe</b>	<b>High Purity Germanium Detector</b>
<b>keV</b>	<b>Thousand Electron Volts</b>
<b>MeV</b>	<b>Million Electron Volts</b>
<b>MCA</b>	<b>Multi-Channel Analyzer</b>
<b>mL</b>	<b>Milliliter</b>
<b>NaI</b>	<b>Sodium Iodide Detector</b>
<b>RDD</b>	<b>Radiation Damage Dating</b>
<b>ROI</b>	<b>Region of Interest</b>
<b>TL</b>	<b>Thermoluminescence</b>
<b>TLD</b>	<b>Thermoluminescent Dosimeter</b>

# **Chapter 1**

## **Introduction**

### **1.1 Background**

The ability to accurately establish the age of an artifact from an ancient civilization is critical to a thorough understanding of their development. The use of naturally occurring radionuclides to assist in this procedure is a concept that has been used for many years (Mejdahl and Wintle, 1984). The most well known radioactive dating technique is carbon dating, but it is limited to about 50,000 years before the present (Aitken, 1985). A technique that is not as well known is that of Radiation Damage Dating (RDD), which has the ability to date certain artifacts for up to a million years before the present. This technique has been in use for over 35 years, but it is a technique that has refined as technology has progressed. Previous studies have compared RDD to carbon dating, and have found that both yield similar results (Benko, 1989). One area that has changed is in the determination of the background dose rate. In particular the development of solid state scintillation detectors has allowed for a much more accurate determination of the activity levels in soil, and therefore a more accurate dose rate.

In this thesis, soil samples from an archeological excavation, of a burial site near Paducah Kentucky, are used to establish a dose rate estimate for artifacts buried at that location. This site contained pottery sherds buried an estimated 500-600 years ago. Analysis of the samples will be accomplished using gamma spectrometry to determine

activity levels, and then several calculational methods will be applied to determine a dose rate from this data. The results of this paper will provide half of the data required for the establishment of an accurate age estimate for the artifacts in question. The other data required, absorbed dose, will not be dealt with in this paper.

## **1.2 Radiation Damage Dating**

A basic understanding of the thermoluminescent properties of various minerals can be traced back approximately 150 years (Mejdahl and Wintle, 1984). Initial work in this area focused on emission characteristics, which were studied and cataloged by scientists at that time. However, it was not until 1905 that it was realized that thermoluminescence in minerals could be induced by naturally occurring radionuclides (Mejdahl and Wintle, 1984). The advent of the photomultiplier tube in the 1940's made it possible to accurately detect the light pulses emitted from thermoluminescent materials. Then in the 1950's, techniques were developed for measuring exposure to ionizing radiation, stemming from initial work at the University of Wisconsin (Aitken, 1985).

The possibility of using the thermoluminescent properties of minerals to date archeological samples was first discovered by Daniels et al, in 1960 (Aitken, 1985). Further work at the universities of Bern and California first measured the thermoluminescence emitted from ancient pottery. Following these discoveries, several laboratories around the world became interested in developing and using this technique as a routine method of dating certain artifacts. In particular, this technique was proven useful for dating ceramics, bricks, and lithics. In the 1960's, laboratories at Oxford,

Kyoto, Wisconsin, Philadelphia, and in Denmark further developed the technique of thermoluminescence for routine use (Aitken, 1985). Today there are more than 40 laboratories that are involved in the application of thermoluminescence (TL) dating techniques for use in archeology and geology.

The practice of radiation damage dating relies on measurement of the effects of natural ionizing radiation on non-conducting solids (materials where the valence band is not completely filled) over time. When these solids are exposed to ionizing radiation, energy is transferred to electrons in the valence band. When this energy is sufficient, these electrons are promoted from the valence band to the conduction band. Once promoted to the conduction band, the electrons become mobile and move into electron traps in the forbidden band (between the valence and conduction bands). If the charges are trapped at a sufficient depth (greater than 1.5 eV), then these charges will remain trapped for a relatively infinite time period. These trapped charges possess energies that are proportional to the absorbed dose. This dose can be measured using one of three techniques: 1) Thermoluminescence (TL); 2) Optical Spin Resonance (OSR); and 3) Electron Spin Resonance (ESR). This paper will deal only with the thermoluminescent technique.

There are certain artifacts that contain minerals capable of giving of a TL signal, if properly measured this signal can be recovered and an absorbed dose can be determined. The artifacts that can be dated using this technique are those that contain minerals with TL properties, and have been heated by ancient man. The heating, or firing, of the artifact

will zero out the TL material and allow for a relative dose, and therefore an absolute age, to be determined. If the artifact were not fired then the dose absorbed would relate back to geologic times (Mejdahl and Wintle, 1984).

The thermoluminescence that comes from constituent minerals in pottery is due to the effect of exposure to the radiation emitted by the radionuclides in the soil, and in the pottery itself. The radioisotopes that result in this exposure are those in the uranium and thorium decay chains, as well as potassium-40. Due to the long half-lives (1 billion years or more) the radiation flux is constant. If the accurate measurement of the dose rate is possible then an age estimate also becomes a possibility.

As more laboratories began to use and further evaluate this technique, more complexities were disclosed than were originally anticipated. Many of these problems related to extracting the total dose from the quartz in archeological samples. These problems ranged from extraction of quartz from the artifact, to correctly interpreting the TL signal that is measured (Mejdahl and Wintle, 1984). Additional problems were noted relating to the determination of an accurate background dose rate.

Being able to accurately establish the dose rate to which an artifact has been exposed, is critical to the establishment of an accurate date for the artifact in question. It was established that the majority of the absorbed dose that an artifact receives is from naturally occurring radionuclides in the soil, so that the contribution of cosmic radiation is minimal and can be accounted for by using existing data (Aitken, 1985). Because of

this it is only necessary to establish an accurate dose rate received from burial in the soil, in order to accurately date the artifact.

### **1.3 Techniques Used for Dose Rate Analysis**

Several techniques for determining the activity have been developed and used to establish the dose rate. These techniques have included alpha scintillation, fission track analysis, neutron activation analysis, thermoluminescent dosimeters (TLD's), as well as gamma spectrometry (Aitken, 1985). Several of these techniques can be performed in a laboratory, while others are done on site. Being able to take soil samples into the laboratory has the advantage of having conditions for counting that are easily reproducible, and also allows experimental conditions to be more easily controlled. In this situation long counting periods are not hard to obtain, making counting statistics more reliable.

In the beginning it was thought that alpha radiation played an important role in producing TL in naturally occurring minerals. Because the lower efficiency of alpha radiation was not known at this time, emphasis was placed on measuring the alpha activity (Mejdahl and Wintle, 1984). The alpha activity was determined at that time using scintillation techniques that are very similar to those used today. Although the contribution of alpha radiation was later proven to be minimal, alpha scintillation is still used by some institutions to establish the uranium and thorium concentrations in the soil.

Both the fission track analysis and neutron activation analysis methods for analyzing uranium and thorium concentrations in soil have been used with some success (Crawford, 1980). However, both techniques require access to a reactor, which is not possible in most facilities. Due to this limitation, these techniques remain rather rare and not practical for most dating applications (Mejdahl and Wintle, 1984).

Another method, probably the most common method, is to place TLD's in the ground at the site of the excavation. This method can be used to calculate both the gamma and beta dose rates from the soil (Mejdahl and Wintle, 1984). These techniques have been proven to work fairly well but have several disadvantages. The biggest disadvantage is that the TLD's need to be left in the ground for periods of time varying from several weeks to several months. This obviously creates problems with ensuring that the site of the reading remains undisturbed, as well as a possible delay in obtaining a dose rate estimate. Also, there are errors inherent in the TLD's themselves. These include fading and individual variations in the makeup of each TLD. In addition, the source of the dose (alpha, beta, or gamma radiation) cannot be determined. This method does have the advantage of being able to measure dose rate directly, rather than measuring radionuclide activity levels and converting them into a dose rate, as with other methods.

The use of various types of gamma spectrometers is an area that has shown a lot of promise, but has been used infrequently until recently. This was due in part to the fact that most of the early scintillation counters were sodium iodide detectors that lacked the necessary resolution for accurate dose rate estimates (Aitken, 1985). The advent of High



Purity Germanium ( HPGe ) detectors have resulted in much improved resolution, which allows for accurate gamma ray spectrometry (ICRU #53, 1994). These techniques can be done on site or in the laboratory, however, most HPGe detectors are not portable so any on site measurements have usually been done with a sodium iodide detector.

When measurement techniques are employed that measure soil activity level, then there must be a conversion to dose rate. This is accomplished by employing calculational methods to approximate the dose that the artifact will receive when buried. These calculations can be done by using dose rate factors, which have been experimentally determined (Till and Meyer, 1983), or by using a computer-based model, such as a Monte Carlo code.

#### **1.4 Objectives of This Thesis**

The main objective of this thesis is to establish a reproducible technique for determining the dose delivered to an artifact buried in soil, to facilitate the dating of these artifacts. In addition, it is hoped that this technique will prove to be able to be accomplished using the existing equipment currently available in the Nuclear Engineering department at UTK. Being able to use this equipment would allow for the accurate calculation of soil activity without having to go to the site of the excavation. The ability to be able to reproduce this technique at UTK could allow for the routine dating of artifacts and eventually lead to further research opportunities in this field.

The calculation of the dose rate from the measured activity is examined using dose rate factors. These results are then compared with the dose conversion currently used in the field of RDD. This is done in order to verify the use of these dose rate factors, and to check the existing factors for agreement.

### **1.5 Organization of This Thesis**

This thesis is organized into five parts; Introduction, Theory of Radiation Damage Dating, Activity Measurements, Dose Rate Calculations, Results and a Conclusion. Chapter II contains the theory behind the Radiation Damage Dating technique. This includes background information on the principles of thermoluminescence as well as specific information on the theory of the RDD procedure.

Chapter III deals with the activity measurements taken with the HPGe system. The setup of the detector and of the entire counting system is covered. In addition, the method for calibration of the detection system is covered along with the sample preparation and the counting geometry.

In chapter IV the method for performing dose rate calculations are detailed. In particular the assumptions associated with the calculations for each type of radiation (alpha, beta, and gamma) are defined. Also the calculation of the Dose Rate Factors for each nuclide are documented.

| In chapter V the results of the activity measurements and dose rate estimates are detailed. The calculations for the activity as well as the counting statistics are included, as well as the dose rate contribution of all individual radionuclides.

Finally, chapter VI contains the conclusions and suggestions for future research and work to improve the results and processes covered in this thesis.

## **Chapter 2**

### **Principles of Radiation Damage Dating**

#### **2.1 Introduction**

The ability to be able to accurately extract the absorbed dose from an artifact requires a working knowledge of the principals behind Radiation Damage Dating (RDD), as well as an understanding of the techniques used, to get the most accurate estimate of the artifacts date that is possible. There are two requirements for establishing an accurate date, a dose rate estimate and a dose estimate. The steps required for estimating the dose fall into two categories: extraction of crystal material, and measurement of the dose from the crystal extracted. Obtaining an accurate dose rate estimate requires a measurement of the dose rate in the soil at the site of excavation.

There are two techniques for extracting quartz crystals from pottery, the quartz extraction technique, and the fine grain technique (Mejdahl and Wintle, 1984). Once the quartz crystals are extracted from the pottery, the dose must be extracted using a thermoluminescent measurement system. And finally the data, glow curves, must be interpreted correctly in order for an accurate dose to be determined. To be able to interpret and use this data effectively a working knowledge of the principles of thermoluminescence is required.

There are many techniques used to obtain dose rate estimates, the method used depends on several factors including cost, time considerations, access to excavation site, and

equipment availability. These techniques, as mentioned in chapter 1, are diverse but have the same goal. That goal is simply to determine the dose rate to which the artifact in question has been exposed. In making this dose rate determination several problems must be addressed in order to obtain meaningful results. These problems include disequilibrium in the decay chain, and the effects of moisture attenuation.

## **2.2 Thermoluminescence**

### **2.2.1 Basic Principles**

Thermoluminescence is the basic principle behind the TL dating technique. Thermoluminescent materials are those capable of storing energy absorbed from ionizing radiation, and then emitting light pulses when heated. These light pulses can then be counted using a photomultiplier tube, and the absorbed dose determined. This is the same principle commonly used in the field of health physics for personnel dosimetry.

The basics of the thermoluminescent process are; a) ionization of electrons by ionizing radiation, b) capture of electrons in traps where they remain until the temperature is raised sufficiently to release the electrons, and c) heating causes eviction from the traps, at a temperature characteristic of the trap. And finally, d) some of these electrons recombine and in the process emit light, the amount of which is proportional to the number of trapped electrons, which is in turn proportional to the amount of nuclear radiation to which the crystal has been exposed (Knoll, 1989).

Specifically, thermoluminescent materials are a class of inorganic crystals that contain enough impurities to allow electrons to be trapped (Knoll, 1989). Because the thermoluminescence of a crystal is dependent upon even minute impurity levels, as well as the thermal history of the material, details about the mechanism of thermoluminescence are important. However, details about thermoluminescent properties are only known for crystals that are grown in the laboratory under strict controls. Because of this, each sample should be calibrated to account for individual sensitivities. It is impractical to try to recalibrate each crystal sample, in addition to introducing other sources of error, so certain assumptions must be made. The specifics of this process are discussed in section 2.3.3, but it is important to note that these procedures are needed due to the different impurity levels.

When exposed to ionizing radiation the electrons will detach from their parent nuclei, allowing the electrons to migrate from the valence band to the conduction band then fall into electron traps in the forbidden band as illustrated in Figure 2-1 (Knoll, 1989). An electron will remain in the trap until it is 'shaken out' by vibrations in the crystal lattice, caused by heating. Several things can happen to an electron once it is shaken out of a trap. It can be re-trapped in a different electron trap, where it can be shaken out again, or to a deeper trap where it is better shielded from being shaken out. If evicted from an electron trap, and not re-trapped, then it will recombine with an ion from which an

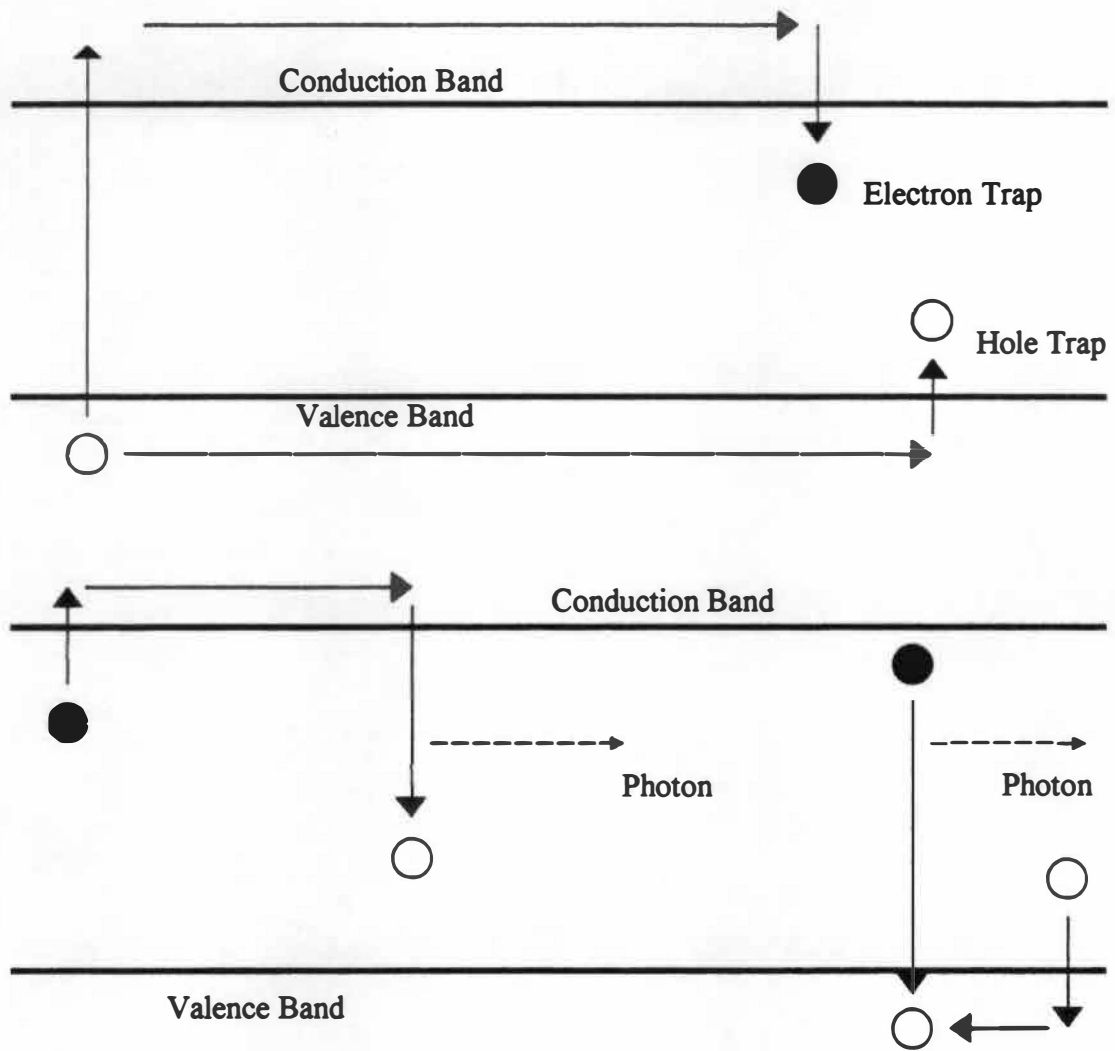


**Figure 2-1.** Electron movement in TL material. The top diagram shows the formation of an electron-hole pair in TL material. The bottom diagram shows the two possible modes of recombination , where a rise in temperature leads to the emission of photons. (From Knoll, 1989)

electron has previously been detached. This recombination can be radiative (with emission of light) or non-radiative (no light emission). If the recombination is radiative it results in thermoluminescence, and the color of the emitted light is characteristic of the impurities in the crystal lattice (Aitken, 1985). These electron traps are located at different energy levels within the forbidden band, with those furthest from the conduction band being the deepest. Some traps are so shallow that they are susceptible to having electrons escape at lower temperatures than desired, or escaping due to exposure to visible light (optical bleaching).

Because of the movement of electrons in the lattice of the crystal, the lifetime of an electron in a trap is considered to be finite. Even at low temperatures, as low as room temperature, there is some probability of escape (Knoll, 1989). The probability may be so slight that the lifetime of the electron is measured in millions of years. Traps such as these are referred to as 'deep' traps. In these traps the temperature required for rapid eviction is high, usually above 400 degrees Celsius. In any given crystal there are many different traps, each with a characteristic temperature. For purposes of dating we are interested only in traps that have lifetimes upward of 1000 years, this usually corresponds to glow curve temperatures of 250 degrees Celsius or higher (Aitken, 1985). As seen in Table 2-1 shallow traps, with glow curve temperatures below 100 degrees Celsius, lifetimes are so short (in hours), that there is no measurable glow curve. Because of the variety of minerals in pottery, each with a number of traps, the individual glow peaks merge together and the glow curve becomes continuous.



**Table 2-1.** Estimate of electron trap lifetimes. Shown in comparison with various glow curve temperatures (From Aitken, 1985)

<b>Peak Temperatures</b>	<b>100 degrees C</b>	<b>200 degrees C</b>	<b>300 degrees C</b>	<b>400 degrees C</b>	<b>500 degrees C</b>
<b>Lifetime for burial at 10 degrees C</b>	<b>2 hours</b>	<b>10 years</b>	<b>600,000 years</b>	<b>30 billion years</b>	<b>2 x 10<sup>15</sup> years</b>
<b>Lifetime for burial at 20 degrees C</b>	<b>.5 hours</b>	<b>2 years</b>	<b>70,000 years</b>	<b>3 billion years</b>	<b>1 x 10<sup>14</sup> years</b>

### 2.2.2 Glow Peak Formation

The probability of escape from a trap rises with the temperature. A typical natural glow curve for calcite is depicted in Figure 2-2. As the temperature is raised the thermoluminescent intensity rises to a maximum and then rapidly decreases to near zero as the traps at that depth empty. The temperature that corresponds to this glow curve peak is frequently referred to as the peak temperature. With the variety of minerals that are in pottery samples, glow curves tend to be broader than those containing a single mineral. This is due to the fact that multiple curves are forming a broader composite glow curve. A typical glow curve seen in pottery is shown in Figure 2-3. In order to obtain glow curves from pottery the samples are heated at a constant rate to about 500 degrees C. Above this temperature, problems occur with incandescence of the sample and the heating plate. Because of this the curve does not return to a baseline level, or zero, prior to reaching the 500 degree C temperature.

The probability of escape from a trap (per second) can be described by the expression:

$$\lambda = s \exp(-E / kT) \quad (2.1)$$

where:

$s$  = the frequency factor (escape frequency,  $\text{sec}^{-1}$ )

$E$  = trap depth (eV)

$k$  = Boltzmann's constant =  $1.38054 \times 10^{-16}$  erg/K

$T$  = absolute temperature (K)

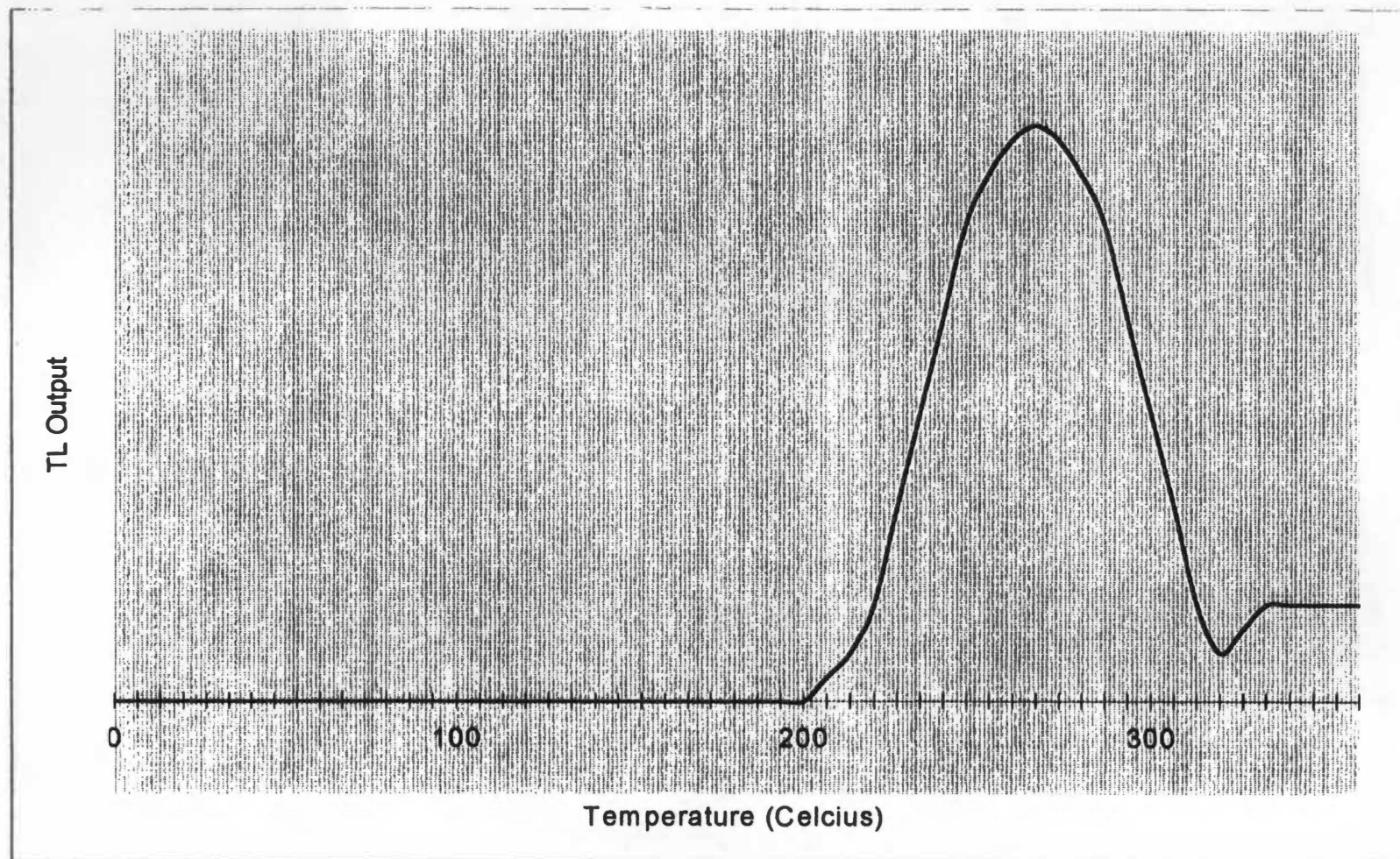


**Figure 2-2.** Typical natural glow curve for calcite (From Mejdahl and Wintle, 1984)

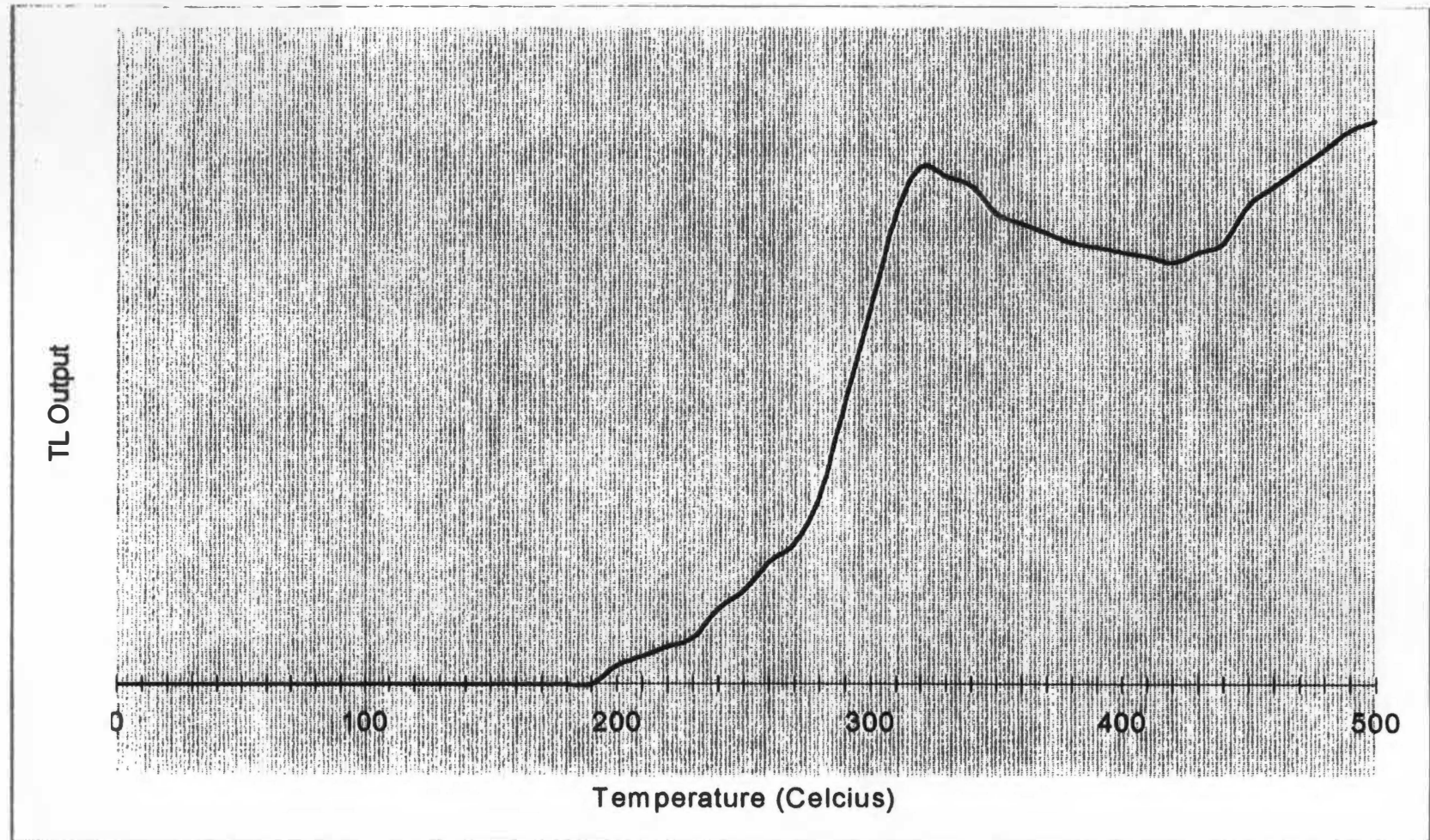


**Figure 2-3.** Typical glow curve for crystals extracted from pottery samples. (Mejdahl and Wintle, 1984)

Glow curves generated by the minerals in pottery are much broader than those seen with TLD's. As mentioned above, glow curves from pottery samples are broad and poorly defined. As seen in Figure 2-4, a lithium fluoride TLD produces a glow curve with much sharper peaks.

### 2.2.3 Lifetime

A concern in the practice of radiation damage dating is what percentage of electrons may have escaped during the period of burial. Because of this it is necessary to determine whether or not the number of escaping electrons are high enough to affect the estimated dose. For a sample held at a constant temperature the probability of escape multiplied by the number remaining trapped will give the rate at which electrons escape. This can be illustrated by (Aitken, 1985):

$$-dn / dt = \lambda n \quad (2.2)$$

where:

$\lambda$  = The probability of escape

$n$  = number of electrons remaining trapped at time  $t$

From this it follows that the number of trapped electrons decays with time according to:

$$n = n_0 \exp(-\lambda T) \quad (2.3)$$

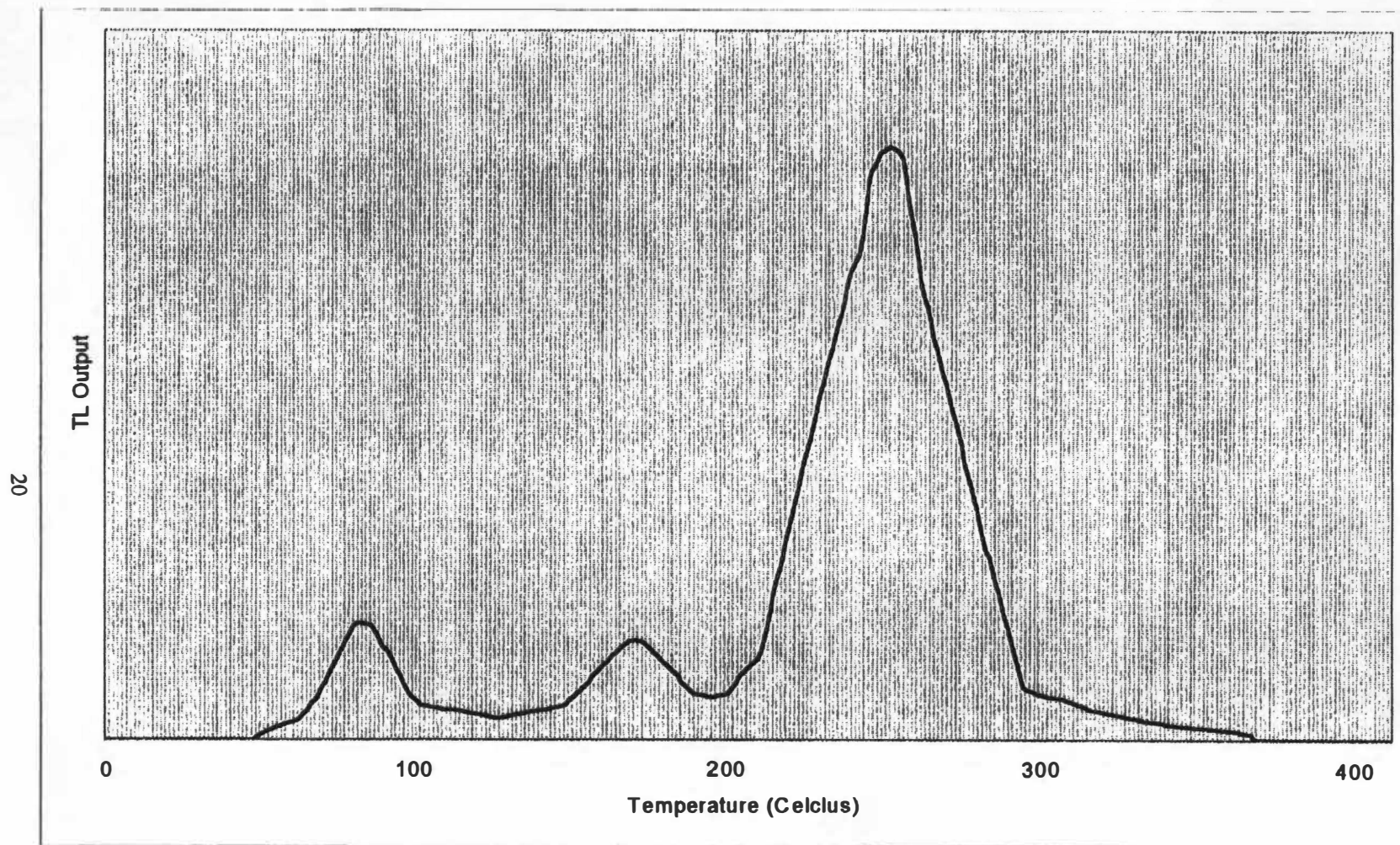


**Figure 2-4.** A typical TLD glow curve. (Turner, 1992)



where:

$$n_0 = n \text{ at } T = 0$$

For exponential decay of this nature it can be said that there is a lifetime, or average residence time in a given trap. For electrons this can be illustrated by:

$$\tau = \lambda^{-1} = s^{-1} \exp(E / kT) \quad (2.4)$$

Equation 2.3 can be rewritten as:

$$n = n_0 \exp(-T / \tau) \quad (2.5)$$

The equation above is defined in terms of lifetime of electrons in the trap, at time  $t = 0$ . When dating pottery there are initially no trapped electrons, and they become trapped at a uniform rate after that point. The fractional loss of thermoluminescence depends upon the burial time and the temperatures that the artifact is exposed to when buried. Several simple formulas have been developed to estimate the percentage of electrons lost over the lifetime of a given sample. If you want no more than a 5% loss, then the lifetime must be at least 10 times the age of the sample. On the other hand if you can tolerate a 10% loss, then 5 times the age is sufficient (Aitken, 1985).

## **2.3 Measurement of Thermoluminescence**

### **2.3.1 Background**

The measurement of the thermoluminescence in the crystals extracted from the pottery is accomplished by using a standard TLD reader. The temperature setting is usually set to increase to about 500 degrees Celsius, which is sufficient to release all electron traps. The use of nitrogen is required to inhibit spurious thermoluminescence, this is especially important in dating because the spurious signals generated can cause a large overestimation of the date for the artifact in question.

Although the basic concept of dose measurement is fairly straightforward, there are several important steps that must be accomplished in order to obtain a meaningful dose. The first step is to extract the crystal from the pottery using either the quartz inclusion or fine grain technique. The second step is to properly evaluate the measured glow curve to obtain a useful dose estimate.

### **2.3.2 Sample Preparation**

One technique of sample preparation for pottery dating is a method known as the quartz inclusion technique (Mejdahl and Wintle, 1984). The basic concept of this technique is that by etching away the outer layer of the crystal you can obtain a sample that has not been penetrated by alpha particles (which have a maximum range of .05 mm). This leaves a sample whose accumulated dose is obtained solely from beta, gamma, and cosmic radiation.



The sample preparation begins by removing a 2 mm layer from the artifact by sawing with a diamond impregnated wheel (Aitken, 1985). The remaining part of the sample is then crushed, usually with a vise. This outer layer is removed because the beta dosage in this outer layer is transitional, by this it is meant that the dosage falls between that in the soil and that in the pottery itself. In addition this technique removes any part of the pottery that may have had reduced level of thermoluminescence due to exposure to sunlight. And finally the removal of the outer layer eliminates any possibility of soil contamination of the sample.

After the sample is crushed it is further reduced using a pestle and mortar. During this process care is taken to avoid crushing the large quartz grains, because the goal is to obtain quartz grains of 90-120 microns (Aitken, 1985). Several techniques are then employed to separate the quartz grains from the rubble. First of all, the sample is sieved to separate grains of the desired size. Then a technique known as magnetic separation is employed to separate the crystalline grains ( non-magnetic) from the clay matrix (slightly magnetic). Finally, calcite grains are removed from the crystalline fraction with dilute hydrochloric acid, and feldspar with concentrated hydrochloric acid. In this last step leaving the crystal in the acid for a sufficient amount of time will sufficiently etch the crystal, as discussed above. All of the above steps are carried out under red light to avoid bleaching effects.

The fine grain technique is a second method of extracting the quartz crystals from the clay matrix (Aitken, 1985). This technique has two requirements. The first is that the

grains must be small enough for full penetration by alpha particles, so they get a dosage corresponding to the radioactivity of the clay matrix. For this to work the grains must be true fine grains, not crushed larger grains. The second requirement is that the grains be obtained in a thin layer suitable for measuring alpha particle dose contribution.

Sample preparation begins as with the quartz inclusion technique, by crushing the pottery sample in a vice. After crushing, the products are washed in acetone, and the different grain sizes are separated. This is accomplished by taking advantage of the different settling times for different grain sizes. Once the grain sizes are separated they then are re-suspended and allowed to deposit on a planchet in a layer of no more than a few microns thick. This planchet is then placed in the TLD reader for the slow measurement and accumulated dose determination. Following this preparation technique allows for the measurement of the thermoluminescent effectiveness of the alpha particles. By taking these prepared samples and performing the additive dose method, an equivalent alpha dose can be calculated. That is the alpha dose at which the measured rate of natural thermoluminescence can be duplicated.

In order to apply this fine grain technique an accurate alpha dose rate must be determined. This will not be discussed in detail in this paper. Obtaining an accurate alpha dose is not easy and is not a commonly used technique. It is brought up in this context only to note that it is a technique used in some laboratories.

### 2.3.3 Dose Evaluation

Once a sample is prepared the thermoluminescence can be measured using a TLD reading system. However, in order for the measured absorbed dose to be properly evaluated, several steps are required. First, in order to establish an area of stability in the glow curve, a test called the plateau test is used (Mejdahl and Wintle, 1984). In addition, some of the crystals are incrementally irradiated by a calibrated artificial source and compared with crystals exposed only to the natural background radiation. This test is known as the additive dose test and it is used for an accurate determination of the accumulated dose (Mejdahl, 1984).

The first step in evaluating glow curves is to perform the plateau test, which can show when an area of stability, in the glow curve, has been reached. As discussed earlier, shallow traps have short lifetimes and are subject to the loss of electrons during the time that the artifact is buried. For the purposes of establishing an accurate date, the only traps that are of interest are those not subject to leakage. This usually means that only traps that occur above 300 degrees Celsius are of interest.

It is important to not only be aware of the importance of this area of stability, but also to be able to make an accurate determination of where the stable region begins. This is where the plateau test is of vital importance (Mejdahl, 1984). This is accomplished by taking a sample that has not been exposed to any artificial radiation, and comparing it to a

sample that has been exposed to an artificial source as well as to the natural radiation. By comparing these two glow curves, illustrated in Figure 2-5, and obtaining a ratio, natural radiation divided by the natural plus artificial radiation, a plateau will be evident when the traps become deep enough so that there has been negligible leakage. To successfully accomplish the artificial irradiation needed, a calibrated radioactive source is required. The most common isotope used for this application is strontium-90 (Mejdahl and Wintle, 1984), although there are several different techniques used to deliver the dose required. The results of this test can be seen visually in Figure 2-6. From this test, it can be assumed that the part of the glow curve under the plateau has had a negligible leakage of electrons. One purpose of this test is to assure that only the dose received since initial firing by ancient man is measured. More importantly, it ensures that there hasn't been a significant loss of trapped charge due to anomalous fading.

Trapped charge stability cannot be assumed without performing this test. It would seem that an assumption could be made that the part of the curve above a certain temperature would be adequate for obtaining a dose. There are several problems with making this assumption, the first being that anomalous fading does not show up (Aitken, 1985). Anomalous fading occurs in some minerals, and the plateau test is considered a minimum requirement for identifying this problem. Another reason that the plateau test is necessary is to check to see if ancient man did an adequate job of firing the artifact. If incompletely fired, electrons would remain in the deeper traps after firing, and there would be no identifiable plateau. A third problem that the plateau test can identify is that of spurious thermoluminescence in the natural glow curve. Just as in the case of a poorly fired

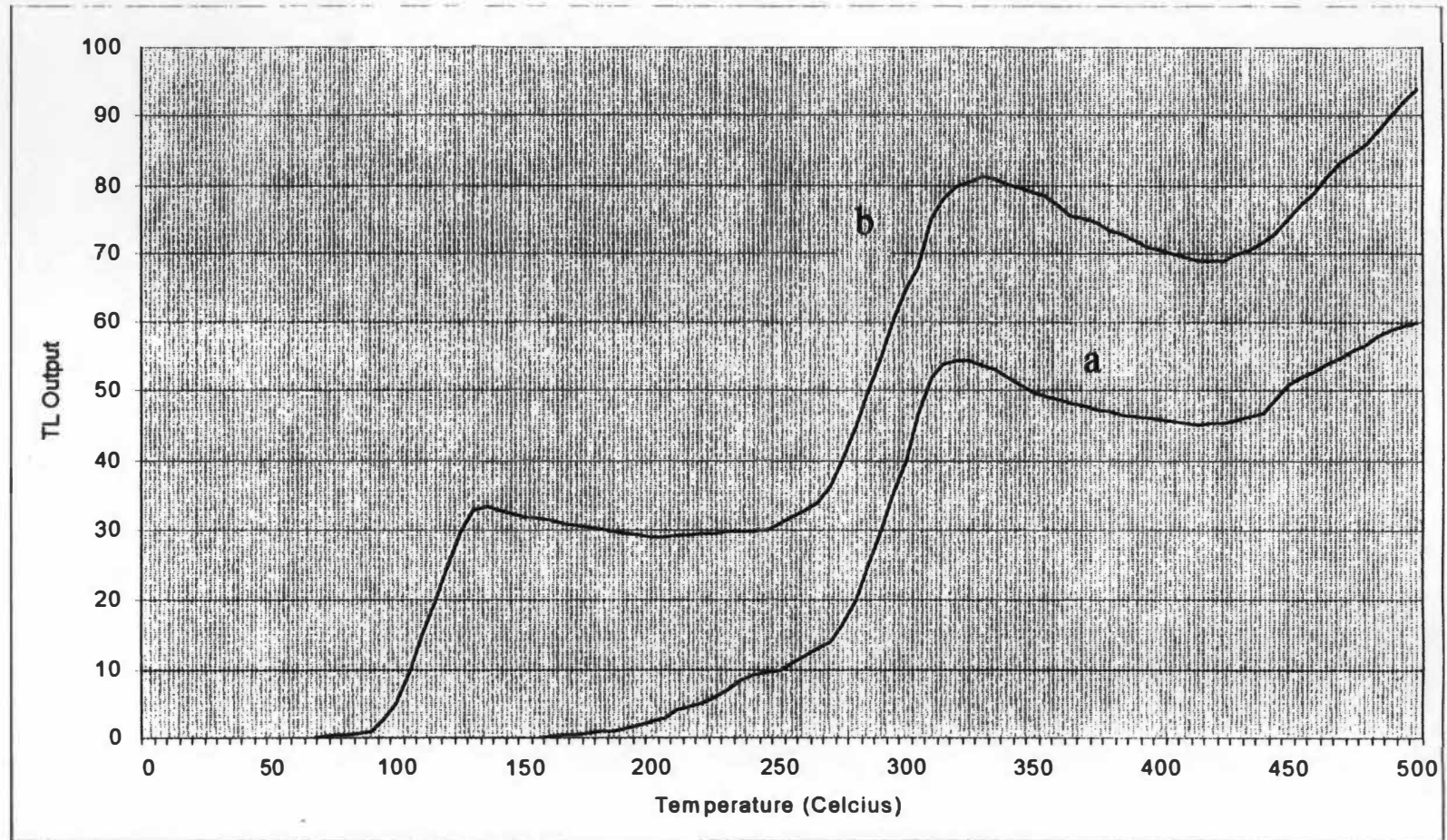


**Figure 2-5.** An example of glow curves from pottery grains; a) from natural TL, and b) natural TL plus additional TL induced by artificial irradiation (Mejdahl and Wintle, 1984)

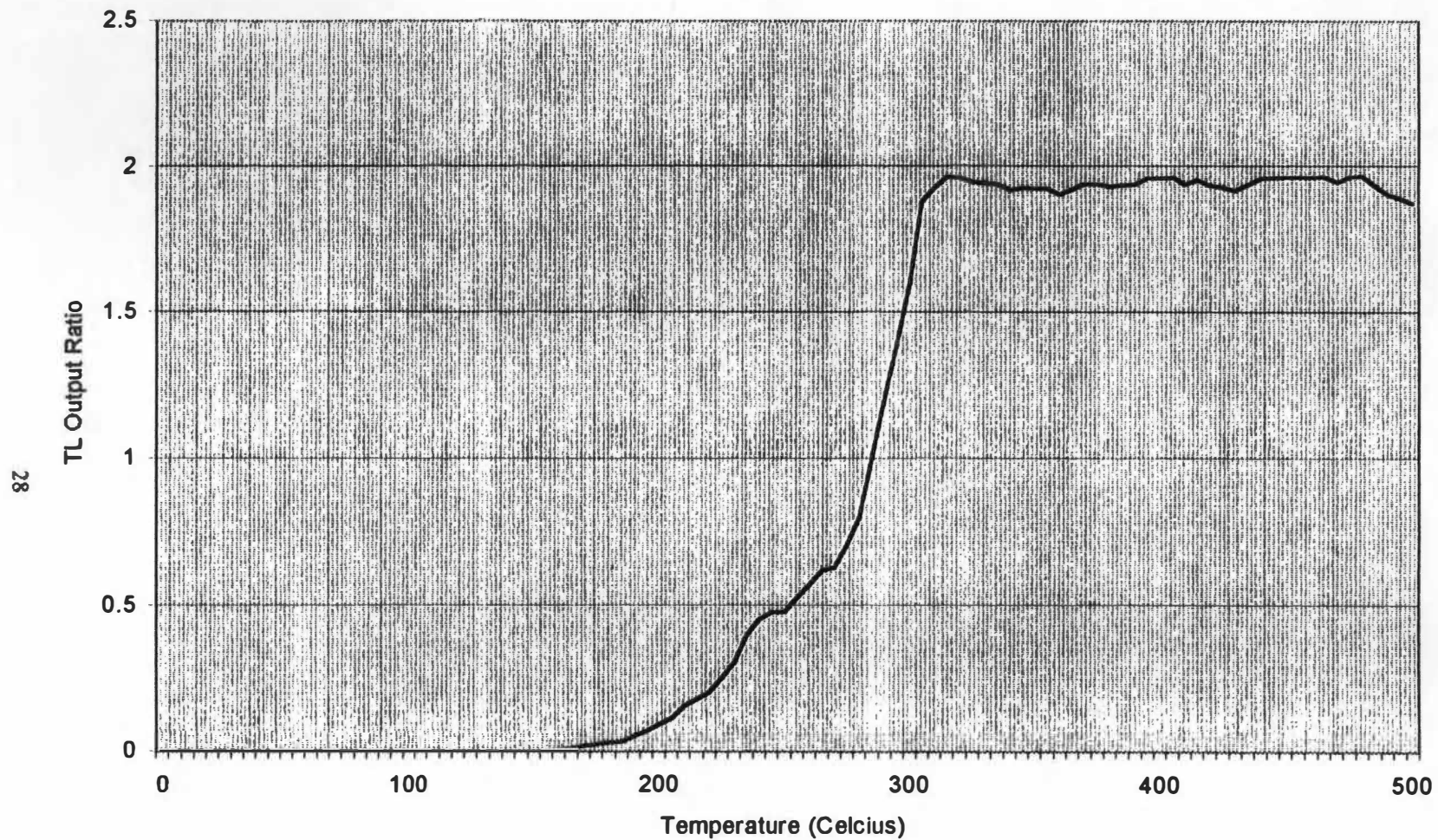


**Figure 2-6.** An example of the results of the plateau test. This shows the area of TL storage stability. (Mejdahl and Wintle, 1984)

artifact, this causes the ratio to rise as temperature increases. And finally, this test can point out any contamination of the sample with a thermoluminescent sensitive mineral during sample preparation. In this case the plateau would be destroyed due to the fact that the contaminant is unlikely to have the same thermoluminescent characteristics as the sample.

Once the sample has been extracted it is a fairly straightforward process to compare the natural thermoluminescence from the quartz to that induced by a known dosage in the same crystals. This procedure requires annealing the quartz and/or re-heating for another reading to be taken. This heating changes the thermoluminescent sensitivity of any minerals, and consequently this method provides only an approximate dose. Because of this a method called the additive dose method was developed to avoid this problem (Aitken, 1985).

The additive dose method requires measurements to be made on a number of weighed portions of quartz grains. Readings are taken with crystals exposed only to the natural dose, and then readings are taken with other crystals with natural plus artificial doses. After these doses are normalized for the sample weight, they are plotted as shown in Figure 2-7. By plotting the dose in this way you can obtain an estimate of the paleodose, denoted by  $Q$ . This is not entirely accurate in that it does not account for the supralinearity effect. To account for this supralinearity, and correct for it, portions of the sample must be irradiated after being annealed, in order to determine this value experimentally.



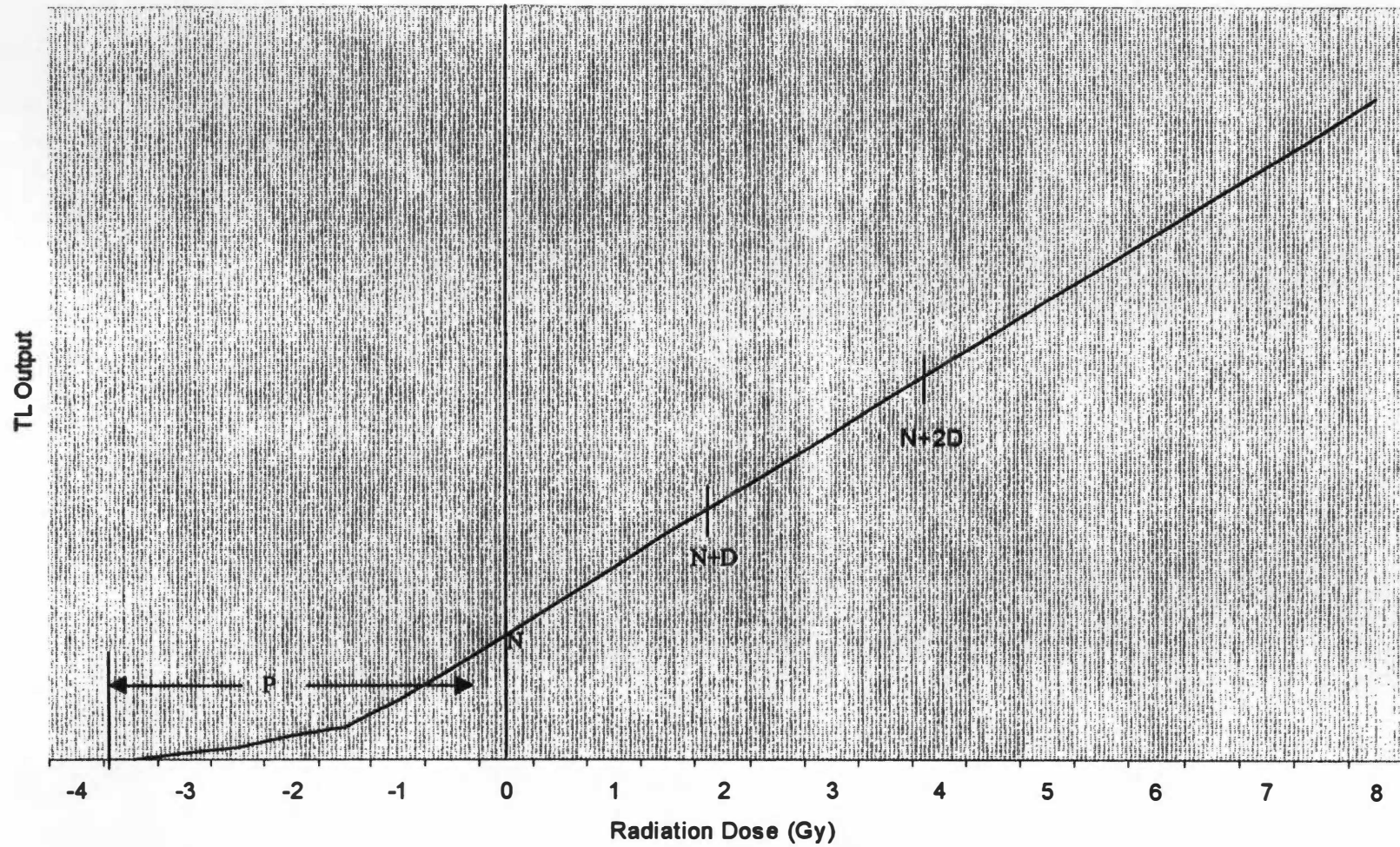


**Figure 2-7.** Illustration of the additive dose method. This is used to determine paleodose (P) (Mejdahl and Wintle, 1984)



## **2.4 Determining Dose Rates**

### **2.4.1 Introduction**

There are several steps that must be undertaken in order to establish a dose rate estimate. First, the source of the dose to the artifact must be understood. This will be a combination of dose from soil, dose from the clay in the artifact (in the case of pottery), and dose from cosmic radiation. Second of all, an understanding of the composition of the radiation sources must be defined. And finally, a measurement technique must be employed to determine the dose rate from these sources.

When taking measurements, in particular soil measurements, an understanding of the radionuclides that are involved is required. In addition, when taking soil measurements the problems of disequilibrium and the effect of moisture content must be accounted for.

### **2.4.2 Contribution to Annual Dose**

The major contributions to the annual dose rate in the environment are made from radionuclides in the Uranium and Thorium decay chains, as well as from potassium. In addition, there are small contributions from cosmic radiation and from rubidium. Because of the much higher proportional contribution of potassium, uranium and thorium these are the most critical values in determining an accurate background dose rate (Mejdahl and Wintle, 1984).

The contribution to the dose of an artifact is from alpha, beta, and gamma radiation in these decay chains. However, the use of separation techniques for extracting the crystal

lattice from pottery samples can be used to eliminate the contribution of alpha particles from the dose. This is helpful in simplifying the calculation of dose rates, as only the beta and gamma contributions to the dose rate need to be estimated. The contribution of rubidium normally either ignored or assumed due to the minimal contribution to the overall dose (Mejdahl and Wintle, 1984).

The contribution of cosmic radiation is normally assumed, due to the availability of consistent measured data and its relatively small contribution to the total dose. For typical pottery dating, cosmic radiation contributes about 5-6% of the total dose (Aitken, 1985). Both the altitude and the latitude of the burial site affect the dose. Only the hard component of cosmic radiation will reach the artifact due the depth of burial. Additionally, it can be assumed that the majority of the cosmic dose is received while the artifact is buried, as compared with any dose received prior to burial (Aitken, 1985).

In dealing with pottery samples, there is an internal dose from radionuclides in the clay. In the case of gamma radiation this is not a factor, the gamma dose will originate from the soil unless the sample is very large. This is due to the range of gamma radiation in soil, about 0.3 meters (Aitken, 1985). For alpha radiation all of the absorbed dose can come from nuclides in the pottery, but this factor can be eliminated by use of the quartz inclusion technique. It is in the case of beta radiation that this internal dose can effect the dose rate estimate. If it is suspected that the content of the clay varies from the soil, then the activity of the clay can be measured separately (Mejdahl and Wintle, 1984). In order to isolate the internal beta emitters from those in soil then the outer 1-2 mm of the sample

must be removed before measuring the dose (Mejdahl and Wintle, 1984). This ensures that the entire beta dose originates from the pottery itself.

### **2.4.3 Measurement Techniques**

As discussed briefly in the introduction, there are several techniques for measuring the activity level in soil. These techniques have evolved as different technologies have grown over time. Measurements can be taken in the laboratory or on site, and dose rate can be measured directly or can be calculated from activity measurements.

The use of TLD's, buried at the archeological site, would appear at first glance to be the most effective technique possible, because it measures dose directly and in the actual geometry of the sample. This technique runs into problems because of the burial duration, and with the composition of the TL phosphor that is used. In fact, it has been determined that this technique has no accuracy advantage over other known techniques. This is due to the fact that TLD's are not made up of exactly the same material as crystals in pottery, in fact their TL characteristics are very different (Aitken, 1985).

Recently, the use of gamma spectrometry has been explored for use in determining background activity. The advent of HPGe detectors has allowed for easier and more accurate activity determinations (Guibert, 1991). This will be explored in detail in chapter three.

#### **2.4.4 Disequilibrium**

Disequilibrium in the Thorium and Uranium decay chains must be accounted for when performing dose calculations. If activity estimates are based on nuclides occurring at a later point in either decay chain, then the dose rate could be underestimated.

Disequilibrium occurs when either radon escapes or there is leaching of some of the parent nuclides (Guibert, 1994). This creates a situation where the concentration of radionuclides later in the decay chain is not equivalent to those that occur earlier. This effect is felt most prominently in the uranium chain, effecting the estimate of beta dose from uranium.

To account for this, an effort must be made to measure nuclide concentration both early and later in the decay chain. If this difference can be measured, then the most accurate results can be obtained. If this is not possible the effects of radon escape, or leaching, can be estimated. Typically the beta dose from uranium constitutes about 15% of the total dose in typical pottery dating. So if radon were to completely escape during burial the error would be about 7%, resulting in an underestimate of age (Mejdahl and Wintle, 1984). The thorium-232 decay chain disequilibrium is much easier to measure, but it can be assumed to have no significant loss if measurement is not possible.

#### **2.4.5 Effects of Moisture Content**

Moisture content in soil has the effect of attenuating the emitted beta radiation, and can effect the overall measured dose. If counts are obtained using a dry sample, then a correction factor must be used to account for this effect. This correction factor can be

determined via measurement or by using published data. Correction factors for pottery are typically around 20% (Aitken, 1985).

Additionally, the average water content of the soil must be estimated. This can be obtained from environmental information such as annual rainfall or ground water level. Most published data indicates that an almost complete saturation level exists for pottery buried in temperate regions at depths exceeding 30 cm (Mejdahl and Wintle, 1984). If no data exists, then a 50-50 saturation to dry level ratio can be assumed (Mejdahl and Wintle, 1984).

## **2.5 Other Applications**

In addition to using this technique for the dating of pottery samples, there are several other materials that can be dated. Many of these can occur outside the 40,000 – 50,000 year limit of carbon dating. Other materials that this technique has been applied to include burnt flint, burnt stones, and volcanic lava (Aitken, 1985). As is the case with the dating of pottery samples care must be taken to insure that the object was properly heated in order to zero out the electron traps. The sample preparation in these cases is basically the same as for pottery with some minor exceptions.

These applications enable, for example, artifacts left by ancient man in the paleolithic period (3.5 – 12 million years before present) to be dated. This predates use of pottery, but flint was commonly used for weapons and tools. In the case of volcanic lava, this

technique has been used to pinpoint the date of volcanic eruptions. In this instance the eruption of the volcano would have zeroed the electron traps.

## **Chapter 3**

### **Activity Measurements**

#### **3.1 Introduction**

The activity of the soil samples are determined using a High Purity Germanium (HPGe) gamma spectrometry system. The germanium detector was chosen because it provides the energy resolution necessary for quantifying environmental samples. This enables the accurate identification of the various energy peaks associated with the gamma spectrum emitted from soil samples. This represents a vast improvement over sodium iodide detectors, whose resolution is not adequate for this application. Because of the lower resolution sodium iodide detectors can have multiple energies hidden in one large peak, but with the germanium detector these peaks can be separated. In being able to analyze soil samples accurately, the ability to separate peaks that are close in energy is critical. An example of this can be seen in Figure 3-1, where the sodium iodide detector shows one large peak, when in fact several peaks are present.

However, there is lower counting efficiency with germanium detectors as compared with sodium iodide, which leads to smaller amplitude peaks (Knoll, 1989). The need for improved resolution for soil analysis overrides this loss of efficiency. Because of this improved resolution, it is now considered common practice to analyze environmental samples using germanium detectors.

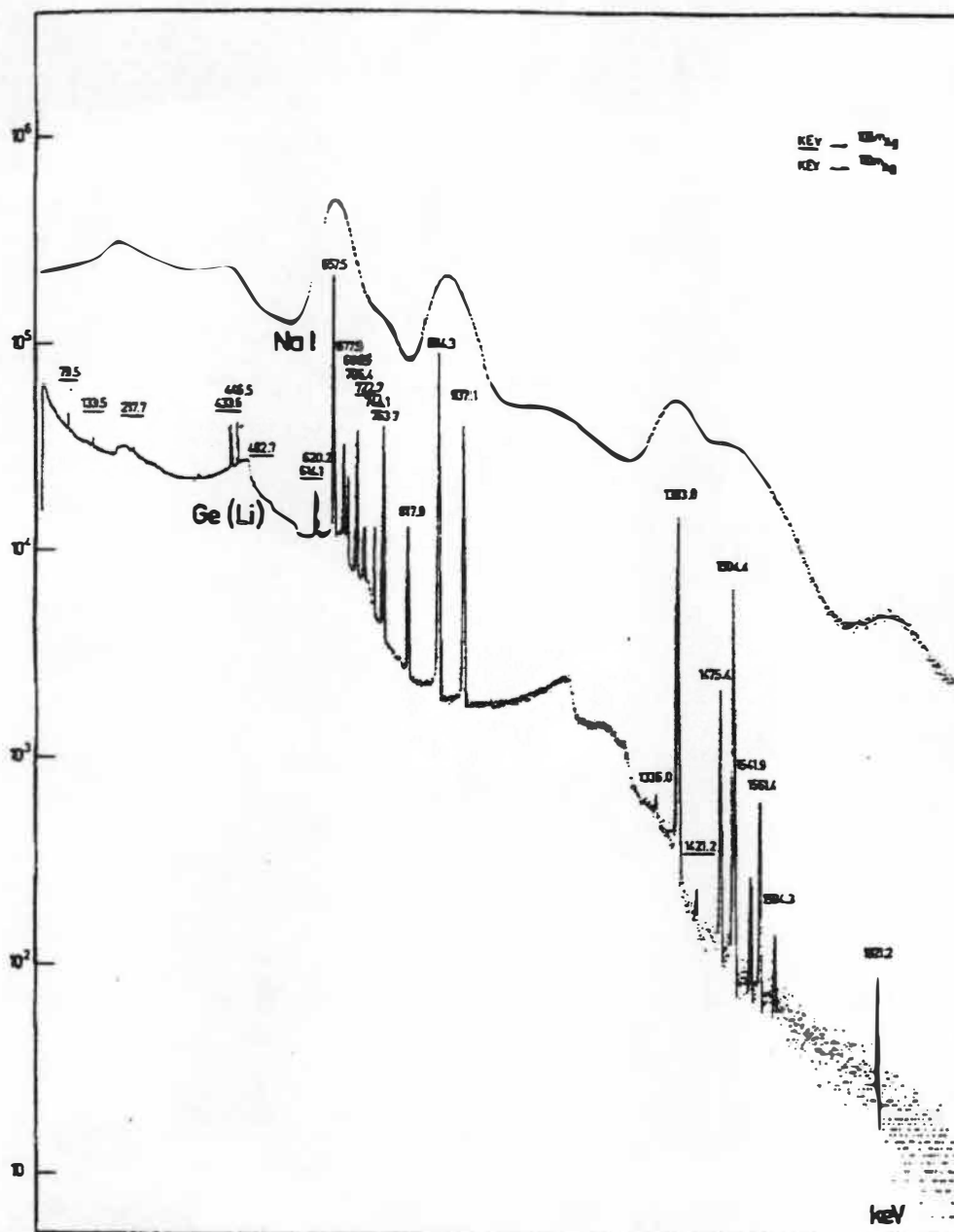


Figure 3-1. Comparison of HPGe and NaI pulse height spectra. Energy in keV (Knoll,1989)



By separating and identifying the peaks in the gamma spectrum then the different nuclides can be identified to allow for quantification of each nuclide in the uranium, thorium, and potassium decay chains. This is critical for identifying key gamma rays throughout the energy spectrum, which is critical for establishing the activity of the sample and identifying potential problems with disequilibrium in the decay chains.

### **3.2 Principles of Gamma Ray Spectrometry**

#### **3.2.1 Detector Types**

The only two types of detectors suitable for measuring gamma ray energies above several hundred keV are inorganic scintillators and germanium semiconductor detectors (Knoll, 1989). The most common type of scintillator is the sodium iodide detector (NaI), whose characteristics are discussed in the introduction to this chapter. The advantages of sodium iodide detectors are their size and material densities, which result in a high interaction probability for gamma rays. This accounts for the higher efficiency as well as the reduced resolution of scintillators as compared to germanium detectors.

Germanium detectors have excellent resolution but peak sizes that can be an order of magnitude smaller than those seen with scintillators. This lack of efficiency can be a problem when measuring small peaks, but is an advantage when analyzing spectra that have tightly spaced energy peaks. There are two primary types of germanium detectors, lithium drifted and HPGe detectors. Most modern germanium detectors are of the HPGe type due to the fact that they only require cooling when in use, while the lithium-drifted detectors require constant cooling.

There are also two types of HPGe detectors available, those made of n-type germanium and those made of p-type germanium. The main difference between these two types of detectors is in the thickness of the dead layer of germanium, which is thicker for the p-type detector. This leads to a decrease in response at energies below 200 keV, however the responses of the two types are identical above 200 keV (Knoll, 1989).

Detectors are normally characterized by their size (for scintillators), relative efficiency (germanium), and energy resolution (both types) (Knoll, 1989). In the case of germanium detectors it is common to define relative efficiency by comparison to a standard sodium iodide crystal. It is also common to relate efficiency by calculating the number of full energy peak counts for a 1.33 MeV photon emitted from Cobalt-60 at a standard distance. Energy resolution is normally characterized by the full width at half maximum (FWHM) of the full energy peak, at the 1.33 MeV peak of Cobalt-60. The FWHM normally increases as the energy increases, so a peak at 100 keV would have a smaller FWHM than a peak at 1 MeV.

### **3.2.2 Gamma Ray Spectra Characteristics**

There are significant differences in the appearance of the energy spectra of germanium detectors and those for scintillators. This discussion will deal only with the characteristics of the spectra produced by germanium detectors. The pulse height spectra observed is the result of the processes of Compton scattering, the photoelectric effect, and pair

production (Knoll, 1989). The probability of each of these different interactions is directly related to the energy of the gamma ray detected.

There are several distinct features of a germanium spectrum, the most prominent of which is the Compton continuum. This continuum of energies results from a single Compton scattering in a small detector (Knoll, 1989). The spectrum of these scattered electrons produces a prominent continuum at the beginning of the displayed spectra. This phenomenon can be seen in Figure 3-2. Sometimes the term peak-to-Compton ratio is referred to as a feature of a given detector. This is usually defined as the ratio of the height of the most prominent photopeak to a typical channel in the Compton continuum, typically chosen in a flat portion of the distribution. It is desirable to have the largest possible peak to Compton ratio, so that small low energy peaks may be more easily identified.

Another feature of germanium spectra is the presence of single escape peaks and double escape peaks. These peaks arise due to the escape of annihilation radiation following pair production. During the pair production process an electron-positron pair is created at the site of the original gamma-ray interaction (Turner, 1992). The positron will then travel some distance and annihilate creating two 0.511 MeV photons. There is some probability that one or both of these photons will escape. The single escape peak will occur when only one of these photons escapes. This will lead to a peak appearing at 0.511 MeV

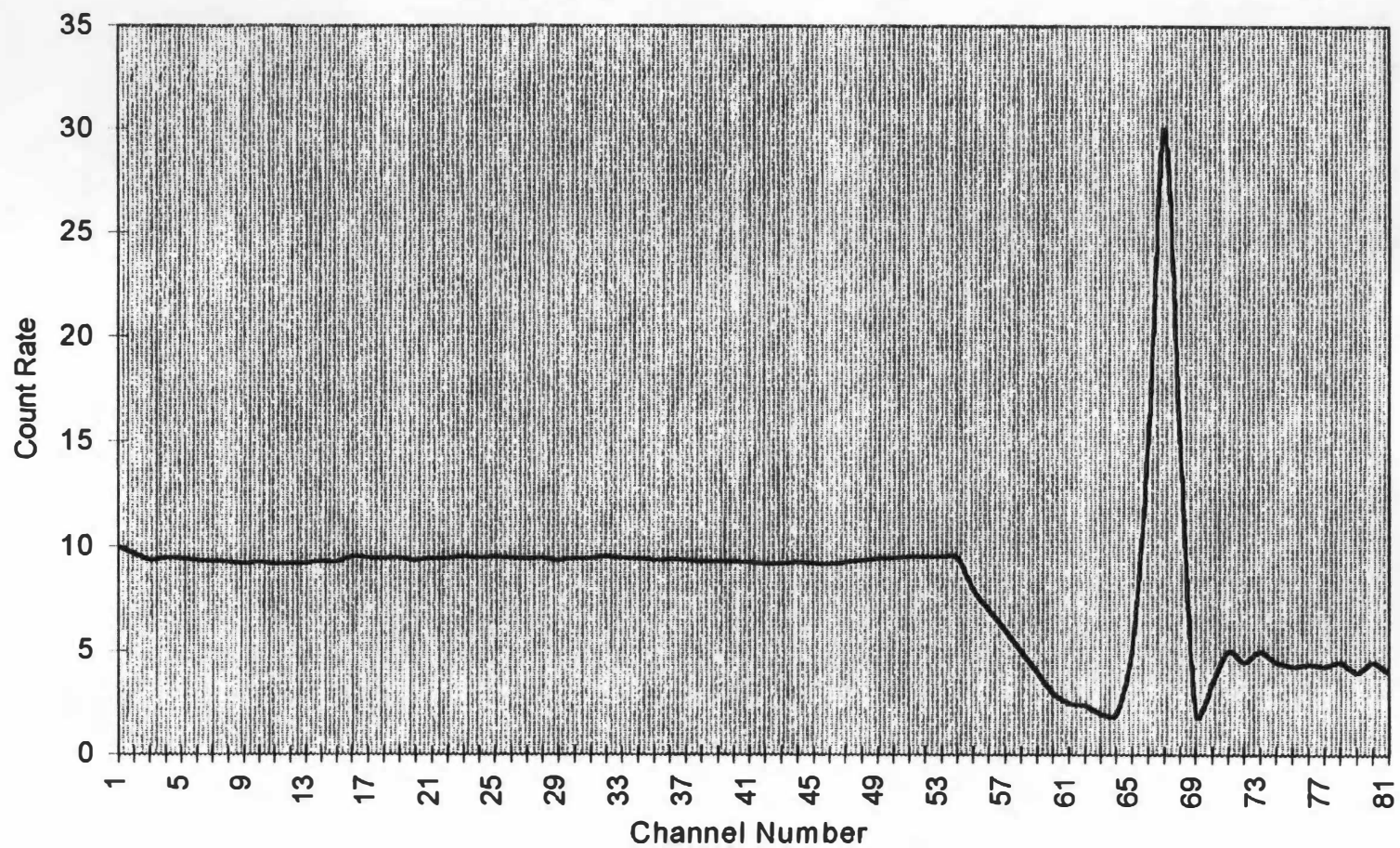


**Figure 3-2.** Example of the Compton Continuum. Example Shown is 662 keV full energy peak from Cs-137

below the full energy peak. A double escape peak occurs when both of the annihilation photons escape, creating a peak 1.022 MeV below the full energy peak. These two peaks are possible when dealing with high-energy gamma rays, above 1.022 MeV, and must be taken into consideration because they take away from the full energy peak. Some gamma rays can be identified by the presence of these escape peaks as readily as with the full energy peak (Knoll, 1989).

### **3.2.3 Gamma Spectrometry System Setup**

The setup of the system used for this paper is illustrated in Figure 3-3. It makes use of a solid state High Purity Germanium (HPGe) detector in conjunction with a multichannel buffer, high voltage power supply, amplifier, and a computer used for data processing. The computer contains a program called Gamma Vision, which provides data analysis. Specifically, the Gamma Vision software package, which is produced by EG&G Ortec, and functions as both a MCA emulator and an analysis tool for gamma ray spectrums (EG&G, 1990). This program allows for the display and manipulation of the spectrum in windows environment. It also has the capability of calculating all peak information with a calculated uncertainty, the details of the counting statistics employed are presented in section 3.6.

The power supply used for this project was made by Tennelec and is capable of providing a maximum of -5,000 volts, although for this paper a bias voltage of -2,000 volts was employed. In addition to supplying the high voltage, this unit also has the capability of detecting when the detector temperature rises, usually due to nitrogen loss.

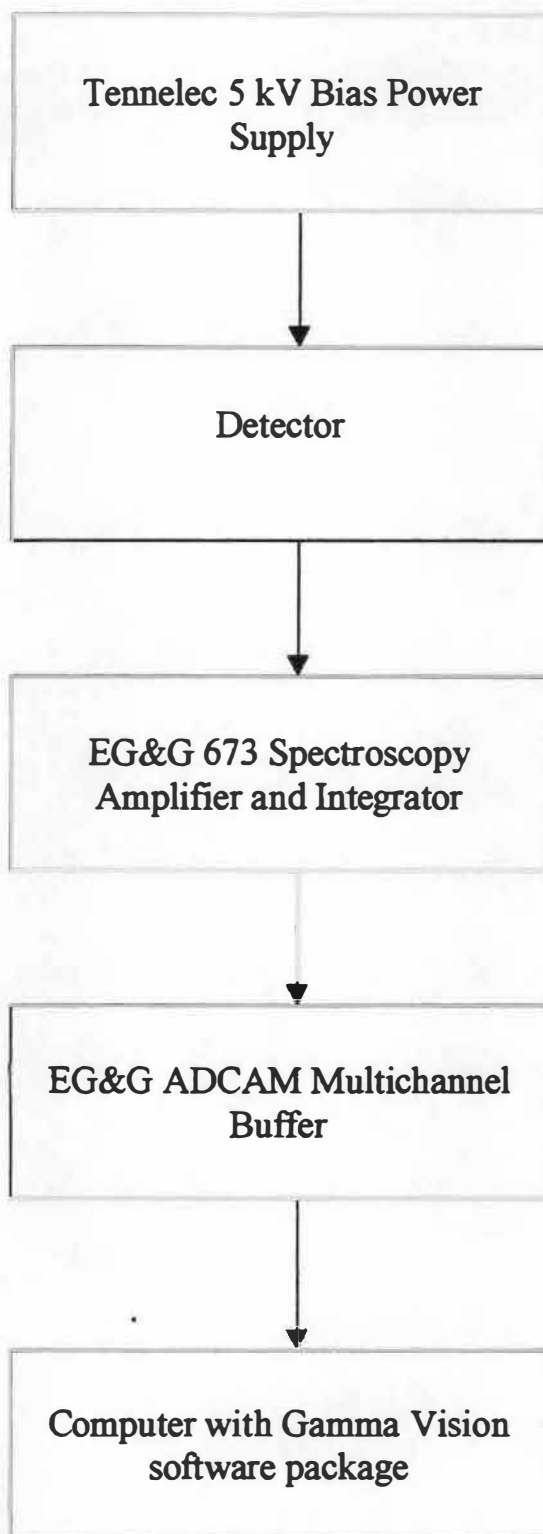


**Figure 3-3. HPGe system setup**

When this temperature rises to a preset point, the voltage is then switched off to protect the detector.

A spectroscopy amp and gated integrator, model 673, manufactured by EG&G Ortec was used as a combination amplifier and gated integrator. There are several features in this amplifier that make it an excellent amplifier for use in gamma spectrometry work. In particular this amplifier provides a unipolar output plus pole-zero cancellation. These features allow for a smooth output pulse, elimination of the undershoot of the output pulse, and a rapid restoration of the baseline after each pulse occurrence. Due to the low count rate being dealt with in these environmental samples, problems with detector saturation were not a concern. This particular model allows for the gain and shaping time to be manually adjusted by the operator.

A multichannel buffer was used to transition the output from the amplifier and provide an input to the MCA emulator. The unit used for this function was the ADCAM 918 multichannel buffer. This unit's primary function was to provide analog to digital conversion of the data before being applied to the computer.

The Gamma Vision software package is designed for use on a PC, and enables MCA emulation for acquisition, analysis and manipulation of the gamma spectrum. This program sorts the data from the buffer and places it into a channel corresponding to the energy of the pulse detected. There were 8100 channels available in the emulator, corresponding to an energy range of 5 MeV. This works out to about .6 keV per channel,

which exceeds any minimum recommended specifications (ICRU, 1994). The data processing functions of this program allow for the calculation of energy and efficiency calibration curves, region of interest manipulation, and the ability to display multiple spectrums simultaneously. In addition, the ability to save both spectrums and calibrations as files allows transfer of spectrum data to other computers.

The detector used here was manufactured by EG&G Ortec and is an n-type coaxial detector of vertical configuration, the geometry of which is shown in Figure 3-4. The detector consists of a germanium crystal connected and mounted in a vacuum tight cryostat, which has been evacuated by the manufacturer. The crystal dimensions measure 48.4 x 47.2 mm, with a resolution of 1.73 keV at the 1.33 MeV peak of Co-60. The effective range of the detector is 3 keV to 10 MeV.

The cryostat is inserted into an insulated dewar that contains the liquid nitrogen that is required to cool the germanium, as is standard with all germanium detectors. The reason that nitrogen is required is due to the small band gap ( .7 eV ) of the germanium crystal. This small band gap creates leakage current at room temperature would ruin the detector resolution. The nitrogen keeps the detector at 77K or cooler through the use of the dewar, through which the reservoir of liquid nitrogen is kept in thermal contact with the detector (Knoll, 1989).



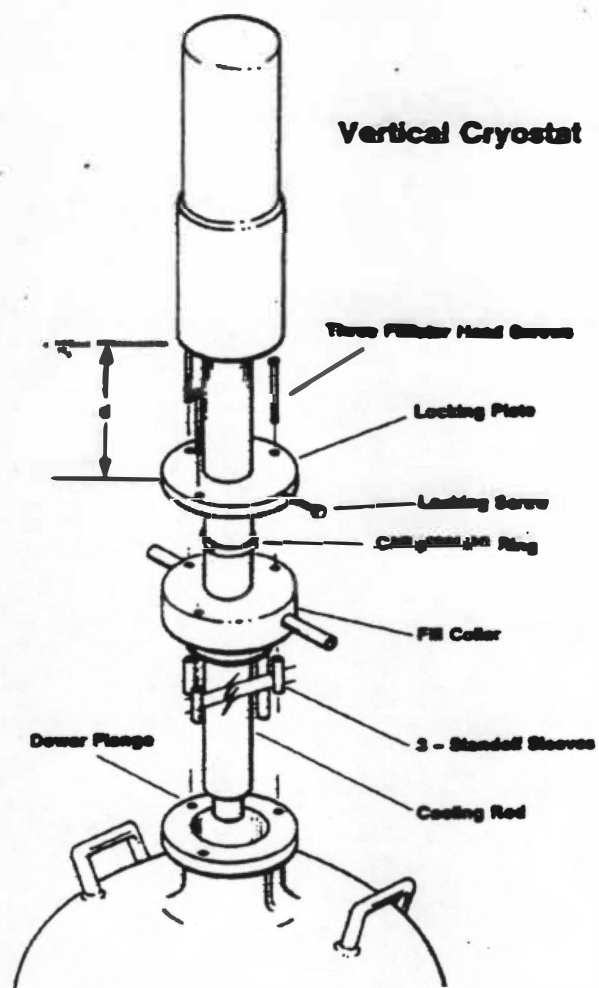


**Figure 3-4.** Vertical HPGe detector configuration (EG&G, 1986)

### **3.3 Calibration**

#### **3.3.1 Energy Calibration**

The first step in calibrating the gamma spectrometry system is to perform an energy calibration that will relate the channel of the MCA to an energy level. The first step in the energy calibration was to obtain a measurement using an Eu-152 source. The gamma rays emitted by this isotope are listed in Table 3-1. Eu-152 is a commonly used isotope for energy calibrations due to its relatively long half-life (13 years), and the wide range of gamma ray energies. The Eu-152 source is also ideal for soil analysis because it emits a range of gamma rays, which cover the spectrum of energies necessary for determining the activity in soil.

A counting time of 15 minutes was employed to allow for sharp peaks at all energies. The length of counting time is not critical as long as it is long enough to allow for sharp peaks. Once the counting was completed, the energy of key peaks had to be determined and then entered into the computer. The calculation of a calibration curve was accomplished by using the Gamma Vision computer program. This allows for energies to be displayed on the spectrum, eliminating the need for manually plotting the calibration curve.

#### **3.3.2 Efficiency Calibration**

Following the energy calibration, an efficiency calibration was performed using a sample of dry sand in a 500-mL container. This is the same container type (size, and

**Table 3-1 – Gamma rays emitted from Eu-152**

<b>Energy (keV)</b>	<b>Relative Intensity</b>
121.8	141
244.7	36.6
344.3	127.2
367.8	4.19
411.1	10.71
444	15
488.7	1.984
586.3	2.24
678.6	2.296
688.7	4.12
778.9	62.6
867.4	20.54
964	70.4
1005.1	3.57
1085.8	48.7
1089.7	8.26
1112.1	65
1212.9	6.67
1299.1	7.76
1408	100
1457.6	2.52

material) used with the soil samples. By using a container of known activity with the same geometry, as was used for the soil counts, the effects of the counting geometry will be negated. By performing an efficiency calibration using this methodology the calibration will yield an efficiency comparable to that of the actual soil counts. The sample of dry sand used for this calibration contained 70 pCi of Th-232, with a sample weight of 508.8 grams.

The first step in the efficiency calibration was to perform a 48-hour count with the known sample. This time period was chosen to ensure good counting statistics, while keeping the time period of the count practical. Defining a practical time period is arbitrary, however the need to have the liquid nitrogen regularly refilled regulated this process. In particular, because the liquid nitrogen required refilling every 10 days, plus a one day delay after refilling, performing four counts in a two week period was all that was realistically possible. A pulse height spectrum from this known sample was obtained as shown in Figure 3-5, with all peaks identified in Table 3-2.

The second step in this procedure was to calculate the emission rate, for each gamma ray, from the known activity levels. Then a comparison was performed using the measured emission rates and the calculated rates. In order to accomplish this calculation the assumption was made that all elements in the Th-232 decay chain are in secular equilibrium. This assumption is based on the extremely long half-life (14 billion years) of Th-232, and has been experimentally determined. By definition, secular equilibrium occurs when the parent has a long half-life, and the daughter builds up to an equilibrium

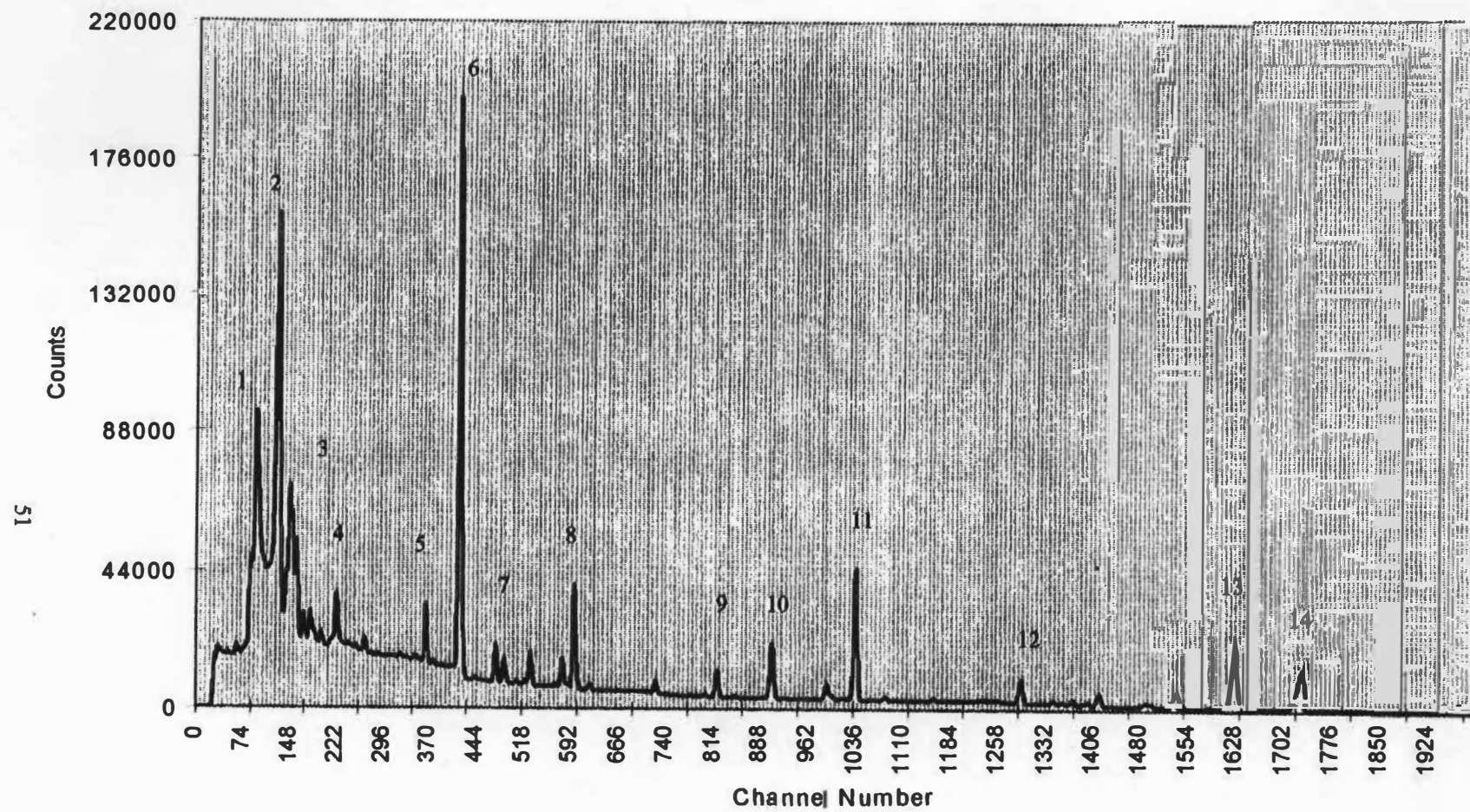


Figure 3-5. Spectrum for sample of known activity

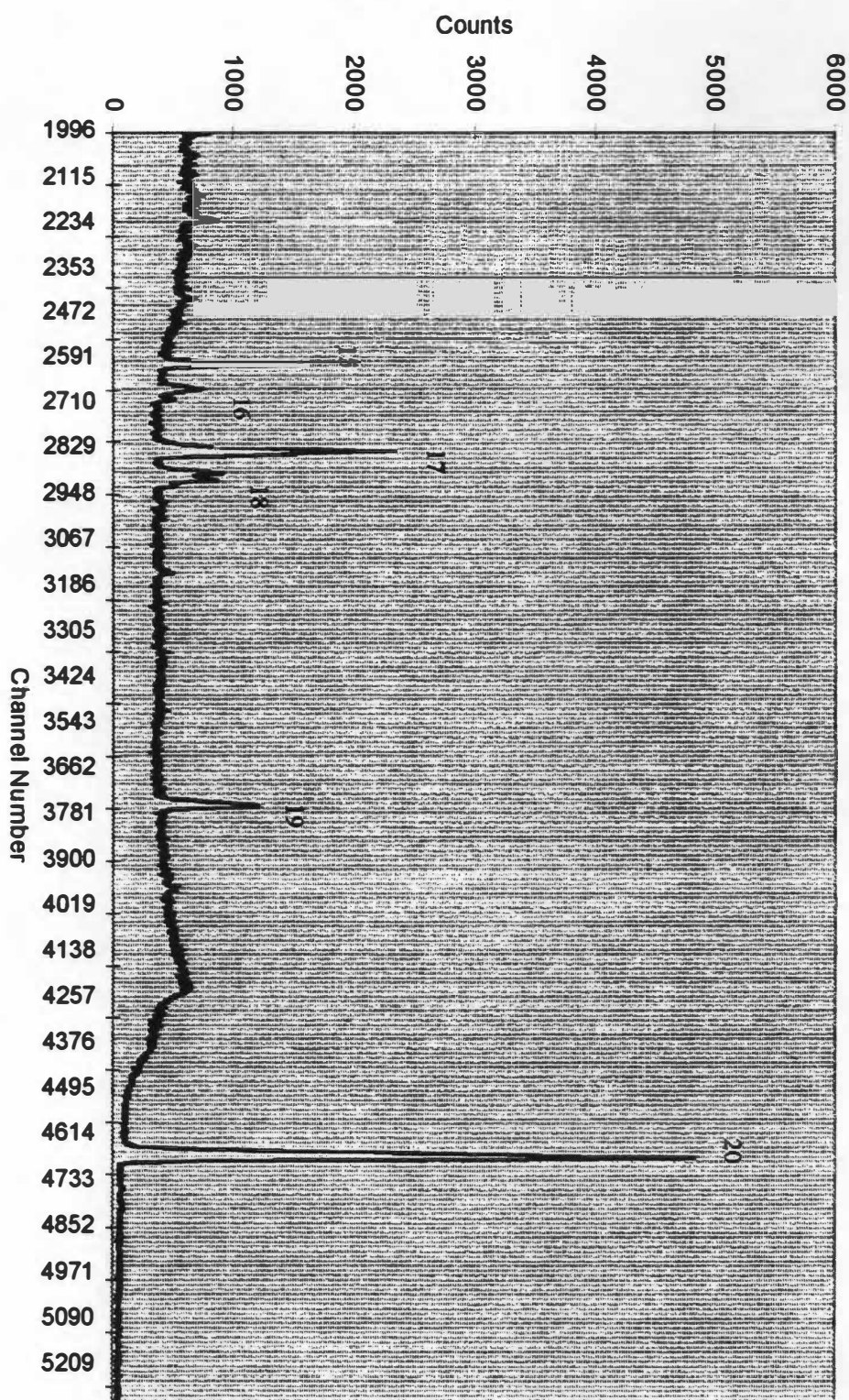


Figure 3-5 (cont'd)

**Table 3-2. Peak identification for known sample**

<b>Peak Number</b>	<b>Energy (keV)</b>	<b>Radionuclide</b>
1	57.2	Ac-228
2	77.1	Pb-212
3	87.3	Pb-212
4	129.1	Ac-228
5	209.3	Ac-228
6	238.6	Pb-212
7	270.2	Ac-228
8	338.3	Ac-228
9	463	Ac-228
10	511	Ann. Peak
11	583.1	Tl-208
12	727.2	Bi-212
13	911.1	Ac-228
14	966/969	Ac-228
15	1459.5	K-40/Ac-228
16	1495.8	Ac-228
17	1588	Ac-228
18	1620/1630	Bi-212/Ac-228
19	2103	SE Tl-208
20	2614.1	Tl-208

amount and then decays at a constant rate (Turner, 1992). In this situation  $\lambda_1 \ll \lambda_2$  and the rate of the daughter formation balances their rate of decay.

This can be expressed by (Aitken, 1985):

$$\frac{dN_2}{dt} = \lambda_1 N_1 - \lambda_2 N_2 \quad (3.1)$$

Therefore,

$$\lambda_1 N_1 = \lambda_2 N_2 \quad (3.2)$$

In the Th-232 decay chain all of the daughter elements build up to an equilibrium level.

This chain can be expressed as:

$$\lambda_1 N_1 = \lambda_2 N_2 = \lambda_3 N_3 = \dots = \lambda_{n-1} N_{n-1} \quad (3.3)$$

From this data a calibration curve was calculated as shown in Figure 3-6. The calibration curve was calculated by means of a curve fit computer program, which ran a best-fit comparison. The Weibull model produced the best fit, and is discussed in detail in section 3.6.



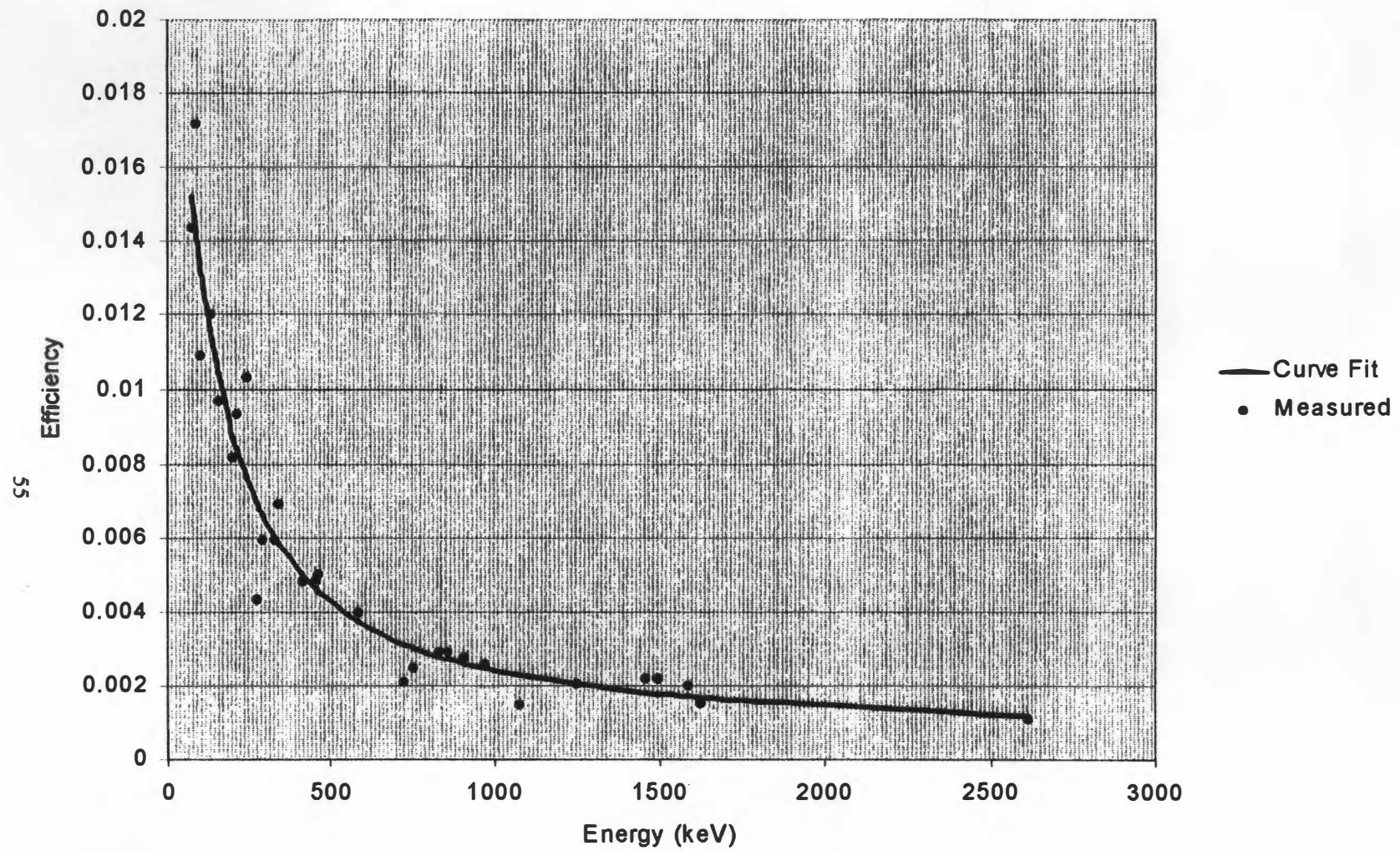


**Figure 3-6.** Efficiency curve generated from known sample

The efficiency calibration curve that was obtained was used to estimate the activity of two additional samples whose activity was known. This comparison produced activity comparisons within 2.3% of the actual activity levels, and is shown in Table 3-3. It should be noted that both of these activity levels were lower than that of the original sample. Both of these samples were thorium-232 of similar sample weight, and using the same container type and size. The container was a 500-ml plastic jar that was used for all counts reported in this paper.

### **3.4 Sample Preparation and Counting**

The soil samples were divided into five separate containers identical to the ones that held the known samples. Each sample was weighed both when saturated and when dry. Then a total of ten 48-hour counts were performed, five when moisture saturated and five when dry. It should be noted that the samples were initially saturated and then dried out in an oven. The reason for this was to determine the effect of moisture attenuation on the measured activity levels. It should be noted that all of the samples were sealed in plastic bags immediately after recovery. This ensured that the moisture content remained unchanged until analysis.

Although it can be difficult to determine the contextual relative humidity (saturation level), certain assumptions can be made relating to the depth of the burial. In the continental United States ceramics buried below 30 cm can be assumed to have been buried in complete saturation (Aitken, 1985). In other geographic regions, or at a

**Table 3-3. Results of activity calculations with known samples**

<b>Sample Number</b>	<b>Known Activity (pCi/gm)</b>	<b>Calculated Activity (pCi/gm)</b>	<b>Percent Difference</b>
2	10.2	10.0	-2%
3	30.5	29.8	-2.3

shallower depth, annual rainfall and water table levels can be used for determining the saturation level. For this project the saturation level used came from the soil in which the pottery sample was buried. These soil samples came from the Wickliffe Mound excavation site in Paducah, Kentucky and, due to the depth of the burial and geographic location, was assumed to be at its normal saturation level.

The archeological site at Wickliffe Mounds consists of several burial mounds located in Western Kentucky. These mounds have been the site of excavations dating back to the 1930's (Matternes, 1994). After these early excavations were conducted, the site was opened to the public and partial excavations were displayed for viewing. Recently, these excavations have continued and attempts have been made to correct for past mistakes, and to properly catalogue and preserve to site. The soil samples analyzed here are part of this effort.

Once the samples were counted then the peaks were cataloged and identified. The Appendix shows the analysis of all ten soil counts, including efficiency data and estimated activity for each of the energy peaks. Details of these counts, including all peak information, are in the Chapter Five.

### **3.5 Activity Calculations**

Each of the various elements has distinctive gamma peaks that are suitable for analysis. These peaks are the most distinguishable and provide the best statistical counting efficiency. For uranium the 185, 295, 351, 609, 1120, and 1764 keV peaks were used.

The 583, 911, 966, and 2614 keV peaks were analyzed for thorium, while the 1460 keV peak was used for potassium. Further comparison was accomplished using the weaker peaks to see how accurate, and to what agreement, these peaks would have. As would be expected the weaker peaks do not provide an accurate picture of the actual soil activity. The complete decay chains for both thorium-232 and uranium-238 are illustrated in Figures 3-7 and 3-8, respectively. Specifically, the activity was determined by using the efficiency curve to determine the emission rate for each gamma ray. Once the various emission rates were known, then the concentration of each nuclide was determined by using published data on the intensity of the emitted gamma rays for each of the nuclides.

The activity can then be calculated using the equation:

$$A = \frac{R}{I, E} \quad (3.4)$$

where:

**R** = Net Count-rate (counts per second)

**E** = Counting efficiency (counts per gamma)

**I<sub>γ</sub>** = Gamma Intensity (gamma per disintegration)

### 3.6 Statistical Analysis

Several different processes are involved in computing energy peak information, necessary for accurate activity estimates. In any gamma spectrometry system, the energy

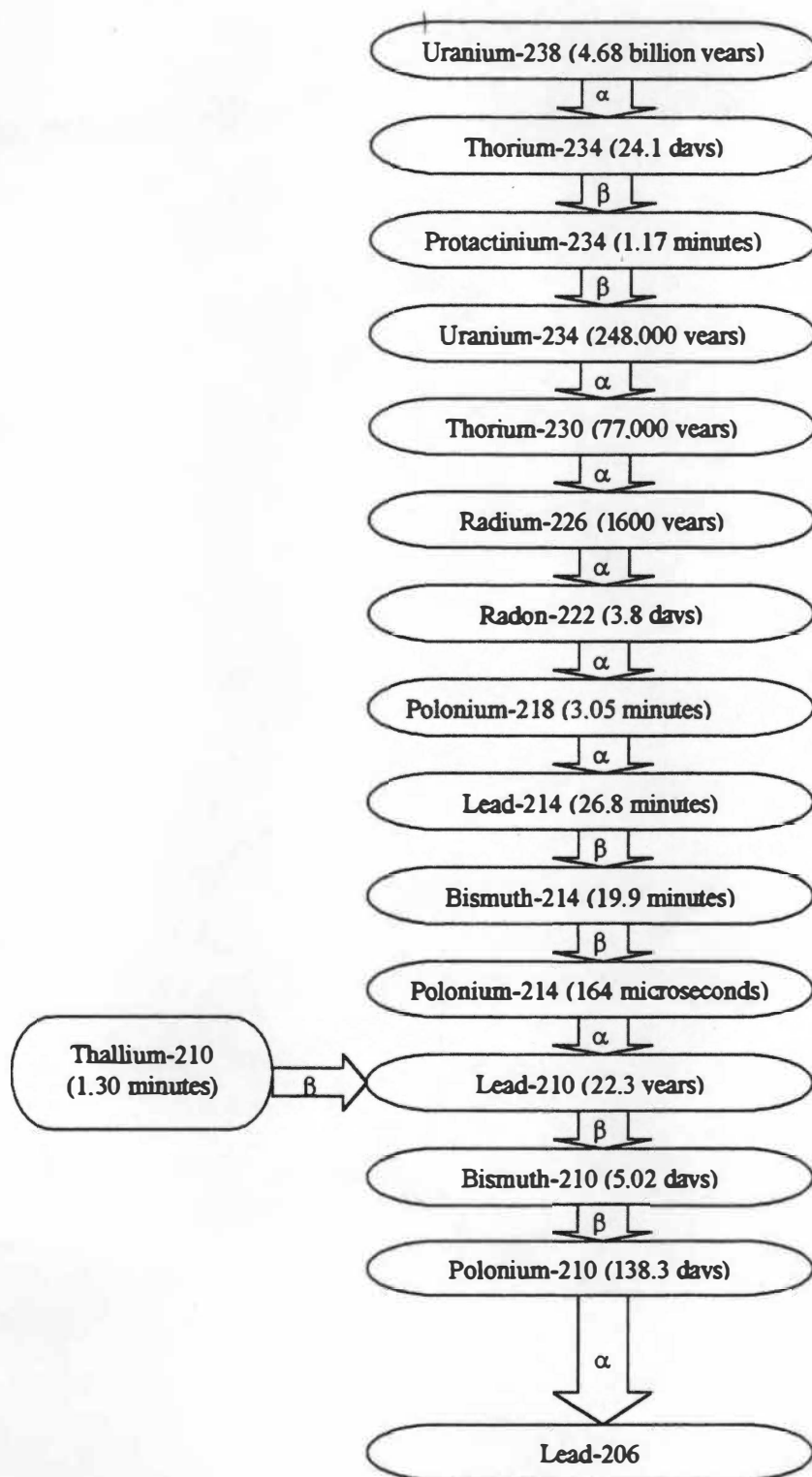


**Figure 3-7. Uranium-238 decay chain**

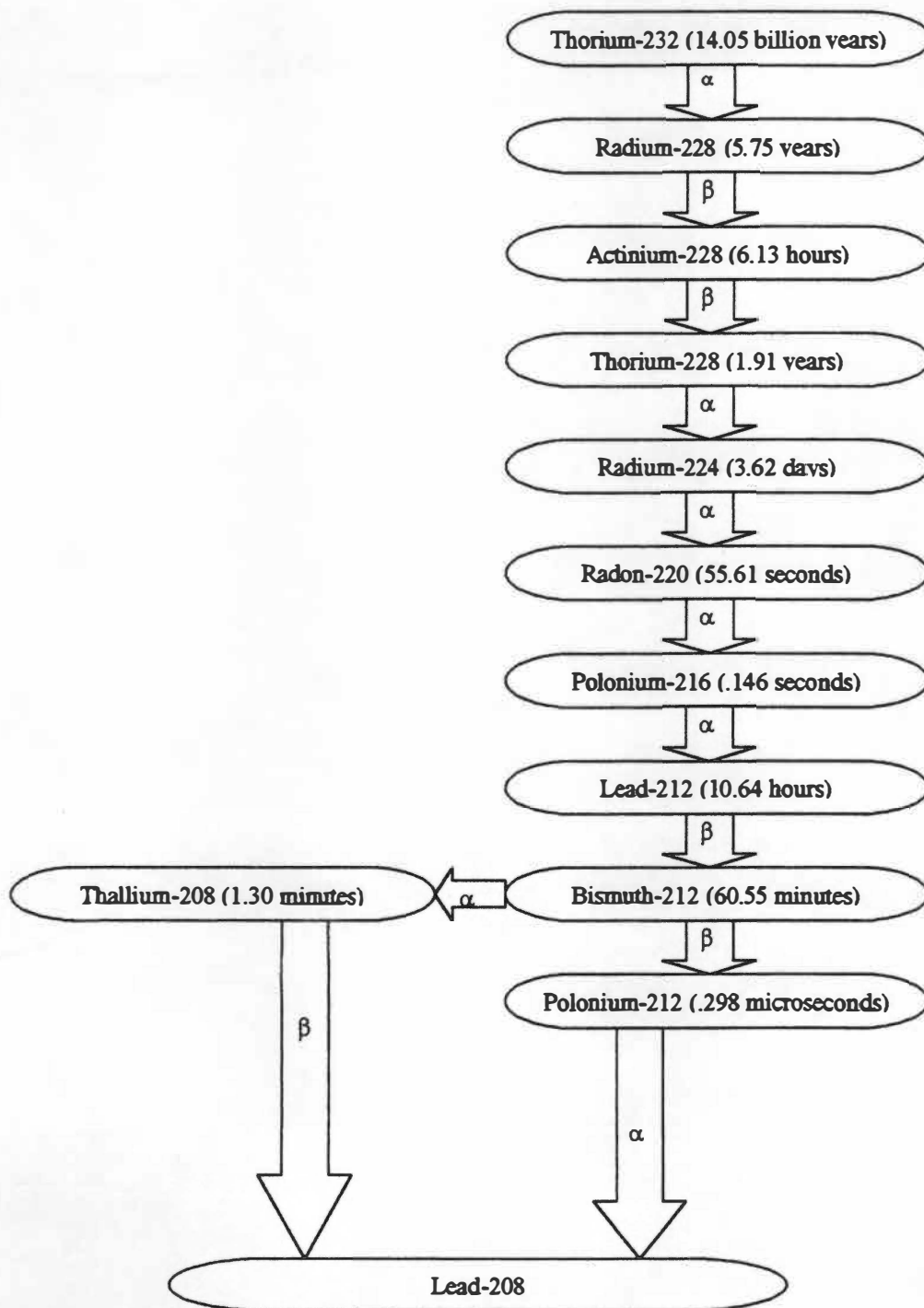


**Figure 3-8.** Thorium-232 decay chain

resolution is a critical factor in obtaining accurate peak information. The resolution determines whether you will be able to separate, and identify, peaks that are close in energy. Another area of concern involves the calculation of the area under the peak, and the uncertainty associated with this number. The area under the peak is critical due to the fact that these numbers are used to calculate the activity for each peak.

### 3.6.1 Energy Resolution

The overall energy resolution of a spectroscopy system depends on several factors. These include the statistical spread in the number of charge carriers, electronic noise, and charge collection efficiency. The full width at half-maximum  $W_t$  of a peak in the spectrum can be broken down as follows (Knoll, 1989):

$$W_t^2 = W_d^2 + W_x^2 + W_e^2 \quad (3.5)$$

where:

$W_d$  = the effect of carrier statistics

$W_x$  = charge carrier collection

$W_e$  = electronic noise

The first factor,  $W_d^2$ , represents the statistical fluctuation in the charge carriers and can be represented as follows:



$$W^2 = (2.35)^2 F \epsilon E \quad (3.6)$$

where:

**F** = the Fano factor

**ε** = the energy necessary to produce one electron-hole pair

**E** = gamma ray energy

The Fano factor is an attempt to quantify the variation of the statistical fluctuations in the number of charge carriers from pure poisson statistics and can be defined by:

$$F = \frac{(\text{Observed Variance in } N)}{(\text{Poisson predicted Variance } (= N))} \quad (3.7)$$

The Fano factor was devised to illustrate the fact that some radiation detectors exhibit values of R that are lower by a factor of 3 or 4 than the minimum value predicted by the statistical argument below. The resolution of this germanium detector falls into this category, with energy resolution of 1.73 keV.

The response of the detector can be assumed to be linear, so the average pulse amplitude can be expressed as  $H_0 = KN$ , with K as the proportionality constant. From this

an expression for the limiting resolution, due only to statistical fluctuations, in a detector with linear response would be (Knoll, 1989):

$$R = \frac{FWHM}{H.} = \frac{2.35K\sqrt{N}}{KN} = \frac{2.35}{\sqrt{N}} \quad (3.8)$$

With R equating to the resolution of the detector calculated only due to the statistical fluctuation of the charge carriers. The Fano factor gives rise to a modification of this equation as follows:

$$R = \frac{2.35K\sqrt{NF}}{KN} = 2.35\sqrt{\frac{F}{N}} \quad (3.9)$$

Figure 3-9 shows the definition of detector energy resolution is in a visual form. This figure assumes that only a single energy is being recorded.

### 3.6.2 MCA Emulator Peak Calculations

The Gamma Vision software package has the capability of calculating peak information including FWHM, and net peak area with a calculated uncertainty. The methodology used to calculate the net area, as defined in the Gamma Vision users guide, begins with a background calculation. The first three and the last three channels of the Region Of

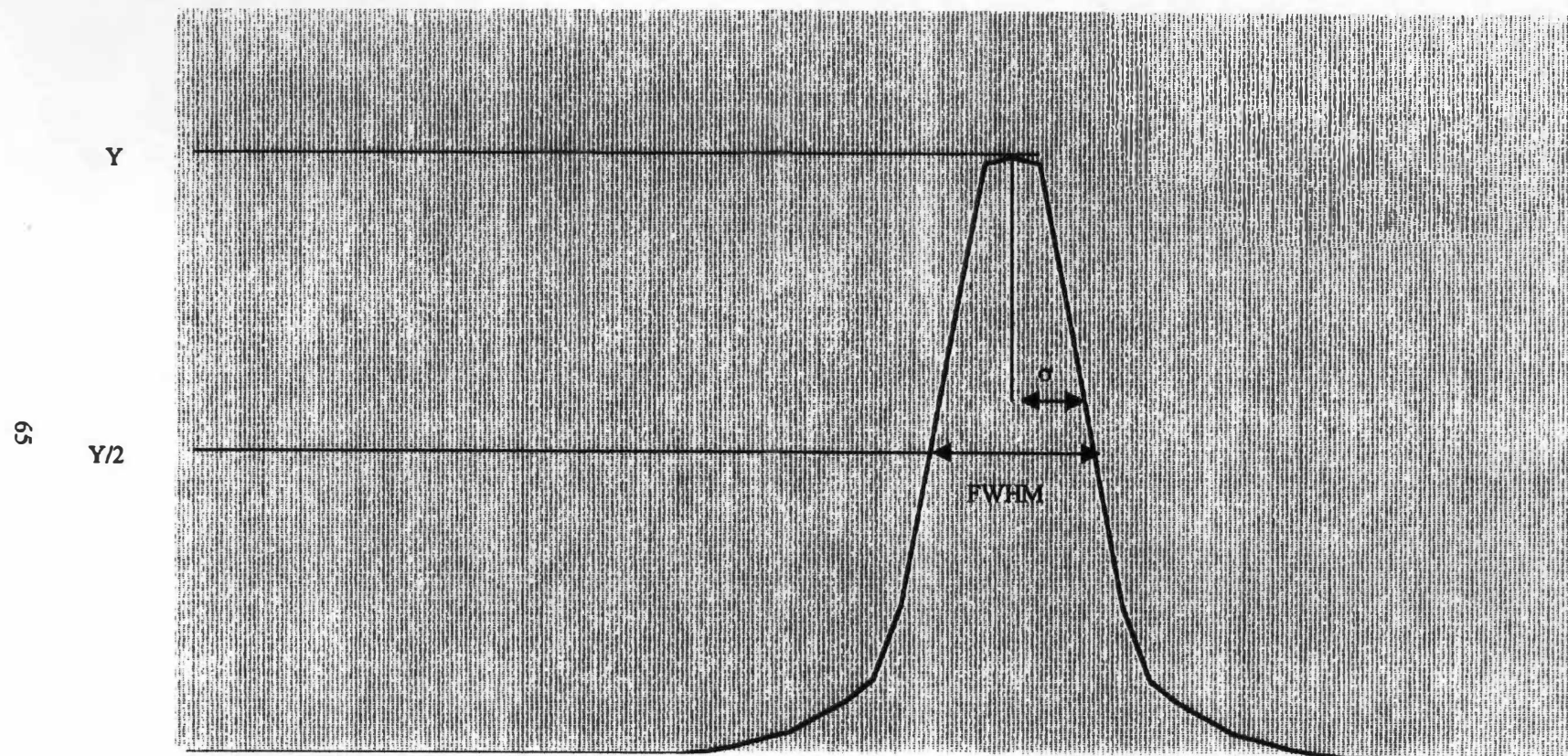


Figure 3-9. Depiction of detector energy resolution (Knoll, 1989)

Interest (ROI) are sampled and then are averaged. The background on the low side of the peak is the average of the first three channels, while the background on the high side of the peak is the average of the last three channels.

This leads to the background equation as follows:

$$B = \left( \sum_{i=l}^{l+2} C_i + \sum_{i=h-2}^h C_i \right) \frac{h-l+1}{6} \quad (3.10)$$

where:

**B** = the background area

**l** = the ROI low limit

**h** = the ROI high limit

**C** = contents of channel **i**

The gross area of all the channels in the ROI is defined by:

$$A_g = \sum_{i=l}^h C_i \quad (3.11)$$

The adjusted gross area is then calculated. It is defined as the sum of all channels marked by the ROI but not used in the background. It is further defined by:

$$A_g = \sum_{i=l+3}^{h-3} C_i \quad (3.12)$$

Finally the net area is calculated by taking the adjusted gross area and subtracting the adjusted calculated background, as follows:

$$A_n = A_g - \frac{B(h-l-5)}{(h-l+1)} \quad (3.13)$$

The program calculates an error for the net area. This error is the square root of the sum of squares of the errors in the adjusted background and of the weighted error of the background. This background error is weighted by the ratio of the adjusted peak width to the number of channels needed for the adjusted background. From this net peak error is defined as follows:

$$\sigma_n = \sqrt{A_g + B\left(\frac{h-l-5}{6}\right)\left(\frac{h-l-5}{h-l+1}\right)} \quad (3.14)$$

### 3.6.3 Calibration Curve Generation

For generating the efficiency calibration curve, a curve fit program called Curve Expert was used. This program checks over thirty curve fit models to find one that best fits the data given. It determined that the Weibull model provided the best curve fit. This model is defined by:

$$y = a - b e^{-ax^b} \quad (3.15)$$

## Chapter 4

### Dose Rate Determination

#### 4.1 Background

The dose rate that an artifact is exposed to, while buried in soil, has to be determined from the measured activity of the soil. Specifically, this means accounting for the contributions of all nuclides in the uranium-238, uranium-235, and thorium-232 decay chains as well as from potassium. This requires assumptions about the distribution of the nuclides in the soil, the relative contributions of each radionuclide in each of the decay chains, and accounting for the differing effects of the alpha, beta, and gamma radiation.

The thermoluminescence induced by radionuclides in the soil is proportional to the amount of ionization, which is proportional to the energy absorbed from the radiation. The thermoluminescence produced for a given amount of absorbed energy is the same for beta and gamma radiation, but can differ for alpha radiation.

In both the thorium and uranium decay chains there are several alpha emitting nuclides. The energy absorbed from alpha radiation is different due to its limited range (.01 to .05 mm in pottery), and due to the fact that it is so densely ionizing. The density of the ionizations at such shallow depths creates a situation where all of the electron traps fill up, so no further thermoluminescence can be induced. In other words, any electrons ionized after the traps are full will simply fall back into the valence band and its energy

will not be absorbed. As a result of this, alpha particles produce much less thermoluminescence per gray than is the case with beta particles or with gamma radiation. As a result there have been several methods for modifying the age equation to account for this difference. The basic age equation can be defined as follows (Aitken, 1985):

$$Age = \frac{\text{Total radiation dose}}{\text{Radiation dose per year}} \quad (4.1)$$

This equation can then be modified to read as follows:

$$Age = \frac{\text{natural TL}}{\chi_{\alpha} D_{\alpha} + \chi_{\gamma} (D_{\alpha} + D_{\gamma} + D_c)} \quad (4.2)$$

where:

$\chi$  = the thermoluminescent sensitivities

$D_{\alpha}$  = alpha dose rate

$D_{\gamma}$  = gamma dose rate

$D_{\beta}$  = beta dose rate

$I$  = lightly ionizing radiation

$D_c$  = cosmic radiation



In terms of the paleodose (total dose received since artifact was heated or fired) this equation can be written as:

$$Age = \frac{P}{D_{\alpha} + D_{\beta} + D_{\gamma} + D_{\text{e}}}$$
(4.3)

where:

P = paleodose

$D_{\alpha}$  = the effective alpha dose rate

Having defined the contributions of the different types of radiation and their contributions to the annual dose rate, there are certain assumptions that can be made in order to simplify the dose rate calculations. First of all, the contribution of the alpha particles will be ignored due to the fact that preparation of the quartz samples will include the removal of the outer 1 micron layer of the quartz itself. The removal of this layer takes away the only part of the crystal affected by alpha emission (Mejdahl and Wintle, 1984). Second of all the assumption of an infinite matrix has been made which will allow calculations to be simplified. Finally, the assumption is made that makeup of the soil is homogenous both in absorption coefficients and radionuclide concentration.

The use of an assumption of an infinite matrix is necessary due to the complexities of different rates of energy deposition by the different types of radiation. One way of approaching this problem is to make detailed calculations of the different radiations and

energy absorption coefficients of the materials in the sample. By using the assumption of an infinite matrix the calculational procedure can be simplified considerably. The range of gamma radiation in soil is about 30 cm (Mejdahl and Wintle, 1984), so the only problem with this assumption could occur in a very shallow burial.

In a volume that exceeds the ranges of the emitted radiation, conservation of energy requires that the rate of energy absorption be equal to the rate of emission. If we carry this concept further and assume a matrix that is uniform in both radioactivity and absorption coefficient then it follows that we can assume that the energy absorbed per unit mass is equal to energy emission per unit mass. The assumption of a uniform distribution is based on the fact that the measurements were made from various samples from around the excavation site, and the activity was calculated using all of these samples. This should diminish the effect of a possible concentration of nuclides in one location.

Using these assumptions, the dose rate was calculated using dose rate factors. This concept is used in dose assessment for human exposure and can be modified for use in this application. In the field of RDD a table of annual dose conversion factors, published by Nambi and Aitken in 1986, are used as the standard values to convert activity levels to dose rates. A comparison of these published rates and those calculated in this thesis are included in Chapter 5.

## 4.2 Dose Rate Calculations Using Dose Rate Factors

### 4.2.1 Background

By assuming that a medium is infinite in extent, certain assumptions can be made to simplify the calculation of the dose rate. In calculating dose rate in soil the only limiting factor in assuming an infinite medium would be the depth of the burial of the artifact. Once an infinite medium and a uniform source concentration are assumed then the following equation is defined for infinite source regions with uniform radionuclide concentrations (Till and Meyer, 1983):

$$D(t) = \dot{\chi}(t) \times DRF \quad (4.4)$$

where:

$\chi(t)$  = the radionuclide concentration

**DRF** = the dose rate factor or dose rate per unit radionuclide concentration

After the radionuclide concentration is determined using methods detailed in Chapter 3, the dose rate can be determined if dose rate factors are calculated. These dose rate factors must be calculated for each individual radionuclide in each decay chain. Once

dose rate factors are determined for a particular radionuclide then they do not have to be calculated again unless the makeup of the medium changes.

#### **4.2.2 Dose Rate Factors**

To calculate the dose rate deposited in an artifact buried in soil, with the assumptions as stated in Section 4.1, dose rate factors must be computed. The dose rate factor in this equation can also be viewed as the dose rate per unit radionuclide concentration. In this basic equation the dose rate factor is obviously the critical value, as the radionuclide concentration is known from earlier measurements. The development of an accurate dose rate factor is the most important aspect of obtaining an accurate dose rate.

Published dose rate factors have not been defined for immersion in soil, but they have been defined for immersion in contaminated air (Till and Meyer, 1983). This is due to the fact that the most common application of these factors is in external dosimetry for humans, and in most cases immersion in a contaminated cloud, or exposure to a contaminated ground surface, is the area of concern. The same concept can be used for determining dose to an artifact by changing some of the values used in the dose rate factor equation.

The dose rate factor expressions for photons  $\gamma$  and electrons  $\epsilon$  in air can be expressed as follows (Till and Meyer, 1983):

$$DRF_i^* = k \frac{1}{\rho_a} \sum_i f_{\gamma} E_{\gamma} \quad (4.5)$$

$$DRF_i^* = k \frac{1}{\rho_a} \left[ \sum_i f_e E_e + \sum_j f_{\beta} \int_0^{E_{j\beta}^{max}} N_{j\beta}(E) E dE \right] \quad (4.6)$$

where:

**DRF** = dose-rate factor in Gy/s per Bq per unit volume

**$\rho_a$**  = density of air in gram per unit air volume

**k** =  $1.6 \times 10^{-10}$  g-Gy/MeV

**$f_{j\beta}$**  = intensity of electrons from jth continuous beta transition  $\beta$  in number per decay

**$f_{ie}$**  = intensity of the ith discrete electron e in number per decay

**$E_{i\gamma}$**  = energy of ith photon in MeV

**$E_{ie}$**  = energy of ith discrete electron in MeV

**$E_{j\beta}^{max}$**  = endpoint energy in MeV for electrons from the jth continuous beta transition

**$N_{j\beta}(E)$**  = probability density function for electrons from the jth continuous beta transition

**$f_{i\gamma}$**  = intensity of ith photon  $\gamma$  in intensity per decay

These expressions will yield the dose rate factors in air for immersion in a contaminated cloud containing an infinite and uniform source concentration. To convert

this equation to account for immersion in soil, the expression for air density ( $\rho_a = .0012 \text{ g/cm}^3$ ) is replaced by soil density ( $\rho_s = 1.7 \text{ g/cm}^3$ ) .

To calculate the dose rate factors for a quartz crystal buried in soil, an additional term must be added to these equations. In the case of the dose rate factor for photons, the photon mass energy-absorption coefficient for quartz is divided by the mass energy-absorption coefficient for soil to obtain a ratio of the two values. This can be expressed as follows:

$$R_\gamma = \left[ \frac{\left( \frac{\mu_{en}}{\rho} \right)_q}{\left( \frac{\mu_{en}}{\rho} \right)_s} \right] \quad (4.7)$$

where:

$\mu_{en} / \rho$  = photon mass energy-absorption coefficient in  $\text{cm}^2 / \text{g}$

For electrons a similar equation can be used only using the ratio of electron mass stopping powers instead of the photon mass absorption coefficients listed above. This can be expressed as:

$$R_e = \left[ \frac{\left( \frac{dE}{\rho dx} \right)_e}{\left( \frac{dE}{\rho dx} \right)_a} \right] \quad (4.8)$$

where:

$dE / \rho dx$  = electron mass stopping power in MeV – cm<sup>2</sup> / g

By combining these equations with the dose rate factor equations listed above we obtain the following:

$$DRF'_r = k \frac{1}{\rho_r} \sum_i f_i E_i R_i \quad (4.9)$$

$$DRF'_r = k \frac{1}{\rho_r} \left[ \sum_i f_i E_i R_i + \sum_j f_j \int_0^{E_j} N_{jr}(E) E R_r(E) dE \right] \quad (4.10)$$

The latter equation can be simplified, resulting in the following equation:

$$DRF' = k \frac{1}{\rho} \sum_i f_i \overline{E}_i R_i \quad (4.11)$$

This simplification results in a more manageable calculation without sacrificing accuracy. It is commonly used in external dosimetry, except in special cases where knowledge of the energy spectrum makes a difference in calculated organ dose, which is not a factor in this application (Till and Meyer, 1983).

### 4.3 Calculations in Soil

To accomplish the dose calculations described above, the different energies of both the beta particles and gamma rays had to be defined. This was accomplished by taking all of the radionuclides in the thorium-232, uranium-238, and potassium-40 decay chains and quantifying the various gamma rays and beta particles emitted. The calculations were accomplished using the published intensities for each of these nuclides (Kocher, 1981). As discussed earlier, the contribution of alpha particles was ignored due to the fact that sample preparation eliminates their effect. If a different sample preparation technique is used then the alpha contribution to the overall dose rate must be taken into account.



During the activity measurements several peaks were not identified, so to account for their effects a dose was calculated for each peak. The results of were incorporated in the final calculations, detailed in Chapter Five.

## **Chapter 5**

### **Results**

#### **5.1 Results of Gamma Spectrometry**

The spectra measured from the soil samples were first evaluated to identify all of the energy peaks and their associated radionuclides. From this initial evaluation the activity of uranium-238, thorium-232, and potassium-40 were determined. In addition, this data was used for determination of any disequilibrium present in the uranium and thorium decay chains. Several of the peaks in the spectra were not identifiable, and their dose contribution not accounted for with the dose calculation.

##### **5.1.1 Gamma Spectrum Analysis**

A total of ten gamma spectra were measured, originating from five soil samples. Each sample was initially counted in a moisture-saturated condition, which is the way it was removed from the archeological site. Following that, each sample was dried in an oven until no moisture remained, and another count was made for each sample. In Table 5-1 the weights of each sample are listed, in both the moisture-saturated and dry conditions.

After the measurements were taken then all of the peaks in the spectrum were identified. Although some of the smaller peaks were missing from some of the spectra, there was good consistency in the displayed peaks. This is to be expected due to the fact that all of the sample weights are similar. In Figure 5-1 a sample spectrum from a

**Table 5-1. Soil sample weights**

<b>Sample number</b>	<b>Weight (grams)</b>
<b>1 – dry</b>	<b>294.8</b>
<b>2 – dry</b>	<b>267.3</b>
<b>3 – dry</b>	<b>344.4</b>
<b>4 – dry</b>	<b>334.2</b>
<b>5 – dry</b>	<b>314.5</b>
<b>1 – saturated</b>	<b>345.6</b>
<b>2 – saturated</b>	<b>313.5</b>
<b>3 – saturated</b>	<b>402.6</b>
<b>4 – saturated</b>	<b>391.8</b>
<b>5 - saturated</b>	<b>368.3</b>

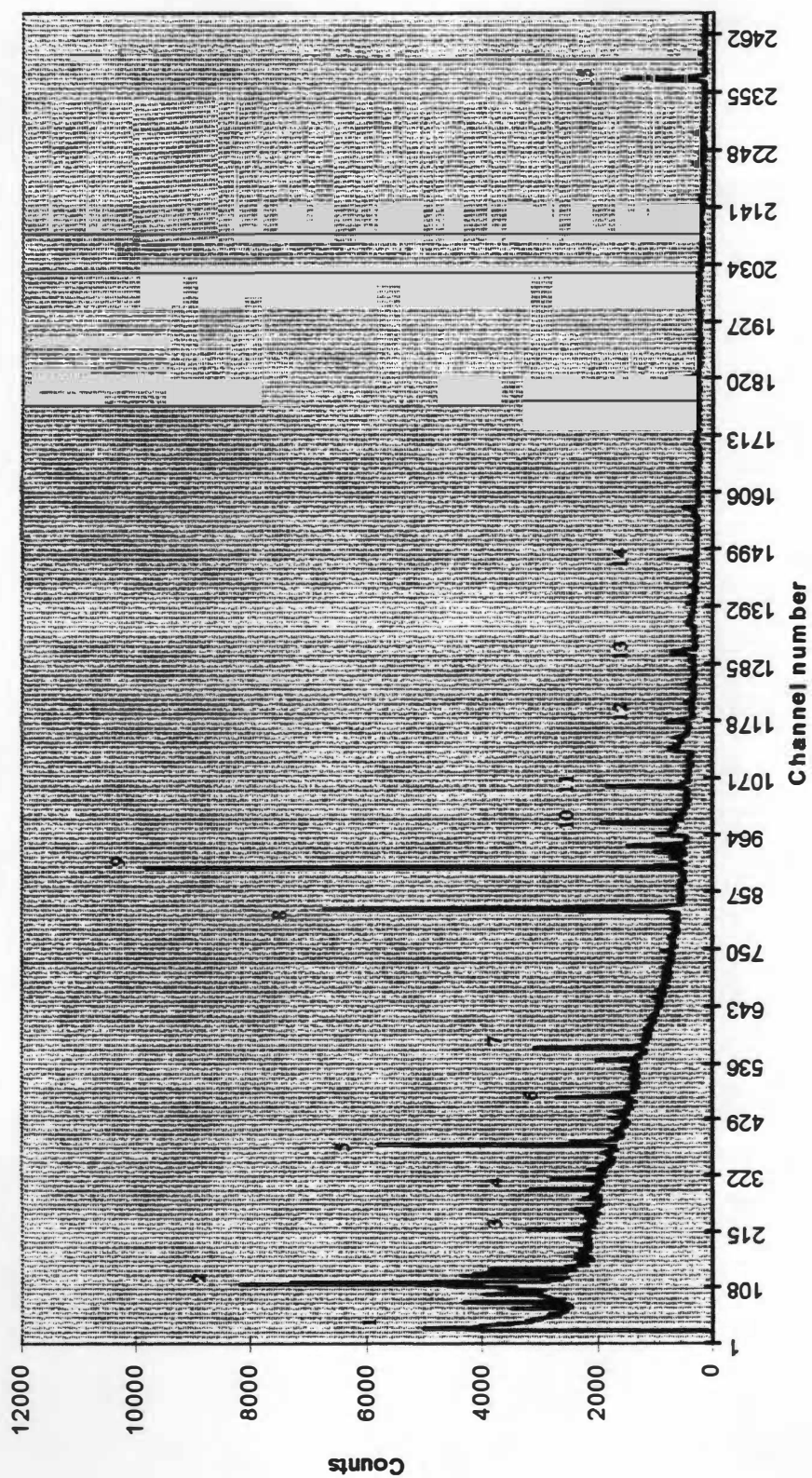


Figure 5-1. Spectrum for soil sample

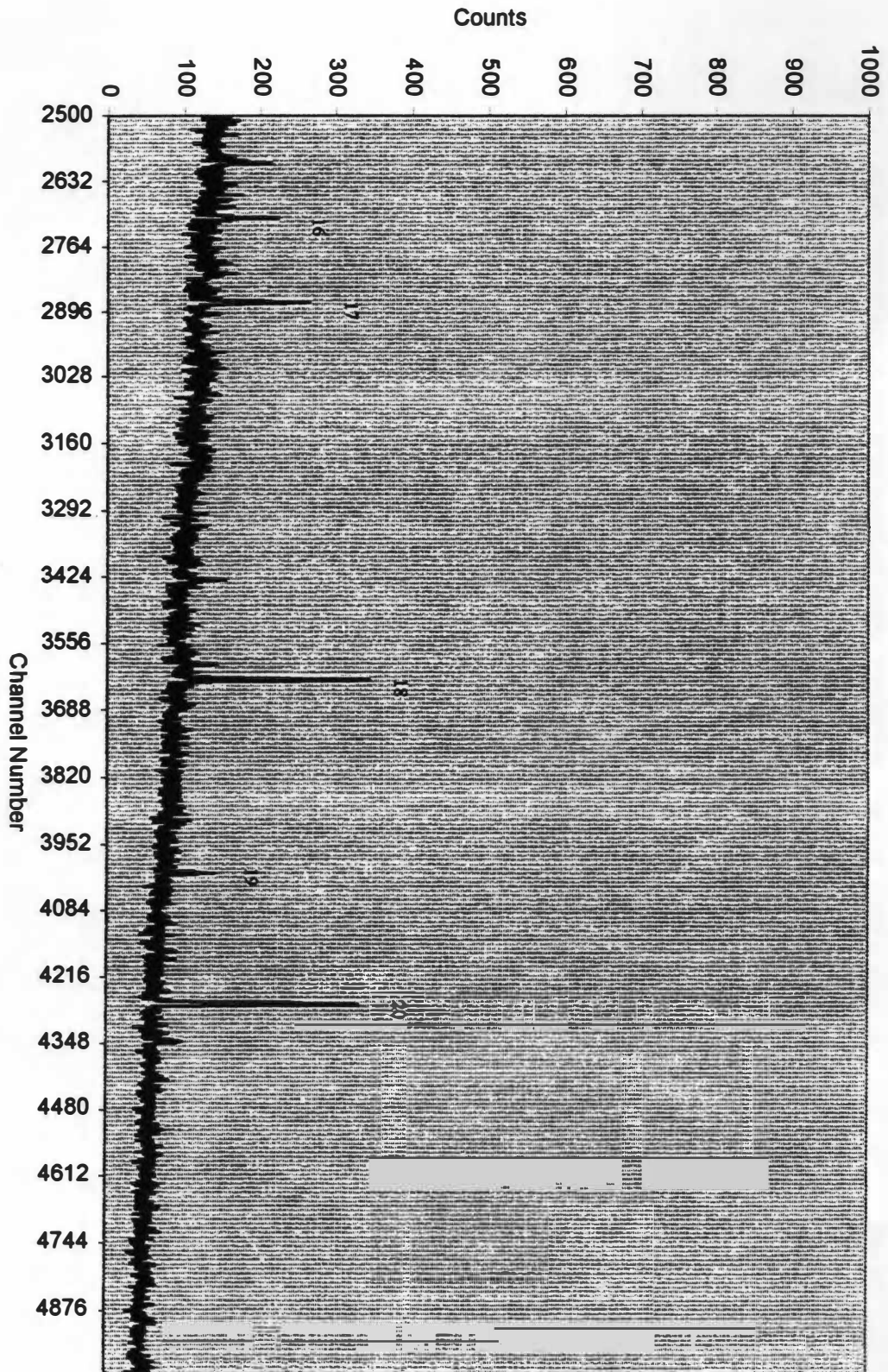


Figure 5-1. (Continued)

moisture saturated sample is shown, this is representative of the spectra observed during measurements. The key peaks for this spectrum are identified in Table 5-2, this includes all peaks observed on the measured spectra. The peak data for all of the spectra are listed in the Appendix, including all peak counts and calculated uncertainties.

Several peaks were used to quantify the concentrations of uranium-238, thorium-232, and potassium-40. For the determination of the potassium-40 concentration, the 1460 keV peak was used. To determine the thorium-232 concentration the 911 keV and 966 keV peaks of Ac-228 and the 580 keV peak of Tl-208 were used. For the uranium-238 concentration the 351 keV peak of Pb-214 and the 609, 1120 and 1764 keV peaks of Bi-214 were used to obtain a radium equivalent concentration (Guibert, 1991). The radium equivalent concentration refers to the nuclide concentration occurring after thorium-230 in the uranium decay chain. The 62 keV Th-234 is used to obtain a value that represents the original concentration of U-238. By taking the ratio of these two numbers, the presence or absence of any disequilibrium effects in the uranium-238 decay chain can be detected (Guibert, 1994). All of the peaks originating from nuclides in the above decay chains were used to check activity estimates.

Identification of all other peaks was attempted in order to check for evidence of the presence of nuclides outside of those contained in the three natural decay chains. There were multiple peaks that were not identifiable using any existing decay data. The existence of these unidentified peaks is common when dealing with environmental samples. This is

**Table 5-2. Peak identification for soil sample spectra**

<b>Peak Number</b>	<b>Energy (keV)</b>	<b>Radionuclide</b>
1	47	Pb-210
2	74	Pb-212/214
3	139	
4	185	U-235/Ra-226
5	238.6	Pb-212
6	295.2	Pb-214
7	351.9	Pb-214
8	510.8	Ann. Peak
9	557	
10	609.3	Bi-214
11	649.6	Bi-210
12	727.1	Bi-212
13	803	Bi-206
14	911	Ac-228
15	1460	K-40
16	1660	
17	1764	Bi-214
18	2224	
19	2458	Bi-214
20	2614	Tl-208

due largely to the presence of fission products, resulting from above ground nuclear testing.

After identification of the individual peaks, then each peak had to be defined and quantified. The Gamma Vision program has a peak search function that will automatically scan the spectrum and display ROI's with calculated peak information. There is a flaw with this due to the fact that some peaks are missed, and others are combined under a single ROI. Because of this the ROI's must be defined, or at least modified, manually. Identifying the peaks requires some judgement as to how much of the background to include, and to be able to delineate the beginning and ending of individual peaks. Also, because of the fact that spectral overlap existed in some areas, especially at the lower energies, the ROI was computed as the sum of these peaks. In the instances where the peaks were far enough apart, they were manually delineated from the adjacent peaks. Where this was not possible, peaks were treated as sum peaks, and identified that way in the Appendix.

None of the peaks subject to spectral overlap were used in calculations, with the exception of the 92.8 keV peak involving U-234 and Ac-228. This was used as a second peak to check for disequilibrium, and is discussed in the section 5.1.3.

### **5.1.2 Activity Calculations**

The activity calculations were performed using Equation 3.4, and obtaining an activity estimate for each peak. The activity estimates are an average of the values obtained from



the peaks of interest, as identified earlier, for each of the decay chains. An estimate was obtained for both the dry soil samples and the moisture saturated samples. In Table 5-3 the results of the calculations for each peak and each sample are detailed. In Table 5-4 the results of all calculations are summed and shown as totals for both the moisture-saturated counts and the dry counts.

Comparison of the activity estimates for the dry and moisture samples were compared for evidence of moisture attenuation. The results of the counting showed an overall attenuation of 18-24% due to the moisture content of the soil. This is illustrated in Table 5-4, where the total activities of both the moisture-saturated and dry samples are displayed. This agreed closely with published data that showed a typical value of between 20-25% (Aitken, 1985). Due to the fact that this soil was obtained from Western Kentucky, the data from the moisture-saturated was used to calculate the dose rate. This assumption is based on the geographic location of the site and is discussed in several publications including Aitken, 1985.

### **5.1.3 Disequilibrium Determination**

Measurements of the ratio of Th-234 to the Pb-214/Bi-214 concentration yielded evidence of disequilibrium in the uranium decay chain. However, the only peak suitable for obtaining good results was the 63 keV peak. This peak was recommended for use in this application by several sources (Guibert, 1994, Durrance, 1986, and Aitken, 1985), along with the 92 keV peak. The results of these calculations are shown in Table 5-5, and indicate a 20% excess of thorium-234. This would appear to show that there is some

**Table 5-3. Activity for each soil sample (Bq/g)**

<i>Decay Series</i>	<i>Peak Energy (keV)</i>	<i>1-dry</i>	<i>2-dry</i>	<i>3-dry</i>	<i>4-dry</i>	<i>5-dry</i>	<i>1-saturated</i>	<i>2-saturated</i>	<i>3-saturated</i>	<i>4-saturated</i>	<i>5-saturated</i>
Th-232	583	.0428	.0448	.0411	.0483	.0512	.0346	.0442	.0314	.0390	.0426
Th-232	911	.0431	.0471	.0411	.0470	.0489	.0379	.0420	.0361	.0394	.0352
Th-232	966	.050	.0587	.0433	.0478	.0467	.0442	.0458	.0393	.0365	.0480
Avg		.0453	.0502	.0418	.0477	.0489	.0389	.0440	.0356	.0383	.0419
U-238	351	.0525	.0579	.0551	.0534	.0507	.0447	.0435	.0429	.0430	.0426
U-238	609	.0535	.0534	.0498	.0494	.0505	.0405	.0444	.0401	.0419	.0398
U-238	1120	.0492	.0520	.0459	.0460	.0507	.0404	.0404	.0385	.0360	.0333
U-238	1764	.0446	.0452	.0540	.0485	.0423	.0438	.0420	.0366	.0380	.0349
Avg		.050	.0521	.0512	.0493	.0486	.0424	.0426	.0395	.0397	.0377
K-40	1460	.658	.665	.578	.641	.687	.558	.563	.524	.538	.524
Avg		.658	.665	.578	.641	.687	.558	.563	.524	.538	.524

**Table 5-4. Total activity of soil samples**

<b>Radionuclide</b>	<b>Activity of dry samples (Bq/g)</b>	<b>Activity of saturated samples (Bq/g)</b>	<b>Moisture Attenuation coefficient</b>
U-238	.0502	.0404	1.24
Th-232	.0468	.0397	1.18
K-40	.646	.541	1.19

**Table 5-5. Disequilibrium in uranium decay chain**

	<b>Calculated Activity (Bq/g)</b>
Th-234	.0478
After Rn-222	.0404
Disequilibrium Ratio	1.18

leaching, or radon loss, in the decay chain. This result was incorporated into the activity calculations. This was accomplished by accounting for the higher concentration of nuclides in the uranium decay chain prior to radon-222.

The 92 keV peak did not prove suitable for this application because of spectral overlap due to the presence of Ac-228 at the same energy. This requires an additional calculation to separate out this peak, introducing a source of error. In addition, the small peak size (approximately 1 count per minute) makes it difficult to obtain good data. The presence of the 90 keV peak also causes a problem in the accurate determination of background levels, because there is not adequate spacing between the peaks.

Previous work has indicated the same problems (Guibert, 1994 ), with regard to spectral overlap. In order to use the 92 keV peak for disequilibrium calculations an alpha spectrometry system should be used in conjunction with the gamma spectrometry system (Krbetschek, 1994).

## **5.2 Dose Rate Calculations using DRF's**

Using the activity levels calculated in Section 5.1, originating from the moisture saturated samples, the dose rate was calculated using dose rate factors. These factors were calculated using the methodology discussed in chapter 4. In order to accomplish these calculations the dose rate factors were calculated for each radionuclide in each decay chain. They were done using the dose rate factor formulas for immersion in air and replacing the air density with the density for soil, the soil density used was  $1.7 \text{ g/cm}^3$

(Aitken, 1985). This gives the dose rate in a soil medium that is assumed to be uniform and infinite in extent, with a uniform radionuclide concentration.

To calculate the dose rate factor for a quartz crystal buried in the soil, the ratios of the photon mass energy-absorption coefficients and electron mass stopping powers were calculated to obtain a correction factor for the photon and electron dose rate factors. These ratios change with the energies of the emitted radiation, so a weighted average must be obtained for each nuclide in order to obtain an accurate result. The equations used for calculating correction factors were equations 4.6 and 4.10 for photons and for electrons, respectively.

Once a dose rate factor was calculated, then the radionuclides for each decay chain were totaled to obtain a total dose rate factor for that particular decay chain. These values were then multiplied by the respective activities of the decay chain they belong to, and an absorbed dose was obtained. For example, all of the dose rate factors for all radionuclides in the uranium-238 decay chain were added up to obtain a single total for the entire chain, and then this value is multiplied by the calculated activity of uranium-238. This total represents the absorbed dose rate for the given concentration of uranium-238. This was repeated for thorium-232 and for potassium-40.

In Table 5-6, a breakdown of the dose rate factors by individual radionuclides is displayed. In Table 5-7, the dose rate factors are totaled for each decay chain and displayed according to the beta and gamma contributions. For each radionuclide the dose

**Table 5-6.** Calculated dose rate factors. For each radionuclide, for quartz immersed in soil (Gy/yr per Bq/cm<sup>3</sup>)

<b>Radionuclide</b>	<b>Electrons</b>	<b>Photons</b>
Pb-210	0	$1.83 \times 10^{-5}$
Bi-210	$1.09 \times 10^{-3}$	0
Pb-214	$6.17 \times 10^{-4}$	$7.00 \times 10^{-4}$
Bi-214	$1.78 \times 10^{-3}$	$4.13 \times 10^{-3}$
Ra-226	$1.89 \times 10^{-5}$	$9.45 \times 10^{-6}$
Th-234	$1.23 \times 10^{-4}$	$2.53 \times 10^{-5}$
Pa-234	$2.31 \times 10^{-3}$	$2.23 \times 10^{-5}$
Rn-222	0	$5.85 \times 10^{-7}$
Th-230	0	$3.60 \times 10^{-6}$
U-234	$4.32 \times 10^{-8}$	$3.85 \times 10^{-6}$
U-238	$1.66 \times 10^{-8}$	$4.86 \times 10^{-9}$
Tl-208	$1.50 \times 10^{-3}$	$9.18 \times 10^{-3}$
Pb-212	$2.65 \times 10^{-4}$	$3.54 \times 10^{-4}$
Bi-212	$1.24 \times 10^{-3}$	$4.94 \times 10^{-4}$
Ra-224	0	$2.30 \times 10^{-5}$
Ac-228	$1.02 \times 10^{-3}$	$2.34 \times 10^{-3}$
Ra-228	$2.66 \times 10^{-5}$	0
K-40	$1.22 \times 10^{-3}$	$4.29 \times 10^{-4}$

**Table 5-7. Dose Rate Factors listed for each decay chain (Gy/yr per Bq/cm<sup>3</sup>)**

<b>Decay Chain</b>	<b>Electrons</b>	<b>Photons</b>
U-238	$6.06 \times 10^{-3}$	$4.99 \times 10^{-3}$
Th-232	$4.04 \times 10^{-3}$	$6.87 \times 10^{-3}$
K-40	$1.22 \times 10^{-3}$	$4.29 \times 10^{-4}$



rate factor was calculated individually using the published intensities of the emitted gamma energies (Kocher, 1981). In the field of RDD thorium and uranium concentrations are normally referred to in parts per million (ppm), while potassium is referred to as a percentage. The published dose conversion factors relate an annual dose in Gray for each radionuclide concentration. For comparison, all the calculated dose rates were converted to the appropriate concentration for comparison. The results of this comparison are listed in Table 5-8, along with the percent difference.

### **5.3 Total Calculated Dose Rate**

The dose rate was calculated from the activity calculations and the dose rate factors using equation 4.3. Table 5-9 shows the total calculated dose rate in mGy/yr. This is in reasonable agreement with recently published studies (Becker, 1994), although calculated dose rates vary widely. It is apparent that several radionuclides contribute little to the overall dose, while a large portion of the dose originates with a few members of this decay chain. This leads to the conclusion that a rough estimate of the dose rate could be obtained by using just a handful of nuclides, while still obtaining a reasonably accurate number.

**Table 5-8.** Comparison of calculated DRF's to published dose conversion factors. Factors calculated for unit concentration indicated.

<b>Radionuclide</b>		<b>Calculated DRF's (<math>\mu\text{Gy/yr}</math>)</b>	<b>Published DCF's (<math>\mu\text{Gy/yr}</math>)</b>	<b>Percent Difference</b>
Th-232 (1 ppm)	Gamma	47.7	52.1	-9.2
	Beta	28.1	28.6	-1.7
U-238 (1 ppm)	Gamma	111	114	-2.7
	Beta	143	147	-2.8
K-40 (1%)	Gamma	230	202	+14.0
	Beta	654	676	-3.4

**Table 5-9. Total calculated dose rate (mGy/yr)**

<b>Decay Chain</b>	<b>Dose Rate</b>
U-238	.759
Th-232	.736
K-40	1.52
<b>Total</b>	<b>3.02</b>

## **Chapter 6**

### **Conclusions**

#### **6.1 Conclusions**

Results from this research indicate that the capability exists at UTK for the accurate determination of dose rate for an artifact buried in soil. In the determination of both the activity level of the soil, and the dose rate from the measured activity, results are obtained that are in agreement with previously published data. The use of the equipment and techniques described in this paper are reproducible, and allow for the future development of a laboratory where this type of work could be performed on a routine basis.

The use of the HPGe system produces spectra that are consistent from sample to sample and provide resolution that is adequate for environmental sampling. The only difficulty that can occur, using this system, is in differentiating energy peaks at low energies (below 100 keV), where spectral overlap is a problem. This does not limit the quantification of most key nuclides in the decay chains, but it can cause some problems with the accurate determination of disequilibrium in these decay chains.

The calculation of dose rate factors provides results that are in reasonable agreement with currently used data. Specifically the dose rate factors vary no more than 10% from published dose conversion data used in the field of TL dating, with the exception of

potassium-40. Because the other DRF's are in agreement with the published data, there could be a problem with the accuracy of the currently used K-40 gamma DCF.

## **6.2 Suggestions for Future Work**

In order to improve the accuracy of the results of this paper several issues could be considered. First, the determination of disequilibrium should be looked at using a combination of alpha spectrometry and gamma spectrometry. This could provide insight into whether the measurements made in this paper are adequate, or whether the combination of alpha and gamma spectrometry would significantly improve results.

A comparison of in-situ gamma spectrometry with in laboratory measurements would be another possible area of study. In particular a comparison using the same soil samples would provide an analysis of the validity of using in laboratory versus in-situ techniques.

Another area that can be explored would be to confirm, or improve on, the calculation of the dose rate factors. This could possibly be accomplished by running a Monte Carlo simulation to verify or improve on the results.

Finally, identification of the unknown gamma peaks could allow for a more accurate dose rate estimate. If most of these peaks did result from fission products from above ground testing, then the dose contribution of these peaks may be minimal relative to contributions of naturally occurring radionuclides.

## REFERENCES

## List of References

Aitken, M.J., (1994). Optical Dating: A Non-Specialist Review. *Quaternary Science Reviews*. Vol 13, P 503-508.

Aitken, M.J., (1985). Thermoluminescent Dating. Academic Press, London.

Becker, H., Goksu, H.Y., and Regulla, D.F., (1994). Combination of Archeomagnetism and Thermoluminescence for Precision Dating. *Quaternary Science Reviews*. Vol 13, p. 563-568.

Benko, Lazar, Horvath, Ferenc, (1989). Radiocarbon and Thermoluminescence Dating of Prehistoric Sites in Hungary and Yugoslavia. *Radiocarbon*. Vol 31, No. 3, p. 992-1002.

Durrance, E.M., (1986). *Radioactivity in Geology*. Ellis Horwood Limited, England.

EG&G Ortec (1990). *Gamma Vision Gamma-Ray Spectrum Analysis and MCA Emulation Software Users Manual*.

Federal Guidance Report No.12, (1993). *External Exposure to Radionuclides in Air, Water, and Soil*.

Geyh, Mebus A., and Schleicher, Helmut, (1990). Absolute Age Determination. Springer-Verlag, Berlin.

Guibert, P., Schvoerer, M., Etcheverry, B. and Ney, C., (1994). IXth Millenium B.C. Ceramics from Niger: Detection of a U-series Disequilibrium and TL Dating. *Quaternary Science Reviews*. Vol 13, p. 555-561.

Guibert, P. and Schvoerer, M. (1991). TL-dating: Low Background Gamma Spectrometry as a Tool for the Determination of the Annual Dose. *Nuclear Tracks and Radiation Measurements*. Vol 14, p. 155-161.

Hassan, A.M., Abdel-Wahab, M., Nada, A. and Khazbak A. (1997). Determination of Uranium and Thorium in Egyptian Monazite by Gamma-Ray Spectrometry. *Applied Radiation and Isotopes*. Vol. 48, No. 1, p. 149-152.

ICRU Report #53, (1994). Gamma Ray Spectrometry in the Environment.

Johnson, R.A., Stipp, J.J., and Tamers, M.A., (1986). Archaeologic Sherd Dating: Comparison of Thermoluminescence Dates by Beta Counting and Accelerator Techniques. *Radiocarbon*. Vol 28, No. 2A, p. 719-725.

Khaykovich, I.M., (1992). Some Theoretical Considerations of Natural Gamma-Ray Spectrometry Calibration. *Nuclear Geophysics*. Vol. 6, No.2, p. 205-212.

Knoll, Glenn F. (1989). Radiation Detection and Measurement, John Wiley & Sons, New York, New York.

Kocher, David C. (1981), Radioactive Decay Data Tables. U.S. Department of Energy.

Krbetschek, M.R., Rieser, U., Zoller, L., and Heinicke, J. (1994). Radioactive Disequilibria in Palaeodosimetric Dating of Sediments. *Radiation Measurements*. Vol. 23, No. 2/3, p. 485-489

MacDonald, J., Gibson, C.J., Fish, P.J. and Assinder, D.J., (1997). A Theoretical Comparison of Methods of Quantification of Radioactive Contamination in Soil Using *In Situ* Gamma Spectrometry. *Journal of Radiation Protection*. Vol 17, No. 1, p. 3-15.

Matternes, Hugh B., (1994). Wickliffe Mound Research Center Report #5

Mejdahl, V. and Wintle, A.G., (1984). Thermoluminescence Applied to Age Determination in Archeology and Geology. Thermoluminescence and Thermoluminescent Dosimetry Vol III. Y.S. Horowitz, Ed. p. 133-190, CRC Press, Boca Raton.

Miller, L.F., (1998). Personal Communication.

Nambi, K.S.V. and Aitken, M.J., (1986). Annual dose conversion factors for TL and ESR dating. *Archaeometry*, Vol 28, P 202-205.

Schilk, A.J., Abel, K.H., and Perkins, R.W., (1995). Characterization of Uranium Contamination in Surface Soils. *Journal of Environmental Radioactivity*. Vol. 26, p. 147-156.

Shenber, M.A., (1997). Measurement of Natural Radioactivity Levels in Soil in Tropoli. *Applied Radiation and Isotopes*. Vol. 48, No. 1, p. 147-148.

Sima, O. and Dovlete, C., (1997). Matrix Effects in the Activity Measurement of Environmental Samples-Implementation of Specific Corrections in a Gamma-Ray Spectrometry Analysis Program. *Applied Radiation and Isotopes*. Vol. 8, No. 1, p. 59-69.

Szegedi, S., El Khayati, N., Saaloki, I. And Reggoug, A., (1994). Determination of Uranium in Rock Samples by Natural Gamma-Ray Spectrometry. *Nuclear Geophysics*. Vol. 8, No. 5, p. 493-497.

Till, J.E., Meyer, H.R., (1983). Radiological Assessment: A Textbook on Environmental Dose Analysis. NUREG/CR-3332. U.S. Nuclear Regulatory Commission.



Turner, James E. (1992). Atoms, Radiation, and Radiation Protection, McGraw-Hill Inc., New York, New York.

Tyler, A.N., Sanderson, D.C.W., Scott, E.M., and Allyson, J.D., (1996). Accounting for Spatial Variability and Field of View in Environmental Gamma Ray Spectrometry. *Journal of Environmental Radioactivity*. Vol. 33, No. 3, p. 213-235.

## **APPENDIX**

# A-1 - Sample #1 saturated

Radionuclide	Gamma Energy (keV)	Emission Rate (y/sec)	Net Peak Count	Uncertainty	Net Count Rate (cps)	Efficiency (c/y)
Pb-210	47	0.64	1924	227	0.0111	0.01741
Pb-214	53.5	1.47	4298	191	0.0249	0.01692
Th-234	63	0.62	1737	99	0.0100	0.01615
	67	0.12	332	62	0.0019	0.01583
	70	102.88	25547	407	0.1478	0.001437
Tl-208	73	SAME	SAME	SAME	SAME	SAME
Pb-212/214	74	SAME	SAME	SAME	SAME	SAME
Pb-212/214	77	SAME	SAME	SAME	SAME	SAME
Tl-208	84	49.01	14534	540	0.0841	0.001716
Pb-212/214	87.2	SAME	SAME	SAME	SAME	SAME
Pb-212	90.1	SAME	SAME	SAME	SAME	SAME
Ac-228/Th-234	93	SAME	SAME	SAME	SAME	SAME
Ac-228	129	0.42	864	262	0.0050	0.01203
	139	1.35	2596	228	0.0150	0.01110
Ac-228	154	0.13	213	121	0.0012	0.00969
	159	0.38	666	374	0.0039	0.01019
	162	SAME	SAME	SAME	SAME	SAME
	174	0.19	307	160	0.0018	0.00959
Ra-226/U-235	185	1.89	3002	243	0.0174	0.00920
Ac-228	199	1.33	1881	256	0.0109	0.00819
Ac-228	209	0.67	1088	154	0.0063	0.00936
Pb-212	238.6	6.15	10928	325	0.0632	0.01029
Pb-214	241.9	SAME	SAME	SAME	SAME	SAME
Ac-228	270	0.45	559	157	0.0032	0.00726
Tl-208	277.3	2.52	3039	121	0.0176	0.00698
Pb-214	295.2	4.16	4676	146	0.0271	0.00650
Ac-228	328	0.57	582	91	0.0034	0.00596
Ac-228	338.3	1.30	1559	181	0.0090	0.00692
Pb-214	351.9	5.45	5334	184	0.0309	0.00566
	415.5	0.45	388	144	0.0022	0.00495
Ac-228	463	0.79	687	131	0.0040	0.00503
	498	0.61	449	122	0.0026	0.00427
Ann. Peak	510.8	41.67	30106	224	0.1742	0.00418
	536	0.45	310	114	0.0018	0.00402
	557	50.41	33915	214	0.1963	0.00389
	567	0.92	609	87	0.0035	0.00384
	574	2.75	1802	91	0.0104	0.00380
Tl-208	583.1	3.61	2492	97	0.0144	0.004
	594	2.08	1328	125	0.0077	0.00369
Bi-214	609.3	6.49	4053	227	0.0235	0.00362

**A-1 – (Continued)**

<b>Radionuclide</b>	<b>Gamma Energy (keV)</b>	<b>Emission Rate (y/sec)</b>	<b>Net Peak Count</b>	<b>Uncertainty</b>	<b>Net Count Rate (cps)</b>	<b>Efficiency (c/y)</b>
	616	1.04	646	94	0.0037	0.00358
Bi-210	649.6	9.02	5343	128	0.0309	0.00343
	692	2.58	1454	115	0.0084	0.00326
	706	0.73	406	113	0.0023	0.00320
Bi-212	727.2	3.11	1677	91	0.0097	0.00313
	746	0.92	484	94	0.0028	0.00306
Bi-214	766.8	0.98	509	93	0.0029	0.00299
Ac-228	794	0.36	183	81	0.0011	0.00291
	801	5.90	2946	110	0.0170	0.00289
Bi-206	803	SAME	SAME	SAME	SAME	SAME
Tl-208	860	0.80	400	80	0.0023	0.0029
	867	0.74	345	88	0.0020	0.00271
Bi-206	881	0.69	319	84	0.0018	0.00267
	897	0.89	403	85	0.0023	0.00263
Ac-228	911	3.63	1737	92	0.0101	0.00277
Bi-214	933	0.36	160	80	0.0009	0.00255
Ac-228	964/969.1	3.24	1441	148	0.0083	0.00257
	1013	0.97	402	79	0.0023	0.00239
	1097	0.35	137	51	0.0008	0.00224
Bi-214	1120.2	2.10	801	81	0.0046	0.00220
	1208.3	2.54	911	76	0.0053	0.00208
Bi-214	1238.1	0.63	222	62	0.0013	0.00204
	1283	1.31	447	66	0.0026	0.00198
	1292	0.84	287	69	0.0017	0.00197
	1300	1.34	453	93	0.0026	0.00196
	1304	SAME	SAME	SAME	SAME	SAME
	1363	2.46	804	70	0.0047	0.00189
	1369	0.49	160	54	0.0009	0.00188
Bi-214	1377.1	0.48	157	53	0.0009	0.00187
	1398	2.44	782	67	0.0045	0.00185
K-40	1460	20.63	6392	108	0.0370	0.00179
	1488	1.69	516	74	0.0030	0.00177
DE Tl-208	1592	N/A	370	80	0.0021	N/A
Bi-214	1764.5	2.39	643	56	0.0037	0.00156
	2102	1.70	404	64	0.0023	0.00137
	2224	6.34	1448	70	0.0084	0.00132
Bi-214	2458	1.84	392	84	0.0023	0.00123
Tl-208	2614	8.63	1595	88	0.0092	0.00107
	2662	1.52	307	55	0.0018	0.00117

A-2 - Sample #2 saturated

Radionuclide	Gamma Energy (keV)	Emission Rate (y/sec)	Net Peak Count	Uncertainty	Net Count Rate (cps)	Efficiency (c/y)
Pb-210	47	0.61	1825	138	0.010561	0.01741
Pb-214	53.5	1.56	4550	168	0.026331	0.01692
Th-234	63	0.64	1788	123	0.010347	0.01615
	67	0.14	376	62	0.002176	0.01583
	70	86.23	21411	344	0.123906	0.001437
Tl-208	73	SAME	SAME	SAME	SAME	SAME
Pb-212/214	74	SAME	SAME	SAME	SAME	SAME
Pb-212/214	77	SAME	SAME	SAME	SAME	SAME
Tl-208	84	4.63	13728	517	0.079444	0.01716
Pb-212/214	87.1	SAME	SAME	SAME	SAME	SAME
Pb-212	90.1	SAME	SAME	SAME	SAME	SAME
Ac-228/Th-234	93	SAME	SAME	SAME	SAME	SAME
Ac-228	129	0.42	864	262	0.005000	0.01203
	139	1.39	2669	130	0.015446	0.01110
Ac-228	154	0.27	457	119	0.002645	0.00969
	159	0.93	1635	292	0.009462	0.01019
	162	SAME	SAME	SAME	SAME	SAME
	174	0.46	759	178	0.004392	0.00959
Ra-226/U-235	185	1.86	2953	298	0.017089	0.00920
Ac-228	199	1.46	2062	199	0.011933	0.00819
Ac-228	209	0.67	1078	227	0.006238	0.00936
Pb-212	238.6	5.93	10542	403	0.061007	0.01029
Pb-214	241.9	SAME	SAME	SAME	SAME	SAME
Ac-228	270	0.38	474	139	0.002743	0.00726
Tl-208	277.3	0.42	512	154	0.002963	0.00698
Pb-214	295.2	3.79	4258	315	0.024641	0.00650
Ac-228	328	0.53	543	100	0.003142	0.00596
Ac-228	338.3	1.30	1560	180	0.009028	0.00692
Pb-214	351.9	5.07	4964	183	0.028727	0.00566
	415.5	0.37	317	117	0.001834	0.00495
Ac-228	463	0.71	620	131	0.003588	0.00503
	476	0.24	184	70	0.001065	0.00443
	498	0.38	283	91	0.001638	0.00427
Ann. Peak	510.84	41.82	30216	223	0.174861	0.00418
	535.5	0.62	429	113	0.002483	0.00402
	557	50.27	33820	214	0.195718	0.00389
	567	0.55	365	76	0.002112	0.00384
	574	2.73	1794	91	0.010382	0.00380
Tl-208	583.1	4.21	2907	112	0.016823	0.004
	594	2.22	1417	124	0.008200	0.00369

**A-2 – (Continued)**

<b>Radionuclide</b>	<b>Gamma Energy (keV)</b>	<b>Emission Rate (y/sec)</b>	<b>Net Peak Count</b>	<b>Uncertainty</b>	<b>Net Count Rate (cps)</b>	<b>Efficiency (c/y)</b>
Bi-214	609.3	6.44	4022	125	0.023275	0.00362
	616	0.76	468	103	0.002708	0.00358
Bi-210	649.6	8.83	5234	129	0.030289	0.00343
	692	2.31	1300	117	0.007523	0.00326
	706	0.95	528	110	0.003056	0.00320
Bi-212	727.2	2.77	1497	90	0.008663	0.00313
	746	0.92	484	94	0.002801	0.00306
Bi-214	766.8	0.70	364	76	0.002106	0.00299
	801	5.98	2983	145	0.017263	0.00289
Bi-206	803	SAME	SAME	SAME	SAME	SAME
Tl-208	860	0.41	207	66	0.001198	0.0029
	867	0.74	345	88	0.001997	0.00271
Bi-206	881	0.65	298	78	0.001725	0.00267
	897	0.71	322	79	0.001863	0.00263
Ac-228	911	3.65	1747	90	0.010110	0.00277
Bi-214	933	0.59	261	80	0.001510	0.00255
Ac-228	964/969.1	3.04	1350	147	0.007813	0.00257
	1097	0.71	275	65	0.001591	0.00224
Bi-214	1120.2	1.91	727	68	0.004207	0.00220
	1208.3	2.30	825	63	0.004774	0.00208
Bi-214	1238.1	0.58	203	86	0.001175	0.00204
	1283	1.10	375	82	0.002170	0.00198
	1292	0.36	121	71	0.000700	0.00197
	1363	2.81	917	66	0.005307	0.00189
	1369	0.58	190	48	0.001100	0.00188
Bi-214	1377.1	0.69	223	70	0.001291	0.00187
	1398	2.47	791	67	0.004578	0.00185
K-40	1460	18.92	5863	106	0.033929	0.00179
	1488	1.57	479	72	0.002772	0.00177
DE Tl-208	1592	0.99	287	67	0.001661	0.00168
	1660	1.68	472	77	0.002731	0.00163
Bi-214	1764.5	2.08	559	77	0.003235	0.00156
	2102	2.16	512	136	0.002963	0.00137
	2224	6.06	1383	78	0.008003	0.00132
Bi-214	2458	1.84	392	84	0.002269	0.00123
Tl-208	2614	8.34	1542	87	0.008924	0.00107
	2662	2.02	409	56	0.002367	0.00117

**A-3 - Sample #3 saturated**

<b>Radionuclide</b>	<b>Gamma Energy (keV)</b>	<b>Emission Rate (y/sec)</b>	<b>Net Peak Count</b>	<b>Uncertainty</b>	<b>Net Count Rate (cps)</b>	<b>Efficiency (c/y)</b>
Pb-210	47	0.58	1738	203	0.010058	0.01741
Pb-214	53.5	1.53	4480	169	0.025926	0.01692
Th-234	63	0.68	1885	124	0.010909	0.01615
	67	0.15	413	63	0.002390	0.01583
	70	10.95	27200	430	0.157407	0.01437
Tl-208	73	SAME	SAME	SAME	SAME	SAME
Pb-212/214	74	SAME	SAME	SAME	SAME	SAME
Pb-212/214	77	SAME	SAME	SAME	SAME	SAME
Tl-208	84	5.12	15188	502	0.087894	0.01716
Pb-212/214	87.1	SAME	SAME	SAME	SAME	SAME
Pb-212	90.1	SAME	SAME	SAME	SAME	SAME
Ac-228/Th-234	93	SAME	SAME	SAME	SAME	SAME
	105	0.08	173	266	0.001001	0.01302
Ac-228	129	0.30	627	266	0.003628	0.01203
	139	1.37	2626	112	0.015197	0.01110
Ac-228	154	0.16	275	991	0.001591	0.00969
	159	0.72	1259	278	0.007286	0.01019
	162	SAME	SAME	SAME	SAME	SAME
	174	0.24	405	258	0.002344	0.00959
Ra-226/U-235	185	2.14	3405	189	0.019705	0.00920
Ac-228	199	1.42	2014	221	0.011655	0.00819
Ac-228	209	0.50	807	155	0.004670	0.00936
Pb-212	238.6	6.90	12276	347	0.071042	0.01029
Pb-214	241.9	SAME	SAME	SAME	SAME	SAME
Ac-228	270	0.60	752	174	0.004352	0.00726
Tl-208	277.3	0.48	581	138	0.003362	0.00698
Pb-214	295.2	3.09	3474	117	0.020104	0.00650
Ac-228	328	0.74	766	118	0.004433	0.00596
Ac-228	338.3	1.49	1785	181	0.010330	0.00692
Pb-214	351.9	6.43	6289	188	0.036395	0.00566
Ac-228	463	0.82	716	108	0.004144	0.00503
	476	0.36	274	128	0.001586	0.00443
	498	0.60	439	122	0.002541	0.00427
Ann. Peak	510.8	N/A	30064	223	0.173981	N/A
	536	0.37	260	114	0.001505	0.00402
	557	51.10	34375	215	0.198929	0.00389
	567	1.03	683	96	0.003953	0.00384
	574	2.90	1904	83	0.011019	0.00380
Tl-208	583.1	3.93	2716	96	0.015718	0.004
	594	2.19	1399	124	0.008096	0.00369



**A-3 – (Continued)**

<b>Radionuclide</b>	<b>Gamma Energy (keV)</b>	<b>Emission Rate (y/sec)</b>	<b>Net Peak Count</b>	<b>Uncertainty</b>	<b>Net Count Rate (cps)</b>	<b>Efficiency (c/y)</b>
Bi-214	609.3	7.47	4665	130	0.026997	0.00362
	616	0.85	525	103	0.003038	0.00358
Bi-210	649.6	9.17	5435	129	0.031453	0.00343
	692	2.12	1194	117	0.006910	0.00326
	706	0.87	482	110	0.002789	0.00320
Bi-212	727.2	3.23	1744	92	0.010093	0.00313
	746	1.32	696	95	0.004028	0.00306
Bi-214	766.8	0.65	336	93	0.001944	0.00299
	786	0.55	281	73	0.001626	0.00293
Ac-228	794	0.95	477	73	0.002760	0.00291
	801	6.10	3044	116	0.017616	0.00289
Bi-206	803	SAME	SAME	SAME	SAME	SAME
Tl-208	860	0.63	316	89	0.001829	0.0029
	867	0.45	211	81	0.001221	0.00271
Bi-206	881	0.36	166	55	0.000961	0.00267
	897	0.71	324	77	0.001875	0.00263
Ac-228	911	4.03	1928	93	0.011157	0.00277
	919	0.38	168	68	0.000972	0.00258
Bi-214	933	0.43	190	103	0.001100	0.00255
Ac-228	964/969.1	3.35	1489	149	0.008617	0.00257
	1000	0.66	273	79	0.001580	0.00241
	1013	0.47	195	66	0.001128	0.00239
	1097	0.68	262	94	0.001516	0.00224
Bi-214	1120.2	2.37	903	70	0.005226	0.00220
	1208.3	2.24	805	63	0.004659	0.00208
Bi-214	1238.1	0.99	350	69	0.002025	0.00204
	1283	1.35	463	82	0.002679	0.00198
	1292	0.81	276	71	0.001597	0.00197
	1304	0.43	146	39	0.000845	0.00196
	1363	2.82	920	71	0.005324	0.00189
	1369	0.48	155	42	0.000897	0.00188
Bi-214	1377.1	1.05	339	75	0.001962	0.00187
	1398	2.18	698	80	0.004039	0.00185
K-40	1460	22.62	7007	110	0.040550	0.00179
	1488	1.41	430	74	0.002488	0.00177
DE Tl-208	1592	1.14	331	88	0.001916	0.00168
	1660	2.02	568	77	0.003287	0.00163
Bi-214	1764.5	2.33	626	78	0.003623	0.00156
	2102	1.11	264	134	0.001528	0.00137
	2224	5.59	1276	74	0.007384	0.00132
Bi-214	2458	1.95	416	82	0.002407	0.00123
Tl-208	2614	9.07	1677	90	0.009705	0.00107
	2662	1.45	294	77	0.001701	0.00117



# A4 - Sample #4 saturated

Radionuclide	Gamma Energy (keV)	Emission Rate (y/sec)	Net Peak Count	Uncertainty	Net Count Rate (cps)	Efficiency (c/y)
Pb-210	47	0.60	1814	201	0.010498	0.01741
Pb-214	53.5	1.26	3685	230	0.021325	0.01692
Th-234	63	0.65	1803	124	0.010434	0.01615
	67	0.05	140	61	0.000810	0.01583
	69	7.41	18399	379	0.106476	0.01437
Tl-208	73	SAME	SAME	SAME	SAME	SAME
Pb-212/214	74	SAME	SAME	SAME	SAME	SAME
Pb-212/214	77	SAME	SAME	SAME	SAME	SAME
Tl-208	84	5.43	16100	515	0.093171	0.01716
Pb-212/214	87.1	SAME	SAME	SAME	SAME	SAME
Pb-212	90.1	SAME	SAME	SAME	SAME	SAME
Ac-228/Th-234	93	SAME	SAME	SAME	SAME	SAME
Ac-228	129	0.30	614	262	0.003553	0.01203
	139	1.32	2525	167	0.014612	0.01110
Ac-228	154	0.06	95	50	0.000550	0.00969
	159	0.89	1566	272	0.009063	0.01019
	162	SAME	SAME	SAME	SAME	SAME
	174	0.11	182	252	0.001053	0.00959
Ra-226/U-235	185	1.93	3071	147	0.017772	0.00920
Ac-228	199	1.53	2163	251	0.012517	0.00819
Ac-228	209	0.56	908	207	0.005255	0.00936
Pb-212	238.6	6.87	12210	260	0.070660	0.01029
Pb-214	241.9	SAME	SAME	SAME	SAME	SAME
Ac-228	270	0.53	669	154	0.003872	0.00726
Tl-208	277	0.59	714	151	0.004132	0.00698
Pb-214	295.2	2.81	3160	113	0.018287	0.00650
Ac-228	327	0.84	870	176	0.005035	0.00596
Ac-228	338.3	1.57	1880	103	0.010880	0.00692
Pb-214	351.9	6.27	6135	180	0.035503	0.00566
	415.5	0.53	450	303	0.002604	0.00495
Ac-228	463	0.78	676	127	0.003912	0.00503
	476	0.18	139	44	0.000804	0.00443
	498	0.25	181	109	0.001047	0.00427
Ann. Peak	510.8		27893	215	0.161418	N/A
	536	0.29	200	61	0.001157	0.00402
	557	45.89	30871	206	0.178652	0.00389
	567	0.97	646	94	0.003738	0.00384
	574	2.50	1641	82	0.009497	0.00380
Tl-208	583.1	4.65	3217	104	0.018617	0.004
	594	1.94	1239	121	0.007170	0.00369

**A-4 – (Continued)**

<b>Radionuclide</b>	<b>Gamma Energy (keV)</b>	<b>Emission Rate (y/sec)</b>	<b>Net Peak Count</b>	<b>Uncertainty</b>	<b>Net Count Rate (cps)</b>	<b>Efficiency (c/y)</b>
Bi-214	609.3	7.60	4748	127	0.027477	0.00362
	616	0.60	369	92	0.002135	0.00358
Bi-210	649.6	8.18	4845	138	0.028038	0.00343
	692	1.91	1077	112	0.006233	0.00326
	706	1.08	595	108	0.003443	0.00320
Bi-212	727.2	3.23	1745	105	0.010098	0.00313
	746	1.17	621	92	0.003594	0.00306
Bi-214	766.8	0.87	450	74	0.002604	0.00299
Ac-228	794	0.52	263	80	0.001522	0.00291
	801	5.75	2868	113	0.016597	0.00289
Bi-206	803	SAME	SAME	SAME	SAME	SAME
Tl-208	860	0.67	338	80	0.001956	0.0029
	867	0.81	381	72	0.002205	0.00271
Bi-206	881	0.44	202	61	0.001169	0.00267
	897	1.01	458	93	0.002650	0.00263
Ac-228	911	4.27	2044	91	0.011829	0.00277
Bi-214	933	0.51	223	73	0.001291	0.00255
Ac-228	964/969.1	3.04	1348	132	0.007801	0.00257
	993	0.32	134	77	0.000775	0.00243
	1013	0.55	227	71	0.001314	0.00239
	1097	0.62	239	70	0.001383	0.00224
Bi-214	1120.3	2.13	811	68	0.004693	0.00220
	1208.3	2.67	956	75	0.005532	0.00208
Bi-214	1238.1	0.72	253	86	0.001464	0.00204
	1282.4	1.20	412	79	0.002384	0.00198
	1292	0.47	161	44	0.000932	0.00197
	1363	2.73	891	68	0.005156	0.00189
	1369	0.43	140	40	0.000810	0.00188
Bi-214	1376	0.56	181	41	0.001047	0.00188
	1398	2.31	741	76	0.004288	0.00185
K-40	1460	22.63	7010	111	0.040567	0.00179
	1488	1.15	350	72	0.002025	0.00177
Bi-214	1592	0.74	214	80	0.001238	0.00168
	1660	1.65	465	75	0.002691	0.00163
Bi-214	1764.5	2.35	633	67	0.003663	0.00156
	2102	0.86	204	82	0.001181	0.00137
	2224	5.45	1244	64	0.007199	0.00132
Bi-214	2458	1.76	375	76	0.002170	0.00123
Tl-208	2614	9.49	1754	84	0.010150	0.00107
	2662	0.97	196	41	0.001134	0.00117

# **A-5 - Sample #5 saturated**

Radionuclide	Gamma Energy (keV)	Emission Rate (y/sec)	Net Peak Count	Uncertainty	Net Count Rate (cps)	Efficiency (c/y)
Pb-210	47	0.52	1568	219	0.009074	0.01741
Pb-214	53.5	1.26	3669	207	0.021233	0.01692
Th-234	63	0.69	1916	122	0.011088	0.01615
	67	0.10	269	61	0.001557	0.01583
	70	7.11	17659	372	0.102193	0.01437
Tl-208	73	SAME	SAME	SAME	SAME	SAME
Pb-212/214	74	SAME	SAME	SAME	SAME	SAME
Pb-212/214	77	SAME	SAME	SAME	SAME	SAME
Tl-208	84	5.00	14824	508	0.085787	0.01716
Pb-212/214	87.2	SAME	SAME	SAME	SAME	SAME
Pb-212	90.1	SAME	SAME	SAME	SAME	SAME
Ac-228/Th-234	93	SAME	SAME	SAME	SAME	SAME
Ac-228	129	0.31	642	219	0.003715	0.01203
	139	1.23	2352	147	0.013611	0.01110
Ac-228	154	0.17	284	97	0.001644	0.00969
	159	0.56	978	252	0.005660	0.01019
	162	SAME	SAME	SAME	SAME	SAME
Ra-226/U-235	185	2.16	3433	256	0.019867	0.00920
Ac-228	199	1.59	2250	176	0.013021	0.00819
Ac-228	209	0.59	959	224	0.005550	0.00936
Pb-212	238.6	6.17	10976	225	0.063519	0.01029
Pb-214	241.9	SAME	SAME	SAME	SAME	SAME
Ac-228	270	0.73	921	153	0.005330	0.00726
Tl-208	277.3	0.62	751	149	0.004346	0.00698
Pb-214	295.2	2.63	2953	112	0.017089	0.00650
Ac-228	328	0.50	513	130	0.002969	0.00596
Ac-228	338.3	1.43	1705	176	0.009867	0.00692
Pb-214	351.9	5.84	5715	180	0.033073	0.00566
	415.5	0.31	268	139	0.001551	0.00495
Ac-228	463	0.56	488	93	0.002824	0.00503
	476	0.25	194	68	0.001123	0.00443
	498	0.16	117	54	0.000677	0.00427
Ann. Peak	510.8	N/A	27655	214	0.160041	N/A
	521	0.37	262	110	0.001516	0.00411
	536	0.29	202	62	0.001169	0.00402
	557	46.36	31189	206	0.180492	0.00389
	567	1.11	737	94	0.004265	0.00384
	574	2.50	1638	79	0.009479	0.00380
Tl-208	583.1	4.23	2921	102	0.016904	0.004
	594	2.26	1442	122	0.008345	0.00369

**A-5 – (Continued)**

<b>Radionuclide</b>	<b>Gamma Energy (keV)</b>	<b>Emission Rate (y/sec)</b>	<b>Net Peak Count</b>	<b>Uncertainty</b>	<b>Net Count Rate (cps)</b>	<b>Efficiency (c/y)</b>
Bi-214	609.3	6.79	4240	124	0.024537	0.00362
	616	0.87	541	91	0.003131	0.00358
Bi-210	649.6	8.80	5213	137	0.030168	0.00343
	692	1.90	1068	112	0.006181	0.00326
	706	1.00	552	108	0.003194	0.00320
Bi-212	727.2	2.88	1553	104	0.008987	0.00313
	746	1.14	603	91	0.003490	0.00306
Bi-214	766.8	0.39	202	90	0.001169	0.00299
Ac-228	794	0.46	230	64	0.001331	0.00291
	801	5.46	2725	134	0.015770	0.00289
Bi-206	803	SAME	SAME	SAME	SAME	SAME
Tl-208	860	0.60	303	73	0.001753	0.0029
	867	0.58	269	63	0.001557	0.00271
Bi-206	881	0.55	253	83	0.001464	0.00267
	897	0.83	377	82	0.002182	0.00263
Ac-228	911	3.59	1718	90	0.009942	0.00277
Ac-228	964/969.1	3.75	1665	143	0.009635	0.00257
	1013	0.37	151	78	0.000874	0.00239
	1097	0.56	218	56	0.001262	0.00224
Bi-214	1120.2	1.60	610	92	0.003530	0.00220
	1208	2.42	867	67	0.005017	0.00208
Bi-214	1238.1	0.71	250	80	0.001447	0.00204
	1283	0.85	291	63	0.001684	0.00198
	1292	0.37	125	73	0.000723	0.00197
	1300	0.79	267	44	0.001545	0.00196
	1304	0.64	216	49	0.001250	0.00196
	1363	2.42	789	53	0.004566	0.00189
	1369	0.35	115	42	0.000666	0.00188
Bi-214	1377.1	0.49	159	73	0.000920	0.00187
	1398	2.29	732	66	0.004236	0.00185
K-40	1460	20.70	6412	107	0.037106	0.00179
	1488	1.67	511	71	0.002957	0.00177
DE Tl-208	1592	1.34	389	74	0.002251	0.00168
	1660	1.11	312	76	0.001806	0.00163
Bi-214	1764.5	2.03	546	76	0.003160	0.00156
	1778	0.70	188	70	0.001088	0.00155
	2102	2.36	559	71	0.003235	0.00137
	2224	5.50	1255	86	0.007263	0.00132
	2458	1.28	273	78	0.001580	0.00123
Tl-208	2614	8.99	1662	86	0.009618	0.00107
	2662	0.86	173	45	0.001001	0.00117

A-6 - Sample #1 dry

Radionuclide	Gamma Energy (keV)	Emission Rate (y/sec)	Net Peak Count	Uncertainty	Net Count Rate (cps)	Efficiency (c/y)
Pb-210	47	0.70	2116	221	0.012245	0.01741
Pb-214	53.5	1.29	3772	183	0.021829	0.01692
Th-234	63	0.66	1852	120	0.010718	0.01615
	67	0.08	216	60	0.001250	0.01583
	70	10.12	25117	402	0.145353	0.01437
Tl-208	73	SAME	SAME	SAME	SAME	SAME
Pb-212/214	74	SAME	SAME	SAME	SAME	SAME
Pb-212/214	77	SAME	SAME	SAME	SAME	SAME
Tl-208	84	5.06	15004	574	0.086829	0.01716
Pb-212/214	87.2	SAME	SAME	SAME	SAME	SAME
Pb-212	90.1	SAME	SAME	SAME	SAME	SAME
Ac-228/Th-234	93	SAME	SAME	SAME	SAME	SAME
Ac-228	129	0.41	857	199	0.004959	0.01203
	139	1.16	2220	221	0.012847	0.01110
Ac-228	154	0.20	333	97	0.001927	0.00969
	159	0.41	719	251	0.004161	0.01019
	162	SAME	SAME	SAME	SAME	SAME
	174	0.40	657	250	0.003802	0.00959
Ra-226/U-235	185	1.91	3039	255	0.017587	0.00920
Ac-228	199	1.37	1934	176	0.011192	0.00819
Ac-228	209	0.45	733	169	0.004242	0.00936
Pb-212	238.6	6.67	11865	271	0.068663	0.01029
Pb-214	241.9	SAME	SAME	SAME	SAME	SAME
Ac-228	270	0.50	621	154	0.003594	0.00726
Tl-208	277.3	0.52	626	150	0.003623	0.00698
Pb-214	295.2	2.82	3173	128	0.018362	0.00650
Ac-228	328	0.65	670	176	0.003877	0.00596
Ac-228	338.3	1.46	1743	161	0.010087	0.00692
Pb-214	351.9	5.75	5626	180	0.032558	0.00566
	415.5	0.42	361	140	0.002089	0.00495
Ac-228	463	0.93	807	116	0.004670	0.00503
	476	0.20	150	80	0.000868	0.00443
	498	0.40	292	118	0.001690	0.00427
Ann. Peak	510.8	N/A	28163	217	0.162980	N/A
	536	0.53	369	111	0.002135	0.00402
	557	47.08	31670	208	0.183275	0.00389
	567	0.34	225	75	0.001302	0.00384
	574	2.86	1874	89	0.010845	0.00380
Tl-208	583.1	3.84	2653	94	0.015353	0.004
	594	2.03	1295	119	0.007494	0.00369



**A-6 – (Continued)**

<b>Radionuclide</b>	<b>Gamma Energy (keV)</b>	<b>Emission Rate (y/sec)</b>	<b>Net Peak Count</b>	<b>Uncertainty</b>	<b>Net Count Rate (cps)</b>	<b>Efficiency (c/y)</b>
Bi-214	609.3	7.31	4565	134	0.026418	0.00362
	616	0.65	405	90	0.002344	0.00358
Bi-210	649.6	8.44	5001	124	0.028941	0.00343
	692	1.69	952	112	0.005509	0.00326
	706	0.98	542	80	0.003137	0.00320
Bi-212	727.2	2.88	1556	104	0.009005	0.00313
	746	0.94	498	92	0.002882	0.00306
Bi-214	766.8	0.47	241	83	0.001395	0.00299
Ac-228	794	0.44	219	71	0.001267	0.00291
	801	5.73	2859	120	0.016545	0.00289
Bi-206	803	SAME	SAME	SAME	SAME	SAME
Tl-208	860	0.28	140	49	0.000810	0.0029
	867	0.50	232	86	0.001343	0.00271
Bi-206	881	0.30	139	61	0.000804	0.00267
	897	0.71	325	83	0.001881	0.00263
Ac-228	911	3.52	1683	88	0.009740	0.00277
Bi-214	933	0.29	126	79	0.000729	0.00255
Ac-228	964/969.1	3.16	1402	137	0.008113	0.00257
	1097	0.65	253	89	0.001464	0.00224
Bi-214	1120.2	2.19	834	92	0.004826	0.00220
	1208.3	2.85	1021	73	0.005909	0.00208
Bi-214	1238.1	0.92	322	85	0.001863	0.00204
	1283	1.48	507	74	0.002934	0.00198
	1292	1.19	405	62	0.002344	0.00197
	1300	0.51	172	34	0.000995	0.00196
	1304	0.36	121	54	0.000700	0.00196
	1363	2.70	882	78	0.005104	0.00189
	1369	0.67	218	57	0.001262	0.00188
Bi-214	1377.1	0.85	276	62	0.001597	0.00187
	1398	2.33	747	76	0.004323	0.00185
K-40	1460	20.75	6429	107	0.037205	0.00179
	1488	1.83	558	72	0.003229	0.00177
DE Tl-208	1592	0.38	109	39	0.000631	0.00168
	1660	1.77	497	74	0.002876	0.00163
Bi-214	1764	2.07	556	63	0.003218	0.00156
	2102	1.18	281	106	0.001626	0.00137
	2224	5.71	1304	86	0.007546	0.00132
	2458	2.49	530	77	0.003067	0.00123
Tl-208	2614	8.51	1573	85	0.009103	0.00107
	2662	1.12	227	190	0.001314	0.00117

### A-7 - Sample #2 dry

Radionuclide	Gamma Energy (keV)	Emission Rate (y/sec)	Net Peak Count	Uncertainty	Net Count Rate (cps)	Efficiency (c/y)
Pb-210	47	0.44	1326	178	0.007674	0.01741
Pb-214	53.5	1.39	4062	22	0.023507	0.01692
Th-234	63	1.13	3163	275	0.018304	0.01615
	67	0.61	1682	96	0.009734	0.01583
	70	0.08	227	59	0.001314	0.01559
Tl-208	73	8.84	21943	338	0.126985	0.01437
Pb-212/214	74	SAME	SAME	SAME	SAME	SAME
Pb-212/214	77	SAME	SAME	SAME	SAME	SAME
Tl-208	84	4.52	13412	505	0.077616	0.01716
Pb-212/214	87.2	SAME	SAME	SAME	SAME	SAME
Pb-212	90.1	SAME	SAME	SAME	SAME	SAME
Ac-228/Th-234	93	SAME	SAME	SAME	SAME	SAME
Ac-228	129	0.50	1037	253	0.006001	0.01203
	139	1.22	2337	144	0.013524	0.01110
Ac-228	154	0.17	287	192	0.001661	0.00969
	159	0.79	1388	267	0.008032	0.01019
	162	SAME	SAME	SAME	SAME	SAME
	174	0.12	206	74	0.001192	0.00959
Ra-226/U-235	185	1.97	3125	253	0.018084	0.00920
Ac-228	199	1.28	1816	139	0.010509	0.00819
Ac-228	209	0.45	724	187	0.004190	0.00936
Pb-212	238.6	6.66	11840	316	0.068519	0.01029
Pb-214	241.9	SAME	SAME	SAME	SAME	SAME
Ac-228	270	0.40	498	169	0.002882	0.00726
Tl-208	277.3	0.49	593	134	0.003432	0.00698
Pb-214	295.2	2.60	2928	126	0.016944	0.00650
Ac-228	328	0.56	576	175	0.003333	0.00596
Ac-228	338.3	1.39	1665	176	0.009635	0.00692
Pb-214	351.9	5.76	5639	179	0.032633	0.00566
	415.5	0.44	376	139	0.002176	0.00495
Ac-228	463	0.66	576	105	0.003333	0.00503
	476	0.29	224	79	0.001296	0.00443
	498	0.51	379	118	0.002193	0.00427
Ann. Peak	510.8	N/A	28267	217	0.163582	N/A
	536	0.50	350	81	0.002025	0.00402
	557	47.48	31941	208	0.184844	0.00389
	567	1.33	885	92	0.005122	0.00384
	574	2.51	1649	78	0.009543	0.00380
Tl-208	583.1	3.64	2514	93	0.014549	0.004
	594	2.16	1381	119	0.007992	0.00369

**A-7 – (Continued)**

<b>Radionuclide</b>	<b>Gamma Energy (keV)</b>	<b>Emission Rate (y/sec)</b>	<b>Net Peak Count</b>	<b>Uncertainty</b>	<b>Net Count Rate (cps)</b>	<b>Efficiency (c/y)</b>
Bi-214	609.3	6.61	4131	123	0.023906	0.00362
	616	0.53	329	90	0.001904	0.00358
Bi-210	649.6	9.14	5418	137	0.031354	0.00343
	692	2.68	1505	113	0.008709	0.00326
	706	0.52	290	108	0.001678	0.00320
Bi-212	727.2	3.31	1787	103	0.010341	0.00313
	746	0.78	414	92	0.002396	0.00306
Bi-214	766.8	0.44	229	89	0.001325	0.00299
Ac-228	794	0.49	245	86	0.001418	0.00291
	801	6.02	3005	132	0.017390	0.00289
Bi-206	803	SAME	SAME	SAME	SAME	SAME
Tl-208	860	0.33	165	79	0.000955	0.0029
	867	0.67	314	63	0.001817	0.00271
Bi-206	881	0.34	158	81	0.000914	0.00267
	897	0.31	139	83	0.000804	0.00263
Ac-228	911	3.49	1669	89	0.009659	0.00277
Bi-214	933	0.90	398	112	0.002303	0.00255
Ac-228	964/969.1	3.33	1478	135	0.008553	0.00257
	1097	0.57	219	70	0.001267	0.00224
Bi-214	1120.2	2.10	801	91	0.004635	0.00220
	1208.3	2.65	951	79	0.005503	0.00208
Bi-214	1238.1	0.94	331	85	0.001916	0.00204
	1283	1.32	451	85	0.002610	0.00198
	1292	0.95	322	67	0.001863	0.00197
	1304	0.46	155	60	0.000897	0.00196
	1363	1.87	612	64	0.003542	0.00189
	1369	0.45	146	40	0.000845	0.00188
Bi-214	1377.1	0.36	117	58	0.000677	0.00187
	1398	2.12	679	76	0.003929	0.00185
K-40	1460	19.03	5897	105	0.034126	0.00179
	1488	1.27	389	71	0.002251	0.00177
DE Tl-208	1592	0.73	212	64	0.001227	0.00168
	1660	1.35	381	74	0.002205	0.00163
Bi-214	1764.5	1.91	514	57	0.002975	0.00156
	2102	0.97	230	81	0.001331	0.00137
	2224	5.53	1262	86	0.007303	0.00132
	2458	2.38	508	77	0.002940	0.00123
Tl-208	2614	8.16	1508	86	0.008727	0.00107
	2663	1.14	230	75	0.001331	0.00117



A-8 - Sample #3 dry

Radionuclide	Gamma Energy (keV)	Emission Rate (y/sec)	Net Peak Count	Uncertainty	Net Count Rate (cps)	Efficiency (c/y)
Pb-210	47	0.41	1248	218	0.007222	0.01741
Pb-214	53.5	1.30	3804	204	0.022014	0.01692
Th-234	63	0.62	1723	96	0.009971	0.01615
	67	0.09	259	60	0.001499	0.01583
	70	102.28	25398	421	0.146979	0.001437
Tl-208	73	SAME	SAME	SAME	SAME	SAME
Pb-212/214	74	SAME	SAME	SAME	SAME	SAME
Pb-212/214	77	SAME	SAME	SAME	SAME	SAME
Tl-208	84	5.07	15023	487	0.086939	0.01716
Pb-212/214	87.1	SAME	SAME	SAME	SAME	SAME
Pb-212	90.1	SAME	SAME	SAME	SAME	SAME
Ac-228/Th-234	93	SAME	SAME	SAME	SAME	SAME
Ac-228	129	0.36	747	253	0.004323	0.01203
	139	1.17	2249	164	0.013015	0.01110
Ac-228	154	0.39	648	174	0.003750	0.00969
	159	1.05	1853	286	0.010723	0.01019
	162	SAME	SAME	SAME	SAME	SAME
	174	0.42	688	249	0.003981	0.00959
Ra-226/U-235	185	1.93	3069	145	0.017760	0.00920
Ac-228	199	1.45	2052	158	0.011875	0.00819
Ac-228	209	0.42	672	151	0.003889	0.00936
Pb-212	238.6	6.98	12416	254	0.071852	0.01029
Pb-214	241.9	SAME	SAME	SAME	SAME	SAME
Ac-228	270	0.57	718	169	0.004155	0.00726
Tl-208	277.3	0.51	616	150	0.003565	0.00698
Pb-214	295.2	3.28	3690	129	0.021354	0.00650
Ac-228	328	0.61	630	174	0.003646	0.00596
Ac-228	338.3	1.41	1689	132	0.009774	0.00692
Pb-214	351.9	7.06	6904	181	0.039954	0.00566
	415.5	0.40	340	139	0.001968	0.00495
Ac-228	463	0.78	607	105	0.003513	0.00453
	476	0.20	153	68	0.000885	0.00443
	498	0.23	166	54	0.000961	0.00427
Ann. Peak	510.8	N/A	28289	215	0.163709	N/A
	536	0.37	256	109	0.001481	0.00402
	557	46.56	31322	207	0.181262	0.00389
	567	0.95	632	94	0.003657	0.00384
	574	2.27	1491	71	0.008628	0.00380
Tl-208	583.1	4.41	3047	102	0.017633	0.004
	594	2.46	1572	120	0.009097	0.00369

# **A-8 – (Continued)**

<b>Radionuclide</b>	<b>Gamma Energy (keV)</b>	<b>Emission Rate (y/sec)</b>	<b>Net Peak Count</b>	<b>Uncertainty</b>	<b>Net Count Rate (cps)</b>	<b>Efficiency (c/y)</b>
Bi-214	609.3	7.94	4963	127	0.028721	0.00362
	616	0.93	575	101	0.003328	0.00358
Bi-210	649.6	9.08	5379	145	0.031128	0.00343
	692	0.77	435	112	0.002517	0.00326
	706	1.07	594	106	0.003438	0.00320
Bi-212	727.2	3.16	1706	104	0.009873	0.00313
	746	1.33	704	92	0.004074	0.00306
Bi-214	766.8	0.72	374	90	0.002164	0.00299
Ac-228	794	0.48	241	80	0.001395	0.00291
	801	6.19	3090	131	0.017882	0.00289
Bi-206	803	SAME	SAME	SAME	SAME	SAME
Tl-208	860	0.46	230	71	0.001331	0.0029
	867	0.53	246	78	0.001424	0.00271
Bi-206	881	0.29	132	60	0.000764	0.00267
	897	1.01	461	81	0.002668	0.00263
Ac-228	911	3.92	1874	90	0.010845	0.00277
Bi-214	933	0.64	282	85	0.001632	0.00255
Ac-228	964/969.1	3.16	1402	139	0.008113	0.00257
	1013	0.56	233	77	0.001348	0.00239
	1097	0.74	288	89	0.001667	0.00224
Bi-214	1120.2	2.39	909	93	0.005260	0.00220
	1208.3	2.57	920	93	0.005324	0.00208
Bi-214	1238.1	0.68	239	85	0.001383	0.00204
	1283	1.22	417	79	0.002413	0.00198
	1292	0.32	110	43	0.000637	0.00197
	1304	0.87	293	56	0.001696	0.00196
	1363	2.91	951	68	0.005503	0.00189
	1369	0.58	190	41	0.001100	0.00188
Bi-214	1377.1	0.45	145	40	0.000839	0.00187
	1398	2.12	680	58	0.003935	0.00185
K-40	1460	21.30	6598	108	0.038183	0.00179
	1488	1.87	570	70	0.003299	0.00177
DE Tl-208	1592	0.80	233	91	0.001348	0.00168
	1660	1.92	541	74	0.003131	0.00163
Bi-214	1764.5	2.94	792	75	0.004583	0.00156
	2102	1.59	377	177	0.002182	0.00137
	2224	5.69	1298	85	0.007512	0.00132
Tl-208	2614	9.15	1691	85	0.009786	0.00107
	2663	0.49	100	82	0.000579	0.00117

# A-9 - Sample #4 dry

Radionuclide	Gamma Energy (keV)	Emission Rate (y/sec)	Net Peak Count	Uncertainty	Net Count Rate (cps)	Efficiency (c/y)
Pb-210	47	0.71	2150	201	0.012442	0.01741
Pb-214	53.5	1.45	4247	185	0.024578	0.01692
Th-234	63	0.66	1838	99	0.010637	0.01615
	67	0.10	269	92	0.001557	0.01583
	70	10.00	24822	348	0.143646	0.01437
Tl-208	73	SAME	SAME	SAME	SAME	SAME
Pb-212/214	74	SAME	SAME	SAME	SAME	SAME
Pb-212/214	77	SAME	SAME	SAME	SAME	SAME
Tl-208	84	4.50	13338	504	0.077188	0.01716
Pb-212/214	87.1	SAME	SAME	SAME	SAME	SAME
Pb-212	90.1	SAME	SAME	SAME	SAME	SAME
Ac-228/Th-234	93	SAME	SAME	SAME	SAME	SAME
Ac-228	129	0.61	1268	260	0.007338	0.01203
	139	1.24	2387	187	0.013814	0.01110
Ac-228	154	0.14	236	76	0.001366	0.00969
	159	0.51	893	254	0.005168	0.01019
	162	SAME	SAME	SAME	SAME	SAME
	174	0.37	620	251	0.003588	0.00959
Ra-226/U-235	185	2.03	3224	148	0.018657	0.00920
Ac-228	199	1.54	2176	189	0.012593	0.00819
Ac-228	208	0.63	1023	134	0.005920	0.00936
Pb-212	238.6	7.18	12760	230	0.073843	0.01029
Pb-214	241.9	SAME	SAME	SAME	SAME	SAME
Ac-228	270	0.71	890	171	0.005150	0.00726
Tl-208	277.3	0.62	744	136	0.004306	0.00698
Pb-214	295.2	3.22	3615	130	0.020920	0.00650
Ac-228	328	0.49	503	177	0.002911	0.00596
Ac-228	338.3	1.72	2056	118	0.011898	0.00692
Pb-214	351.9	6.64	6494	183	0.037581	0.00566
Ac-228	463	1.01	788	117	0.004560	0.00453
	476	0.11	87	56	0.000503	0.00443
	498	0.39	286	88	0.001655	0.00427
Ann. Peak	510.8	N/A	28318	217	0.163877	N/A
	520	0.38	267	111	0.001545	0.00412
	536	0.50	345	111	0.001997	0.00402
	557	46.41	31223	207	0.180689	0.00389
	567	0.38	249	75	0.001441	0.00384
	574	2.57	1689	80	0.009774	0.00380
Tl-208	583.1	4.91	3392	104	0.019630	0.004
	594	2.66	1696	122	0.009815	0.00369

**A-9 – (Continued)**

<b>Radionuclide</b>	<b>Gamma Energy (keV)</b>	<b>Emission Rate (y/sec)</b>	<b>Net Peak Count</b>	<b>Uncertainty</b>	<b>Net Count Rate (cps)</b>	<b>Efficiency (c/y)</b>
Bi-214	609.3	7.64	4773	126	0.027622	0.00362
	616	0.67	412	91	0.002384	0.00358
Bi-210	649.6	8.17	4840	125	0.028009	0.00343
	692	2.83	1590	113	0.009201	0.00326
	706	0.58	321	110	0.001858	0.00320
Bi-212	727.2	3.27	1768	104	0.010231	0.00313
	746	1.53	811	91	0.004693	0.00306
Bi-214	766.8	0.49	252	91	0.001458	0.00299
Ac-228	794	0.37	186	72	0.001076	0.00291
	801	5.72	2853	127	0.016510	0.00289
Bi-206	803	SAME	SAME	SAME	SAME	SAME
Tl-208	860	0.81	406	73	0.002350	0.0029
	867	0.46	215	86	0.001244	0.00271
Bi-206	881	0.27	124	54	0.000718	0.00267
	897	1.02	465	82	0.002691	0.00263
Ac-228	911	4.35	2080	91	0.012037	0.00277
Bi-214	933	0.52	227	51	0.001314	0.00255
Ac-228	964/969.1	3.35	1488	139	0.008611	0.00257
	1013	0.99	409	77	0.002367	0.00239
	1097	0.14	53	91	0.000307	0.00224
Bi-214	1120.2	2.32	884	93	0.005116	0.00220
	1208.3	2.64	948	94	0.005486	0.00208
Bi-214	1238.1	1.11	391	87	0.002263	0.00204
	1283	1.48	507	75	0.002934	0.00198
	1292	0.77	263	73	0.001522	0.00197
	1304	0.36	121	44	0.000700	0.00196
	1363	2.79	911	80	0.005272	0.00189
	1369	0.45	146	41	0.000845	0.00188
Bi-214	1377.1	0.87	282	52	0.001632	0.00187
	1398	2.39	766	65	0.004433	0.00185
K-40	1460	22.90	7095	110	0.041059	0.00179
	1488	1.37	419	72	0.002425	0.00177
DE Tl-208	1592	0.98	284	80	0.001644	0.00168
	1660	1.82	511	74	0.002957	0.00163
Bi-214	1764.5	2.56	688	76	0.003981	0.00156
	2102	1.42	336	98	0.001944	0.00137
	2205	0.85	194	80	0.001123	0.00133
	2224	5.51	1257	70	0.007274	0.00132
	2458	1.91	408	61	0.002361	0.00123
Tl-208	2614	9.28	1716	86	0.009931	0.00107
	2662	1.39	281	53	0.001626	0.00117

# A-10 - Sample #5 dry

Radionuclide	Gamma Energy (keV)	Emission Rate (y/sec)	Net Peak Count	Uncertainty	Net Count Rate (cps)	Efficiency (c/y)
Pb-210	47	0.59	1777	201	0.010284	0.01741
Pb-214	53.5	1.43	4195	186	0.024277	0.01692
Th-234	63	0.70	1952	124	0.011296	0.01615
	67	0.09	257	61	0.001487	0.01583
	70	9.59	23820	348	0.137847	0.01437
Tl-208	73	SAME	SAME	SAME	SAME	SAME
Pb-212/214	74	SAME	SAME	SAME	SAME	SAME
Pb-212/214	77	SAME	SAME	SAME	SAME	SAME
Tl-208	84	5.07	15046	519	0.087072	0.01716
Pb-212/214	87.1	SAME	SAME	SAME	SAME	SAME
Pb-212	90.1	SAME	SAME	SAME	SAME	SAME
Ac-228/Th-234	93	SAME	SAME	SAME	SAME	SAME
Ac-228	129	0.43	896	221	0.005185	0.01203
	139	1.26	2408	166	0.013935	0.01110
Ac-228	154	0.41	688	159	0.003981	0.00969
	159	0.46	807	253	0.004670	0.01019
	162	SAME	SAME	SAME	SAME	SAME
	174	0.17	282	216	0.001632	0.00959
Ra-226/U-235	185	2.23	3548	239	0.020532	0.00920
Ac-228	199	1.26	1778	122	0.010289	0.00819
Ac-228	209	0.67	1079	115	0.006244	0.00936
Pb-212	238.6	7.20	12796	229	0.074051	0.01029
Pb-214	241.9	SAME	SAME	SAME	SAME	SAME
	252	0.34	437	189	0.002529	0.00735
Ac-228	270	0.57	715	138	0.004138	0.00726
Tl-208	277.3	0.57	687	182	0.003976	0.00698
Pb-214	295.2	3.00	3370	129	0.019502	0.00650
Ac-228	328	0.65	674	177	0.003900	0.00596
Ac-228	338.3	1.63	1951	103	0.011291	0.00692
Pb-214	351.9	5.93	5800	181	0.033565	0.00566
	415.5	0.32	278	293	0.001609	0.00495
Ac-228	463	0.91	715	106	0.004138	0.00453
	476	0.27	210	57	0.001215	0.00443
	498	0.17	129	120	0.000747	0.00427
Ann. Peak	510.8	N/A	28225	216	0.163339	N/A
	536	0.57	394	110	0.002280	0.00402
	557	46.97	31597	207	0.182853	0.00389
	567	0.51	335	84	0.001939	0.00384
	574	2.42	1591	79	0.009207	0.00380
Tl-208	583.1	4.89	3382	105	0.019572	0.004



**A-10 – (Continued)**

Radionuclide	Gamma Energy (keV)	Emission Rate (y/sec)	Net Peak Count	Uncertainty	Net Count Rate (cps)	Efficiency (c/y)
	594	1.98	1265	123	0.007321	0.00369
Bi-214	609.3	7.35	4595	135	0.026591	0.00362
	616	0.42	257	92	0.001487	0.00358
Bi-210	649.6	8.37	4959	132	0.028698	0.00343
	692	1.11	623	112	0.003605	0.00326
	706	0.63	349	109	0.002020	0.00320
Bi-212	727.2	3.09	1669	105	0.009659	0.00313
	746	1.37	725	92	0.004196	0.00306
	766.8	0.95	489	121	0.002830	0.00299
	784	0.42	213	71	0.001233	0.00294
Ac-228	794	0.55	275	80	0.001591	0.00291
	801	5.73	2859	127	0.016545	0.00289
Bi-206	803	SAME	SAME	SAME	SAME	SAME
	834	0.28	133	91	0.000770	0.00279
Tl-208	860	0.50	249	72	0.001441	0.0029
	867	0.58	269	70	0.001557	0.00271
Bi-206	881	0.31	144	69	0.000833	0.00267
	897	0.60	272	82	0.001574	0.00263
Ac-228	911	4.24	2031	91	0.011753	0.00277
Bi-214	933	0.50	221	63	0.001279	0.00255
Ac-228	964/969.1	3.11	1381	135	0.007992	0.00257
	1000	0.44	185	116	0.001071	0.00241
	1097	1.05	405	76	0.002344	0.00224
Bi-214	1120.2	2.41	917	93	0.005307	0.00220
	1208.3	3.05	1093	98	0.006325	0.00208
Bi-214	1238.1	1.07	376	86	0.002176	0.00204
	1283	0.97	332	82	0.001921	0.00198
	1292	0.35	119	51	0.000689	0.00197
	1304	0.52	177	68	0.001024	0.00196
	1363	2.53	825	73	0.004774	0.00189
	1369	0.44	142	35	0.000822	0.00188
Bi-214	1376	0.45	147	52	0.000851	0.00188
	1398	2.19	700	76	0.004051	0.00185
K-40	1460	23.14	7170	110	0.041493	0.00179
	1488	1.18	361	72	0.002089	0.00177
DE Tl-208	1592	0.65	190	50	0.001100	0.00168
	1660	1.34	376	76	0.002176	0.00163
Bi-214	1764.5	2.23	601	62	0.003478	0.00156
	2102	1.44	342	82	0.001979	0.00137
	2224	5.34	1219	87	0.007054	0.00132
	2458	2.18	464	77	0.002685	0.00123
Tl-208	2614	10.15	1876	85	0.010856	0.00107
	2662	0.83	167	35	0.000966	0.00117

## **Vita**

Daniel James Chase was born in Libertyville, Illinois, on November 1, 1966. He later moved to Santa Cruz, California, and graduated from Santa Cruz High School in June, 1984. After high school he served four years on active duty with the U.S. Air Force, ending in 1988. He completed his B.S. in Applied Physics at Eastern Kentucky University in December, 1990. He followed this by completing his M.S. in Nuclear Engineering at the University of Tennessee in May, 1998. He is currently employed by the Military Department of Tennessee.